UCD-97-5
March, 1997

Higgs Boson Discovery and Properties *

Authors and Conveners

J.F. Gunion[1,3,5] (U.C. Davis), L. Poggioli[2,3,5] (CERN), R. Van Kooten[2,3,5] (Indiana)
C. Kao[4,5] (Wisconsin), P. Rowson[4] (SLAC)

Working Group Members

S. Abdullin[5] (ITEP), V. Barger[5] (Wisconsin), M. Berger[5] (Indiana), D. Bauer[5] (U.C. Santa Barbara), M. Carena (CERN), C. Damerell[5] (SLAC), M. Fortner (FNAL), R. Frey (Oregon), H.E. Haber[5] (U.C. Santa Cruz), T. Han[5] (U.C. Davis), X.-G. He[5] (Melbourne), D. Hedin (FNAL), C. Heusch (U.C. Santa Cruz), D. Jackson[5] (SLAC), R. Jesik[5] (Indiana), J. Kelly[5] (U.C. Davis/Wisconsin), S. Kim[5] (Tsukuba), S. Kuhlmann[5] (FNAL), C. Loomis[5] (Rutgers), P. Martin[5] (U.C. Davis), T. Moroi[5] (LBL), K. Pitts[5] (FNAL), L. Reina (BNL), R. Sobey[5] (U.C. Davis), N. Stepanov[5] (ITEP), R. Szalapski (KEK), R. Vega (SMU), C. Wagner (CERN), J. Womersley (FNAL), W.-M. Yao[5] (LBL), R.-Y. Zhu (Cal. Tech.)

1) Primary Author; 2) Contributing Author; 3) Property Subgroup Convener;
4) Discovery Subgroup Convener; 5) Author of Summarized Contribution

ABSTRACT

We outline issues examined and progress made by the Light Higgs Snowmass 1996 working group regarding discovering Higgs bosons and measuring their detailed properties. We focused primarily on what could be learned at LEP2, the Tevatron (after upgrade), the LHC, a next linear e^+e^- collider and a $\mu^+\mu^-$ collider.

I. INTRODUCTION

The three accelerators that exist or are certain of being constructed are:

- LEP2, for which we assume $\sqrt{s} = 192\,\mathrm{GeV}$, and total integrated luminosity during the time before LEP2 is shut down for LHC construction of $L = 250\ \mathrm{pb}^{-1}$ at each of the four detectors for a total of $L = 1000\ \mathrm{pb}^{-1}$, assuming that data from the four detectors can be combined;
- the Main Injector at the Tevatron, with $\sqrt{s} = 2\,\mathrm{TeV}$ and $L = 2\ \mathrm{fb}^{-1}$ per year for CDF and D0, each, for a total of $L = 4\ \mathrm{fb}^{-1}$ per year or $L = 12\ \mathrm{fb}^{-1}$ for three years; and
- the LHC, with $\sqrt{s} = 14\,\mathrm{TeV}$ and $L = 100\ \mathrm{fb}^{-1}$ for each detector (ATLAS and CMS), for a total of $L = 200\ \mathrm{fb}^{-1}$ per year, or $L = 600\ \mathrm{fb}^{-1}$ for three years of operation.

Possible upgrades and future machines include:

- an upgrade of the Main Injector so as to enable $30\ \mathrm{fb}^{-1}$ each to be accumulated by CDF and D0;
- a Next Linear e^+e^- Collider (NLC) with $\sqrt{s} = 500\,\mathrm{GeV}$ and four-year integrated luminosity of about $200\ \mathrm{fb}^{-1}$;
- a First Muon Collider (FMC) with four-year integrated luminosity of $L = 200\ \mathrm{fb}^{-1}$ which could be spread out between operation at $\sqrt{s} = 500\,\mathrm{GeV}$ and running at $\sqrt{s}$ in the vicinity of the mass of an already detected Higgs boson or in a range designed to scan for an undiscovered Higgs boson.

Notational Convention: In the following discussions, we use the notation NLC for results that could be achieved in either e^+e^- or $\mu^+\mu^-$ collisions[1] at $\sqrt{s} = 500\,\mathrm{GeV}$. The notation FMC will be reserved for s-channel Higgs production results.

During the Snowmass workshop, we were able to pursue only a limited set of projects. The results obtained by various members of the group will be summarized and their overall impact

* To appear in *Proceedings of the 1996 DPF/DPB Summer Study on "New Directions in High Energy Physics" (Snowmass, 96)*, June 25 - July 12, 1996, Snowmass, Colorado.

[1] At $\sqrt{s} = 500\,\mathrm{GeV}$, $\mu^+\mu^-$ collision results will be similar to e^+e^- collision results if new detector backgrounds are not an issue.

shall also outline an ongoing program for delineating the role that the various machines mentioned above will play in pinning down the properties of a Higgs boson with Standard Model-like properties. Our discussion will be confined to five models:

- the Standard Model (SM), with a single Higgs boson, $h_{\rm SM}$.
- the minimal supersymmetric standard model (MSSM) with exactly two Higgs doublets resulting in five Higgs eigenstates: two CP-even bosons, h^0 and H^0 with $m_{h^0} \leq m_{H^0}$; one CP-odd Higgs, A^0; and a charged Higgs pair, $H^{\pm}$.
- the non-minimal supersymmetric standard model (NMSSM) with a single Higgs singlet field added to the two Higgs doublet fields — if CP is conserved, this adds a third CP-even eigenstate and a second CP-odd eigenstate to the spectrum.
- a general two-Higgs-doublet model (2HDM) of type-II (see Ref. [1]). In such a model, the masses and couplings of the three neutral Higgs bosons are free parameters; the neutral Higgs bosons can be CP-mixed states.
- a Higgs sector containing a doubly-charged Higgs boson (Δ^{--}).

This report is not intended as a general review of Higgs boson physics. It is designed to be read in conjunction with the recent review of Ref. [1], the NLC Physics report Ref. [2], and the muon-collider Higgs physics study of Ref. [3].

II. THE SM OR A SM-LIKE HIGGS BOSON

Although there has been extensive study of the $h_{\rm SM}$, we found a remarkably large number of new projects to pursue. In particular, we found that a detailed delineation of the extent to which the fundamental properties of the $h_{\rm SM}$ could be determined at a given accelerator or combination of accelerators was lacking. In what follows we present results obtained during the course of the workshop and summaries of earlier work in the following areas:

A) the discovery reach of TeV33;

B) strategies for verifying the fundamental properties of the $h_{\rm SM}$ using a combination of LEP2, TeV33, and LHC data, including some first estimates of errors;

C) optimizing the measurements of $\sigma BR(h_{\rm SM} \to b\bar{b})$, $\sigma BR(h_{\rm SM} \to c\bar{c})$ and $\sigma BR(h_{\rm SM} \to WW^\star)$ at the NLC for various production modes and determining ratios of branching ratios.

D) determining $\sigma BR(h_{\rm SM} \to \gamma\gamma)$ at the NLC;

E) determining the $ZZh_{\rm SM}$ coupling at the NLC;

F) determining the branching ratios and $WWh_{\rm SM}$ coupling at the NLC;

of the $h_{\rm SM}$, including relevance and current status of measuring a) the total width by s-channel scanning at the FMC and b) $\Gamma(h_{\rm SM} \to \gamma\gamma)$ at the $\gamma\gamma$ collider facility at the NLC — this section ends with a summary of the errors/precisions with which fundamental $h_{\rm SM}$ properties can be determined using NLC data alone, s-channel FMC data alone and a combination of NLC and s-channel FMC data;

H) determining the mass of the $h_{\rm SM}$ at TeV33, the LHC, the NLC and the FMC;

I) verifying the spin, parity and CP of the $h_{\rm SM}$.

Many new results are contained in these summaries.

Throughout our discussions, the branching ratios of the $h_{\rm SM}$ will play a major role, especially those for the $b\bar{b}$, $WW^\star$ and $ZZ^\star$ channels. These three branching ratios are tabulated for $m_{h_{\rm SM}} \leq 170\,{\rm GeV}$ in Table I for later reference. (For a full figure, see Ref. [1].) Note, in particular, that the $WW^\star$ mode only really begins to be competitive with the $b\bar{b}$ mode when $m_{h_{\rm SM}} \gtrsim 130\,{\rm GeV}$, and that it causes a precipitous decline in the $b\bar{b}$ branching ratio by $m_{h_{\rm SM}} \gtrsim 150\,{\rm GeV}$. In some of the error estimates to be presented, we have extrapolated simulations performed at only a few masses to a larger range of masses using the mass dependence of the $b\bar{b}$ and $WW^\star$ branching ratios. Another important point is also immediately apparent. For $m_{h_{\rm SM}} \leq 170\,{\rm GeV}$, $BR(h_{\rm SM} \to ZZ^\star)$ is always much smaller than $BR(h_{\rm SM} \to WW^\star)$. At the NLC, where backgrounds in the $WW^\star$ channel are not a particular problem (since a Higgs mass peak can be reconstructed in the four-jet $WW^\star$ final state), this has meant that detection of the $h_{\rm SM}$ in its $ZZ^\star$ decay mode has received little attention. However, at the LHC the $ZZ^\star$ channel has been the preferred channel due to the inability to detect $WW^\star$ in its four-jet mode (because of the large jet backgrounds in pp collisions) and the lack of a clear mass peak in the purely-leptonic or mixed modes. The much larger $WW^\star$ branching ratio has led us to pay increased attention to the $WW^\star$ mode at the LHC in this report.

Table I: $b\bar{b}$, $WW^\star$ and $ZZ^\star$ branching ratios for the $h_{\rm SM}$ in the $m_{h_{\rm SM}} < 2m_Z$ mass region.

Mass (GeV)	110	120	130	140	150	170
$BR(b\bar{b})$	0.78	0.69	0.53	0.34	0.17	0.008
$BR(WW^\star)$	0.04	0.13	0.29	0.50	0.70	0.97
$BR(ZZ^\star)$	0.002	0.01	0.03	0.06	0.08	0.02

Also of considerable importance is the expected width of a SM-like Higgs boson. The predicted width, $\Gamma^{\rm tot}_{h_{\rm SM}}$, is plotted in Fig. 1 as a function of $m_{h_{\rm SM}}$. The main features to take note of are:

- $\Gamma^{\rm tot}_{h_{\rm SM}}$ is very small for $m_{h_{\rm SM}} \lesssim 2m_W$. Indeed, for $m_{h_{\rm SM}} \lesssim 140\,{\rm GeV}$, $\Gamma^{\rm tot}_{h_{\rm SM}} < 10\,{\rm MeV}$.

of $h_{\rm SM} \to W^+W^-, ZZ$ decays.

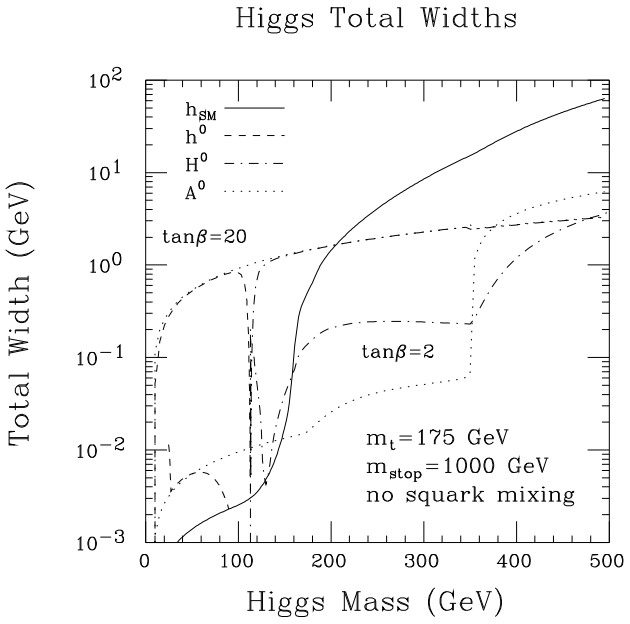

Figure 1: Total width versus mass of the SM and MSSM Higgs bosons for $m_t = 175\,\text{GeV}$. In the case of the MSSM, we have plotted results for $\tan\beta = 2$ and 20, taking $m_{\tilde{t}} = 1\,\text{TeV}$ and including two-loop/RGE-improved Higgs mass corrections and neglecting squark mixing; SUSY decay channels are assumed to be absent.

A. Discovery of $h_{\rm SM}$ in the $Wh_{\rm SM}$ and $Zh_{\rm SM}$ modes at TeV33

A thorough assessment of the $Wh_{\rm SM} \to \ell\nu b\bar{b}$ [4] and $Zh_{\rm SM} \to (\nu\overline{\nu}, \ell^+\ell^-)b\bar{b}$ [5] channels at TeV33 was made. In addition, a first exploration of $Zh_{\rm SM}$ detection in the $4b$ final state was initiated [6].

Earlier results for the $Wh_{\rm SM}$ mode were improved upon by:

- using the CDF soft lepton b-tagging and loose secondary vertex b-tagging in addition to the CDF secondary vertex b-tagging;
- requiring that $|\cos(\theta)| < 0.8$, where θ is the scattering angle of the Higgs in the W-Higgs c.m. system.

With these additional cuts, it is found that the SM Higgs with $m_{h_{\rm SM}} = 60, 80, 100, 120\,\text{GeV}$ could be discovered at the $\sqrt{s} = 2\,\text{TeV}$ TeV33 with integrated luminosity of $L = 3.5$, 5.5, 11 and $24.5\ \text{fb}^{-1}$, respectively — $30\ \text{fb}^{-1}$ would probably probe up to $m_{h_{\rm SM}} = 125\,\text{GeV}$. If results from both CDF and D0 could be combined, one might even reach $m_{h_{\rm SM}} = 130\,\text{GeV}$. The $Zh_{\rm SM}$ study showed that this channel can provide support for $m_{h_{\rm SM}} = 90$, 100, 110 and $120\,\text{GeV}$, respectively. In both the $Wh_{\rm SM}$ and $Zh_{\rm SM}$ channels, the above results require reconstructing the mass of the two tagged b-jets. Accepted $b\bar{b}$ mass intervals were in the range from $24\,\text{GeV}$ (at $m_{h_{\rm SM}} \sim 60\,\text{GeV}$) to $39\,\text{GeV}$ (at $m_{h_{\rm SM}} \sim 120\,\text{GeV}$).

The above results assume increased importance in the context of the MSSM, in which the upper bound on the probably SM-like h^0 is of order $130\,\text{GeV}$. Indeed, values of m_{h^0} in the $80 - 120\,\text{GeV}$ range are most typical in grand-unified (GUT) models with GUT-scale boundary conditions that yield automatic electroweak symmetry breaking (EWSB) via the renormalization group equations (RGE's), provided the squark masses are small enough to avoid naturalness problems. It seems that TeV33 has a good chance of discovering the h^0 of the MSSM. However, in the NMSSM the lightest Higgs need not have full coupling to WW and ZZ. Even if its mass lies in the $\lesssim 125\,\text{GeV}$ range, the other parameters of the model can easily be chosen so that it would not be detectable at TeV33.

If a SM-like Higgs boson is sufficiently light to be discovered at TeV33 (more generally if a SM-like Higgs has mass below $2m_W$) both the NLC and the FMC would be highly desirable machines capable of measuring crucial properties of a SM-like Higgs boson. In particular, for $m_{h_{\rm SM}} \lesssim 2m_W$, a FMC optimized for $\sqrt{s} = m_{h_{\rm SM}}$ running would be a Higgs factory [3] capable of directly measuring (by scanning) the total Higgs width and coupling ratios with great accuracy. Indeed, our final summary tables for the $h_{\rm SM}$ show that if $m_{h_{\rm SM}} \lesssim 150\,\text{GeV}$ then it would be extremely desirable to have both the NLC (or FMC running at $\sqrt{s} = 500\,\text{GeV}$) and a FMC devoted to $\sqrt{s} = m_{h_{\rm SM}}$ measurements in the s-channel. However, observation of a Higgs boson at TeV33 is unlikely to come soon enough to guide us should a decision between the FMC and the NLC (or a second NLC) become necessary.

Finally, a few brief remarks regarding the $Zh_{\rm SM} \to 4b$ final state detection mode. Final results have not yet been obtained, but progress has been made [6]. First, it is found that it will be possible to trigger with about 60% efficiency on the $4b$ final states using a "standard" (*i.e.* as employed in top quark studies) lepton plus jets trigger, where the lepton comes from semi-leptonic decay of one of the b's. Somewhat higher efficiency can probably be achieved with increased electron triggering acceptance and by employing secondary vertex triggers. Using the various codes for the $4b$ final state backgrounds [7] (which are in good agreement) a reasonable signal over background is found if two pairs of b's are required to have high mass.[2] On the other hand, $gg \to h_{\rm SM}b\bar{b}$ looks hard since the associated $b\bar{b}$ does not generally have a high pair mass; in particular, it would probably be necessary to veto charm at the 1% level.[3]

[2] This means that signal to background will possibly also be acceptable for supersymmetric model h^0A^0 Higgs pair production.

[3] Of course, for high $\tan\beta$ in the MSSM, the $gg \to A^0b\bar{b}$ and either $gg \to H^0b\bar{b}$ (for $m_{A^0} \gtrsim 130\,\text{GeV}$) or $gg \to h^0b\bar{b}$ (for $m_{A^0} \lesssim 130\,\text{GeV}$) rates are greatly enhanced relative to $gg \to h_{\rm SM}b\bar{b}$ and detection above some minimum value of $\tan\beta$ would become possible.

$h_{\rm SM}$ using LEP2, TeV33 and LHC data only [8]

In this continuing project, the goal is to fully enumerate the important strategies and measurements at LEP2, the Tevatron and the LHC that will be required to maximize information regarding the couplings of a Standard-Model-like Higgs boson and, thereby, our ability to verify its SM-like nature. Ultimately, as we shall discuss in later subsections, experimental data from the NLC and/or FMC will also be available that will vastly expand our ability to verify the properties of a SM-like Higgs boson. However, in the next decade or so, the challenge will be to extract maximal information from the former three operating accelerators. Ideally, one would wish to determine, *in a model-independent fashion*, all of the tree-level and one-loop couplings of the $h_{\rm SM}$, its spin, parity, and CP nature, and its total width. Here we outline the extent to which this will be possible using data from the three machines.

1. Enumeration of mass regions and reactions

The discussion divides naturally into five different mass regions:

M1: $m_{h_{\rm SM}} \lesssim 95\,{\rm GeV} - 100\,{\rm GeV}$. Detection of the $h_{\rm SM}$ should be possible at all three machines: LEP2, the Tevatron, and the LHC.

M2: $95 - 100\,{\rm GeV} \lesssim m_{h_{\rm SM}} \lesssim 130\,{\rm GeV}$. Detection should be possible at the Tevatron and the LHC, but not at LEP2. Note that we are adopting the optimistic conclusions discussed above that the mass range for which detection at TeV33 will be viable in the $Wh_{\rm SM}$, $h_{\rm SM} \to b\bar{b}$ mode includes the region between 120 and 130 GeV, and that up to 130 GeV some information can also be extracted at TeV33 from the $Zh_{\rm SM}$ mode. At the LHC, modes involving $h_{\rm SM} \to b\bar{b}$ are currently regarded as being quite problematic above 120 GeV. Nonetheless, we will consider them. Of course, $h_{\rm SM} \to ZZ^\star$ and $WW^\star$ decay modes will not yet be significant, and the Higgs remains very narrow.

M3: $130\,{\rm GeV} \lesssim m_{h_{\rm SM}} \lesssim 150 - 155\,{\rm GeV}$. Detection is only possible at the LHC, $ZZ^\star$ and $WW^\star$ decay modes emerge and become highly viable, the Higgs remains narrow.

M4: $155 \lesssim m_{h_{\rm SM}} \lesssim 2m_Z$. The real WW mode turns on, $ZZ^\star$ reaches a minimum at $m_{h_{\rm SM}} \sim 170\,{\rm GeV}$. The inclusive $\gamma\gamma$ mode is definitely out of the picture. The Higgs starts to get broad, but $\Gamma^{\rm tot}_{h_{\rm SM}} \lesssim 1\,{\rm GeV}$.

M5: $m_{h_{\rm SM}} \gtrsim 2m_Z$. Detection will only be possible at the LHC, ZZ and WW modes are dominant, and the Higgs becomes broad enough that a *direct* determination of its width becomes conceivable by reconstructing the $ZZ \to 4\ell$ final state mass (probable resolution being of order $1\% \times m_{h_{\rm SM}}$ at CMS and $1.5\% \times m_{h_{\rm SM}}$ at ATLAS). erties of the $h_{\rm SM}$ at each of the three machines are listed below. Even very marginal modes are included when potentially crucial to measuring an otherwise inaccessible Higgs property.

<u>LEP2</u>

LP1: $e^+e^- \to Z^\star \to Zh_{\rm SM} \to Zb\bar{b}$

LP2: $e^+e^- \to Z^\star \to Zh_{\rm SM} \to Z\tau^+\tau^-$

LP3: $e^+e^- \to Z^\star \to Zh_{\rm SM} \to ZX$

<u>Tevatron/TeV33</u>

T1: $W^\star \to Wh_{\rm SM} \to Wb\bar{b}$

T2: $W^\star \to Wh_{\rm SM} \to W\tau^+\tau^-$

T3: $Z^\star \to Zh_{\rm SM} \to Zb\bar{b}$

T4: $Z^\star \to Zh_{\rm SM} \to Z\tau^+\tau^-$

<u>LHC: $m_{h_{\rm SM}} \lesssim 2m_W, 2m_Z$</u>

L1: $gg \to h_{\rm SM} \to \gamma\gamma$

L2: $gg \to h_{\rm SM} \to ZZ^\star$

L3: $gg \to h_{\rm SM} \to WW^\star$

L4: $WW \to h_{\rm SM} \to \gamma\gamma$

L5: $WW \to h_{\rm SM} \to ZZ^\star$

L6: $WW \to h_{\rm SM} \to WW^\star$

L7: $W^\star \to Wh_{\rm SM} \to W\gamma\gamma$

L8: $W^\star \to Wh_{\rm SM} \to Wb\bar{b}$

L9: $W^\star \to Wh_{\rm SM} \to W\tau^+\tau^-$

L10: $W^\star \to Wh_{\rm SM} \to WZZ^\star$

L11: $W^\star \to Wh_{\rm SM} \to WWW^\star$

L12: $t\bar{t}h_{\rm SM} \to t\bar{t}\gamma\gamma$

L13: $t\bar{t}h_{\rm SM} \to t\bar{t}b\bar{b}$

L14: $t\bar{t}h_{\rm SM} \to t\bar{t}\tau^+\tau^-$

L15: $t\bar{t}h_{\rm SM} \to t\bar{t}ZZ^\star$

L16: $t\bar{t}h_{\rm SM} \to t\bar{t}WW^\star$

<u>LHC: $m_{h_{\rm SM}} \gtrsim 2m_W, 2m_Z$</u>

H1: $gg \to h_{\rm SM} \to ZZ$

H2: $gg \to h_{\rm SM} \to WW$

H3: $WW \to h_{\rm SM} \to ZZ$

H4: $WW \to h_{\rm SM} \to WW$

H5: $W^\star \to Wh_{\rm SM} \to WWW$

For $m_{h_{\rm SM}} \gtrsim 2m_W, 2m_Z$, we ignore $b\bar{b}$ decays of the $h_{\rm SM}$ as having much too small a branching ratio, and $t\bar{t}$ decays are not relevant for $m_{h_{\rm SM}} \lesssim 2m_t$.

We now tabulate the reactions of potential use in the five different mass regions, M1, M2, M3, M4 and M5.

M1: LP1, LP2, LP3, T1, T2, T3, T4, L1, L4, L7, L8, L9, L12, L13, L14.

M2: T1, T2, T3, T4, L1, L4, L7, L8, L9, L12, L13, L14.

M3: L1, L2, L3, L4?, L5, L6, L7, L10, L11, L12?, L15, L16.

M4: L2, L3, L5, L6, L10, L11, L15, L16.

M5: H1, H2, H3, H4, H5, H6.

2. Using Observed Rates to Extract Higgs Couplings

Again, we divide our discussion according to the five different mass regions listed above.

M1

Rates for reactions LP1, LP3, T1, T3, L1, L7, L8, L12, L13 will be well measured. Our ability to observe reactions LP2, T2, T4, L4, L9, L14 and determine with some reasonable accuracy the ratio of the rates for these reactions to the better measured reactions and to each other is less certain. Considering only the well-measured rates to begin with we find that we should be able to determine the following quantities.

- Measurement of the rate for LP3 (*i.e.* $Zh_{\rm SM} \to ZX$ with $Z \to e^+e^-, \mu^+\mu^-$) determines the $ZZh_{\rm SM}$ coupling (squared). For $m_{h_{\rm SM}} \sim 90 - 100\,{\rm GeV}$, $\sigma(Zh_{\rm SM}) \sim 0.5$ pb ($\sqrt{s} = 192\,{\rm GeV}$), implying for $L = 1000\ {\rm pb}^{-1}$ an event rate of about $0.06 \times 500 = 30$. Taking $S/B \sim 1$[4] for $m_{h_{\rm SM}} \sim m_Z$ (we cannot use b-tagging for this inclusive mode) gives a 1σ error, $\pm\sqrt{S+B}/S$, of $\pm 26\%$ on $\sigma(Zh_{\rm SM})$, corresponding to a $\sim \pm 12\%$ error on the $ZZh_{\rm SM}$ coupling. For $m_{h_{\rm SM}}$ significantly below m_Z, B/S will be smaller, and S larger, implying smaller errors.

- LP1/LP3 gives $BR(h_{\rm SM} \to b\bar{b})$, which can be checked against the SM prediction, but on its own does not allow a model-independent determination of the $h_{\rm SM} \to b\bar{b}$ coupling. For $m_{h_{\rm SM}} \sim m_Z$, using $BR(h_{\rm SM} \to b\bar{b}) \sim 0.89$ and a b-tagging efficiency of 50% per b, we get $S = 500 \times 0.89 \times (1 - [0.5]^2) \sim 334$ in the $Zb\bar{b}$ channel. The net efficiency associated with the use of the various Z decay modes is probably not more than 70%, implying a usable $S = 233$. Taking $S/B = 1$ (b-tagging included) we get $\sqrt{S+B}/S \sim 0.1$ for the 1σ error on $\sigma(Zh_{\rm SM})BR(h_{\rm SM} \to b\bar{b})$. The error on $BR(h_{\rm SM} \to b\bar{b})$ will then be dominated by the $\sigma(Zh_{\rm SM})$ error of $\sim \pm 26\%$.

- The ratio T1/LP1 yields the $(WWh_{\rm SM})^2/(ZZh_{\rm SM})^2$ coupling-squared ratio, and multiplying by the LP3 determination of $(ZZh_{\rm SM})^2$ we get an absolute magnitude for from the results presented in Ref. [4]. For $m_{h_{\rm SM}} \sim m_Z$, we average the S and B values presented in Table I of Ref. [4] for $m_{h_{\rm SM}} = 80\,{\rm GeV}$ and $m_{h_{\rm SM}} = 100\,{\rm GeV}$, obtaining $S \sim 75$ and $B \sim 324$, implying $\sqrt{S+B}/S \sim 0.26$, for $L = 10\ {\rm fb}^{-1}$. Going to 60 ${\rm fb}^{-1}$ ($L = 30\ {\rm fb}^{-1}$ for each of the two detectors) would reduce the fractional error to ~ 0.11. Combining with the ~ 0.1 error on LP1 implies an error for T1/LP1 of order $\sim \pm 15\%$. Systematic uncertainty would probably also be present in relating the $\sigma(Wh_{\rm SM})$ factor in the T1 rate to the $WWh_{\rm SM}$ coupling, and in the exact efficiencies for isolating the $T1$ reaction. It is hard to imagine that $(WWh_{\rm SM})^2/(ZZh_{\rm SM})^2$ could be determined to better than $\sim \pm 20\%$.

- The ratio T1/T3 gives an independent determination of $(WWh_{\rm SM})^2/(ZZh_{\rm SM})^2$. The T3 error can be estimated from the results presented in Ref. [5], Table I. For $L = 60\ {\rm fb}^{-1}$, at $m_{h_{\rm SM}} = 90\,{\rm GeV}$ we find $S \sim 216$ and $B \sim 1066$, implying $\sqrt{S+B}/S \sim 0.16$. combining this with the T1 error quoted above and including systematics, which might not be so large for this type of ratio, we might achieve a $\sim \pm 20\%$ determination of $(WWh_{\rm SM})^2/(ZZh_{\rm SM})^2$. If this and the previous determination can be combined, then a net error of order $\pm 14\%$ would appear to be possible. Given the $\sim \pm 26\%$ error in the determination of $(ZZh_{\rm SM})^2$ from $\sigma(Zh_{\rm SM})$, we obtain an error of $\sim \pm 30\%$ for $(WWh_{\rm SM})^2$.

- The ratio T1/$BR(b\bar{b})$ gives $(WWh_{\rm SM})^2$ and T3/$BR(b\bar{b})$ gives $(ZZh_{\rm SM})^2$. Given the $\sim \pm 26\%$ error on $BR(b\bar{b})$ from LP1/LP3 and the $\sim \pm 15\%$ and $\sim \pm 19\%$ errors on T1 and T3 (treated individually, implying that systematic errors — we take 10% — should be included), we obtain about $\pm 30\%$ and $\pm 32\%$ error on the absolute magnitudes of the individual $(WWh_{\rm SM})^2$ and $(ZZh_{\rm SM})^2$ couplings-squared, respectively. Combining with the previously discussed determinations we see that errors on $(WWh_{\rm SM})^2$ and $(ZZh_{\rm SM})^2$ of order $\sim \pm 20\%$ and $\sim \pm 22\%$ are to be expected, respectively.

- The ratios L7/L8 and L12/L13 yield two independent determinations of $BR(\gamma\gamma)/BR(b\bar{b})$. Alternatively, if it is difficult to separate L7 from L12 and/or L8 from L13 (*i.e.* $Wh_{\rm SM}$ from $t\bar{t}h_{\rm SM}$ production), we can take (L7+L12)/(L8+L13) to get a single determination. Multiplying by $BR(b\bar{b})$, we get $BR(\gamma\gamma)$.

  - A first estimate of the errors for L7 and L12, performed in Ref. [1], gave errors of $\sim \pm 13\%$, assuming no inefficiencies associated with separating L7 from L12. The individual errors on L7 and L12 were re-examined for this report, the new estimates being $\sim \pm 15\%$. If we combine L7+L12, the net error on the sum would then be of order $\sim \pm 10\%$.

  - Remarkably, the errors associated with separating L7 from L12 are small. For example, misidentification of $t\bar{t}h_{\rm SM}$ as $Wh_{\rm SM}$ would mean that (a) both b-jets

[4] Here, and in what follows, we denote the signal event rate by S and the background event rate by B.

the t's observed in the leptonic decay mode the second W must decay to two jets with mass different from m_W or to $\ell\nu$ where the ℓ is mis-identified.[5] The net probability for $t\bar{t}h_{\rm SM}$ misidentification would then be of order 2.5%.

– Modes L8 and L13 ($Wb\bar{b}$ and $t\bar{t}b\bar{b}$) are still under study by CMS. The ATLAS study [9] states that isolation of L8 may be impossible at high luminosity because of the difficulty of vetoing extra jets. The error on the L13 mode event rate can be estimated for $m_{h_{\rm SM}} \sim m_Z$ using Table 11.8 from Ref. [9]. Averaging 80 GeV and 100 GeV results yields $S \sim 1355$ and $B \sim 37850$ for $L = 100\,{\rm fb}^{-1}$. At $L = 600\,{\rm fb}^{-1}$, $S/\sqrt{B} \sim 17$ and $\sqrt{S+B}/S \sim 0.06$. In the next item, we assume that the amount of contamination from L8 is small.

– Thus, so long as the (large) backgrounds in the $b\bar{b}$ channels are well-understood, extraction of $BR(\gamma\gamma)/BR(b\bar{b})$ in the form L12/L13 would be possible. Using the above estimates of $\pm 15\%$ for L12 and $\pm 6\%$ for L13, a statistical error of $\pm 17\%$ would be found for $BR(\gamma\gamma)/BR(b\bar{b})$. Combining with the $\pm 26\%$ error on $BR(b\bar{b})$ from LEP2 implies error on $BR(\gamma\gamma)$ of $\sim \pm 31\%$.

Table II: We tabulate the approximate error in the determination of $\sigma(gg \to h_{\rm SM})BR(h_{\rm SM} \to \gamma\gamma)$ as a function of $m_{h_{\rm SM}}$ (in GeV) assuming $L = 300\ {\rm fb}^{-1}$ for the CMS and ATLAS detectors at the LHC.

Mass	90	110	130	150
CMS Error	$\pm 9\%$	$\pm 6\%$	$\pm 5\%$	$\pm 8\%$
ATLAS Error	$\pm 23\%$	$\pm 7\%$	$\pm 7\%$	$\pm 10\%$
Combined Error	$\pm 8.5\%$	$\pm 4.5\%$	$\pm 4.0\%$	$\pm 6.2\%$

- L1/$BR(\gamma\gamma)$ yields the magnitude of the $(gg h_{\rm SM})^2$ coupling-squared, which is primarily sensitive to the $t\bar{t}h_{\rm SM}$ coupling. The error on the L1 rate is quite different for ATLAS and CMS. At $m_{h_{\rm SM}} \sim m_Z$, for $L = 300\ {\rm fb}^{-1}$ ATLAS [9] expects $S \sim 1650$ and $B \sim 142800$ yielding an error of $\sim \pm 23\%$; CMS (see Fig. 12.3 and associated tables in Ref. [10]) expects $S \sim 3825$ and $B \sim 115429$ yielding $\sqrt{S+B}/S \sim 0.09$. (For later reference, we give the errors on the L1 event rate for CMS and ATLAS with $L = 300\ {\rm fb}^{-1}$ in Table II.) The much better CMS result derives from: i) CMS includes a QCD correction factor of $K = 1.5$ in the L1 rate, whereas ATLAS does not; ii) for $m_{h_{\rm SM}} \sim m_Z$, ATLAS reduces the γ efficiency from 80% to 72% (needed to reject the Z continuum). As a compromise, we adopt the approach of computing the net L1 error ing an error on the L1 rate of $\sim \pm 8\%$. In any case, it will be much smaller than the error of $\sim \pm 31\%$ on $BR(\gamma\gamma)$, which will therefore dominate the error on $(gg h_{\rm SM})^2$.

- L12/L7 and L13/L8 yield independent determinations of the $t\bar{t}h_{\rm SM}/WWh_{\rm SM}$ event rate ratio. By multiplying by the previously determined value of $(WWh_{\rm SM})^2$ we get an absolute magnitude for the $(t\bar{t}h_{\rm SM})^2$ coupling-squared which can be checked against the $gg h_{\rm SM}$ result. As noted earlier, L12 can be efficiently separated from L7, whereas isolation of L8 is very uncertain at high luminosity. Since the L7 and L12 rates have errors of $\sim \pm 15\%$ (see above), we predict an error on L12/L7 of about $\pm 21\%$, not including any systematic uncertainty. Given the $\sim \pm 20\%$ error in $(WWh_{\rm SM})^2$, an error of $\sim \pm 30\%$ for $(t\bar{t}h_{\rm SM})^2$ is anticipated, *i.e.* comparable to that coming from the $(gg h_{\rm SM})^2$ coupling-squared determination.

What is missing from the above list is any determination of the $(b\bar{b}h_{\rm SM})$, $(\tau^+\tau^- h_{\rm SM})$ and $(\gamma\gamma h_{\rm SM})$ couplings, any check that fermion couplings are proportional to the fermion mass (other than the $(t\bar{t}h_{\rm SM})$ coupling magnitude), and the Higgs total width. Given the $(WWh_{\rm SM})$ and $(t\bar{t}h_{\rm SM})$ couplings we could compute the expected value for the $(\gamma\gamma h_{\rm SM})$ coupling, and combine this with $BR(\gamma\gamma)$ to get a value for $\Gamma^{\rm tot}_{h_{\rm SM}}$. $BR(b\bar{b})\Gamma^{\rm tot}_{h_{\rm SM}}$ then yields $b\bar{b}h_{\rm SM}$ and we would have a somewhat indirect check that $b\bar{b}h_{\rm SM}/t\bar{t}h_{\rm SM} = m_b/m_t$. Some systematic uncertainty in the correct values of m_b and m_t would enter into this check, but the propagation of the already rather significant statistical errors would be the dominant uncertainty.

In the above, a very critical ingredient was the small probability of mis-identifying a $t\bar{t}h_{\rm SM}$ event as a $Wh_{\rm SM}$ event, and vice versa. Further careful studies of this issue by the detector groups would be useful.

Let us now ask what we would gain by adding reactions LP2, T2, T4, L4, L9, and L14. LP2/LP1, T2/T1, T4/T3 L9/L8 and L14/L13 would all allow different determinations of $\tau^+\tau^- h_{\rm SM}/b\bar{b}h_{\rm SM}$. This would certainly be of significant value, but with what accuracy could these ratios be measured? After including efficiencies for τ identification, the rate for $Zh_{\rm SM} \to 2j + 2\tau$ at LEP2 is about 8 events over a background of 5 for $L = 1\ {\rm fb}^{-1}$, for $m_{h_{\rm SM}} \simeq m_Z$. This makes use of the estimated mass resolution $\sigma_m \sim 2 - 3\,{\rm GeV}$ for a 2τ pair. The known Z branching fractions could then be used to extract the $h_{\rm SM} \to \tau^+\tau^-$ portion of the net rate. At best, LP2/LP1 could be extracted with $\sim \pm 50\%$ accuracy implying (taking the square root) that the $(\tau^+\tau^- h_{\rm SM})/(b\bar{b}h_{\rm SM})$ coupling ratio could be extracted with an error of order $\sim \pm 30\%$.

What about $Wh_{\rm SM}$ and $t\bar{t}h_{\rm SM}$ production with $h_{\rm SM} \to \tau^+\tau^-$ at TeV33 (T2 and T4) and the LHC (L9 and L14)? At the time that this report is being prepared, the status of T2 and T4 at TeV33 is still being debated. We will not attempt any estimates. At the LHC, L9 and L14 are not deemed observable at $m_{h_{\rm SM}} \lesssim 100\,{\rm GeV}$ because of the very large backgrounds associated with $Z \to \tau^+\tau^-$.

Finally, the unstudied mode L4 does not provide any crucial new information given that the $WWh_{\rm SM}$ coupling cannot be

[5] Thus, misidentification has a probability of $(1-\epsilon_{b-tag})^2[BR(W \to 2j)Prob(m_{2j} \not\sim m_W) + BR(W \to \ell\nu)\epsilon_{\ell-misid}]$ estimated at $(0.5)^2[0.8 \cdot 0.1 + 0.2 \cdot 0.1] \sim 0.025$.

ficult to separate $WW \to h_{\rm SM}$ fusion from $gg \to h_{\rm SM}$ fusion for the low values of $m_{h_{\rm SM}}$ appropriate to mass region M1.

We end by summarizing in Table III the errors on fundamental branching ratios, couplings-squared, and ratios thereof as obtained above at $m_{h_{\rm SM}} \sim m_Z$ by combining LEP2, TeV33 and LHC data.

Table III: Summary of approximate errors for branching ratios and couplings-squared at $m_{h_{\rm SM}} \sim m_Z$ in the M1 mass region. Where appropriate, estimated systematic errors are included. Quantities not listed cannot be determined in a model-independent manner. As discussed in the text, directly measured products of couplings-squared times branching ratios can often be determined with better accuracy.

Quantity	Error
$BR(b\bar{b})$	$\pm 26\%$
$(WWh_{\rm SM})^2/(ZZh_{\rm SM})^2$	$\pm 14\%$
$(WWh_{\rm SM})^2$	$\pm 20\%$
$(ZZh_{\rm SM})^2$	$\pm 22\%$
$(\gamma\gamma h_{\rm SM})^2/(b\bar{b}h_{\rm SM})^2$	$\pm 17\%$
$BR(\gamma\gamma)$	$\pm 31\%$
$(ggh_{\rm SM})^2$	$\pm 31\%$
$(t\bar{t}h_{\rm SM})^2/(WWh_{\rm SM})^2$	$\pm 21\%$
$(t\bar{t}h_{\rm SM})^2$	$\pm 30\%$

M2

Rates for reactions T1, T3, L1, L7, L8, L12, L13 will be well measured. Reactions T2, T4, L4, L9, L14 are less robust. Relative to mass region M1, we suffer the crucial loss of a measurement of the magnitude of the $(ZZh_{\rm SM})$ coupling-constant-squared. Considering first the well-measured rates, we should be able to determine the following quantities.

- The ratio T1/T3 gives a determination of $(WWh_{\rm SM})^2/(ZZh_{\rm SM})^2$. Following a similar procedure as at $m_{h_{\rm SM}} \sim m_Z$, the statistical error for T1 can be estimated from the results presented in Ref. [4]. For $m_{h_{\rm SM}} \sim 100, 120\,{\rm GeV}$, Table I of Ref. [4] shows $S \sim 52, 27$ and $B \sim 257, 137$, implying $\sqrt{S+B}/S \sim 0.34, 0.47$, for $L = 10\ {\rm fb}^{-1}$. Going to $60\ {\rm fb}^{-1}$ would reduce the fractional error to $\sim 0.14, 0.19$. Table I of Ref. [5] for reaction T3 implies $S \sim 184, 102$ and $B \sim 990, 756$ for $L = 60\ {\rm fb}^{-1}$, implying fractional error of $\sim 0.19, 0.29$ at $m_{h_{\rm SM}} = 100, 120\,{\rm GeV}$. The resulting error on the ratio of the couplings-squared, $(WWh_{\rm SM})^2/(ZZh_{\rm SM})^2$, would then be $\sim \pm 23\%, \pm 34\%$ at these two masses.

- The errors for L7 and L12 are predicted to be similar in the M2 mass range to those found in the M1 mass range, *i.e.* of order $\pm 15\%$.

- The utility of the $b\bar{b}$ final states at the LHC, modes L8 and L13, is still being debated. No explicit CMS results are available at the time of writing. ATLAS states [9] that it may be possible to observe the $h_{\rm SM} \to b\bar{b}$ mode when $h_{\rm SM} \to b\bar{b}$. Here, we note that even if L8 and L13 are not viable discovery channels, it may still be possible to get a semi-accurate measurement of important ratios of branching ratios once the Higgs has been discovered. A rough estimate of the accuracy with which L13 can be measured is possible from Table 11.8 in Ref. [9]. For $L = 100\ {\rm fb}^{-1}$, ATLAS expects $S = 870, 420, 283$ and $B = 35100, 28300, 20000$ at $m_{h_{\rm SM}} = 100, 120, 130\,{\rm GeV}$ (where the $130\,{\rm GeV}$ numbers are obtained by extrapolation). Assuming that CMS studies will ultimately yield similar results we upgrade these numbers to $L = 600\ {\rm fb}^{-1}$, and find accuracies for the L13 rate of $\pm 9\%, \pm 16\%, \pm 21\%$ at the above respective masses.

- The ratios L7/L8 and L12/L13 yield two independent determinations of $BR(\gamma\gamma)/BR(b\bar{b})$. At the moment we can only estimate the accuracy of the L12/L13 determination of $BR(\gamma\gamma)/BR(b\bar{b})$: using $\pm 15\%$ for the error in L12 and the above estimates for the L13 errors we obtain errors for L12/L13 of $\pm 17\%, \pm 22\%, \pm 25\%$ at $m_{h_{\rm SM}} = 100, 120, 130\,{\rm GeV}$.

- L12/L7 and L13/L8 yield independent determinations of $(t\bar{t}h_{\rm SM})^2/(WWh_{\rm SM})^2$. Since L8 is dubious, we focus on L12/L7. Since the numerator and denominator errors are both of order $\pm 15\%$ in the M2 mass region, the error on this ratio is of order $\pm 21\%$, substantially better than the TeV33 expectation of $\sim \pm 34\%$.

Thus, we will have ways of determining the $(WWh_{\rm SM})$: $(ZZh_{\rm SM})$: $(t\bar{t}h_{\rm SM})$ coupling ratios, but no absolute coupling magnitudes are directly determined, and there is no test of the fermion-Higgs coupling being proportional to fermion mass. Once again, an important ingredient in determining the $(WWh_{\rm SM})^2/(t\bar{t}h_{\rm SM})^2$ ratio is the ability to separate $Wh_{\rm SM}$ from $t\bar{t}h_{\rm SM}$ final states in the $\gamma\gamma$ decay mode of the $h_{\rm SM}$.

To proceed further, requires more model input. Given that we know (in the SM) how to compute $BR(\gamma\gamma)$ from the $WWh_{\rm SM}$ and $t\bar{t}h_{\rm SM}$ couplings, and given that we know the ratio of the latter, $BR(\gamma\gamma)/BR(b\bar{b})$ would yield a result for $t\bar{t}h_{\rm SM}/b\bar{b}h_{\rm SM}$ which could then be checked against the predicted m_t/m_b.

Let us now ask what we would gain by adding reactions T2, T4, L4, L9, and L14. T2/T1, T4/T3, L9/L8 and L14/L13 would all allow different determinations of $(\tau^+\tau^- h_{\rm SM})^2/(b\bar{b}h_{\rm SM})^2$. This would allow a model independent check of the predicted $m_\tau^2/[3m_b^2(m_{h_{\rm SM}})]$ result. A first look at the LHC L9 and L14 rates is described below; recall that $m_{h_{\rm SM}} \gtrsim 100\,{\rm GeV}$, *i.e.* in the M2 mass region, is required in order that the $Z \to \tau^+\tau^-$ backgrounds to L9 and L14 be manageable. (We continue to leave aside the $\tau^+\tau^-$ modes T2 and T4 at TeV33 as being too uncertain.) Reaction L4 does not provide new information, and will not be considered.

We have estimated rates for L9 at the LHC. At $m_{h_{\rm SM}} = 110\,{\rm GeV}$, $\sigma BR(Wh_{\rm SM} \to l\nu\tau^+\tau^-) \sim 19$ fb. The $\Delta m_{\tau^+\tau^-}$ would be about $11\,{\rm GeV}$ ($21\,{\rm GeV}$) at low (high) luminosity. The acceptance factor (which takes into account the kinematical cuts, mass bin acceptance, the τ identification efficiency

only about 0.15% (0.07%), at low (high) L. At high L with 600 fb^{-1} (3 years running), this would leave us with $N = 600\ \text{fb}^{-1} \times 19\ \text{fb} \times 0.0007 = 8$ events. This is clearly a very marginal rate.

An alternative approach to identifying the $\tau^+\tau^-$ final state is to use $\tau^+\tau^- \to \ell + hadron + X$, which has an effective $BR \sim 50\%$, implying about 25 events per detector at low luminosity ($L = 30$ fb^{-1}). For $L = 600$ fb^{-1} one would have 500 events. But substantial cuts would be need to eliminate backgrounds from $W\tau^+\tau^-$, $t\bar{t}$ and $WW \to \ell\nu\ell\nu$.

The final mode is $\tau^+\tau^- \to \ell\nu\ell\nu$ with $BR \sim 0.12$, implying about 12 events for a detector-summed $L = 60$ fb^{-1} (low luminosity) or 120 events for total $L = 600$ fb^{-1}. However, this is before any cuts required to eliminate backgrounds.

We are not optimistic that L9 can be measured at a useful level of accuracy at the LHC. It appears that any determination of the $(\tau^+\tau^- h_{\rm SM})^2/(b\bar{b}h_{\rm SM})^2$ coupling-squared ratio will be extremely rough.

Finally, if signal L4 proves viable, L1/L4 would give $(ggh_{\rm SM})^2/(WWh_{\rm SM})^2$, which in the SM would yield a determination of $(t\bar{t}h_{\rm SM})^2/(WWh_{\rm SM})^2$ that could be checked against the L12/L7 determination. The key question is whether the WW fusion reaction can be separated from the gg fusion reaction in order to get at L1/L4. Some work by the ATLAS collaboration [11] showed that this may be very difficult at Higgs masses in the 100 GeV range.

We summarize as a function of $m_{h_{\rm SM}}$ in Table IV the errors for the few coupling-squared ratios that can be determined in the M2 mass region.

Table IV: Summary of approximate errors for coupling-squared ratios at $m_{h_{\rm SM}} = 100, 110, 120, 130$ GeV in the M2 mass region. As discussed in the text, directly measured products of couplings-squared times branching ratios can often be determined with better accuracy.

Quantity	Errors			
Mass (GeV)	100	110	120	130
$(WWh_{\rm SM})^2/(ZZh_{\rm SM})^2$	$\pm 23\%$	$\pm 26\%$	$\pm 34\%$	–
$(\gamma\gamma h_{\rm SM})^2/(b\bar{b}h_{\rm SM})^2$	$\pm 17\%$	$\pm 19\%$	$\pm 22\%$	$\pm 25\%$
$(t\bar{t}h_{\rm SM})^2/(WWh_{\rm SM})^2$	$\pm 21\%$	$\pm 21\%$	$\pm 21\%$	$\pm 21\%$

M3

Of the potential channels listed under M3, only L1 and L2 are thoroughly studied and certain to be measurable over this mass interval. L1 should be viable for $m_{h_{\rm SM}} \lesssim 150$ GeV. L2 (the $gg \to h_{\rm SM} \to ZZ^\star$ reaction) should be good for $m_{h_{\rm SM}} \gtrsim 130$ GeV. With these two modes alone, we discover the Higgs, and for $130 \lesssim m_{h_{\rm SM}} \lesssim 150$ GeV we can determine $BR(\gamma\gamma)/BR(ZZ^\star)$. The errors for the measurement of L2 have been estimated from the high luminosity results presented in Table 29 of Ref. [12]. For $L = 600$ fb^{-1} we find the errors listed in Table V. As expected, quite decent results are obtained for $m_{h_{\rm SM}} \gtrsim 130$ GeV. The errors in the $\gamma\gamma$ mode L1 rate obtained by combining ATLAS and CMS results would be $\pm 4\% - \pm 5\%$ for $m_{h_{\rm SM}}$ in the $110 - 130$ GeV range, rising $(\gamma\gamma h_{\rm SM})^2/(ZZh_{\rm SM})^2$ deriving from the L1/L2 ratio are tabulated in Table VII. This ratio is interesting, but cannot be unambiguously interpreted.

Table V: We tabulate the error in the determination of $\sigma(gg \to h_{\rm SM})BR(h_{\rm SM} \to 4\ell)$ as a function of $m_{h_{\rm SM}}$ (in GeV) assuming $L = 600$ fb^{-1} at the LHC.

Mass	120	130	150	170	180
Error	$\pm 25\%$	$\pm 9.5\%$	$\pm 5.3\%$	$\pm 11\%$	$\pm 6.1\%$
Mass	200	220	240	260	280
Error	$\pm 7.8\%$	$\pm 6.9\%$	$\pm 6.2\%$	$\pm 6.2\%$	$\pm 6.2\%$
Mass	300	320	340	360	380
Error	$\pm 6.2\%$	$\pm 6.2\%$	$\pm 6.1\%$	$\pm 6.0\%$	$\pm 6.4\%$
Mass	400	500	600	700	800
Error	$\pm 6.7\%$	$\pm 9.4\%$	$\pm 14\%$	$\pm 20\%$	$\pm 28\%$

The L3 mode was first examined in detail in Ref. [13]. They found that with some cuts it might be possible to dig out a signal in the $\ell\nu\ell\nu$ decay mode of the $WW^\star$ final state. A more recent study [14] focusing on the $m_{h_{\rm SM}} \gtrsim 155$ GeV mass region finds that additional cuts are necessary in the context of a more complete simulation, but that very promising $S/\sqrt{B}$ can be obtained. Here we give a rough extrapolation into the $130 - 150$ GeV mass region of their results by simply using the mass dependence of $BR(h_{\rm SM} \to WW^\star)$. We do not include the rise in the cross section as $m_{h_{\rm SM}}$ decreases since it is likely that there will be a compensating decrease in the efficiency with which the cuts of Ref. [14] accept events. We begin with the $m_{h_{\rm SM}} = 155$ GeV, $L = 5$ fb^{-1} result from their Table 2 of $S = 49$ and $B = 92$. We upgrade to $L = 600$ fb^{-1} and correct for $BR(h_{\rm SM} \to WW^\star)$ to obtain the statistical errors for $\sigma(gg \to h_{\rm SM} \to WW^\star)$ listed in Table VI; this table also includes the $m_{h_{\rm SM}} \geq 155$ GeV results. Presumably, one must also allow for a $\sim \pm 10\%$ systematic uncertainty in absolute normalization. This would then be the dominant error! However, we do not include this systematic error in the errors quoted for the $(WWh_{\rm SM})^2/(ZZh_{\rm SM})^2$ coupling-squared ratio as computed from L3/L2. The amount of systematic error that should be incorporated in estimating the error for such a ratio requires further study. The resulting statistical $(WWh_{\rm SM})^2/(ZZh_{\rm SM})^2$ errors are tabulated in Table VII. Apparently L3/L2 will provide a decent measurement of the $(WWh_{\rm SM})^2/(ZZh_{\rm SM})^2$ coupling-squared ratio, thereby allowing a check that custodial SU(2) is operating, so long as the systematic error is $\lesssim 10\%$.

The L4 mode could become of critical importance, since L4/L1 yields a determination of $(WWh_{\rm SM})^2/(gggh_{\rm SM})^2$ which (assuming only SM particles in the loops) yields a value of $(WWh_{\rm SM})^2/(t\bar{t}h_{\rm SM})^2$. But, at best the L4 mode might survive for $m_{h_{\rm SM}} \lesssim 140$ GeV. Further, the ability to separate WW fusion from gg fusion production has not been studied at $m_{h_{\rm SM}}$ values this low. The WW fusion rate is $\sim 1/5$ of the gg fusion rate; see Fig. 15, Ref. [1].

Let us now turn to other modes. Consider L10, L11, L15, and

Table VI: We tabulate the statistical error in the determination of $\sigma(gg \to h_{\rm SM} \to WW^\star)$ as a function of $m_{h_{\rm SM}}$ (in GeV) assuming $L = 600$ fb^{-1} at the LHC. For $m_{h_{\rm SM}} \leq 150\,{\rm GeV}$, the errors are based on extrapolation from $m_{h_{\rm SM}} \geq 155\,{\rm GeV}$ results. See text.

Mass	120	130	140	150	$155-180$
Error	$\pm 12\%$	$\pm 6\%$	$\pm 3\%$	$\pm 3\%$	$\pm 2\%$

Table VII: We tabulate the statistical errors at $m_{h_{\rm SM}} = 120, 130, 150\,{\rm GeV}$ in the determinations of $(\gamma\gamma h_{\rm SM})^2/(ZZh_{\rm SM})^2$ and $(WWh_{\rm SM})^2/(ZZh_{\rm SM})^2$, assuming $L = 600$ fb^{-1} at the LHC.

Quantity	Errors		
Mass (GeV)	120	130	150
$(\gamma\gamma h_{\rm SM})^2/(ZZh_{\rm SM})^2$	$\pm 25\%$	$\pm 11\%$	$\pm 10\%$
$(WWh_{\rm SM})^2/(ZZh_{\rm SM})^2$	$\pm 27\%$	$\pm 11\%$	$\pm 6\%$

L16. To begin, we relate L15 to L2. The maximum rate for $gg \to h_{\rm SM} \to ZZ^\star \to 4\ell$ is 69 events at $m_{h_{\rm SM}} = 150\,{\rm GeV}$ for $L = 100$ fb^{-1}, implying about 410 events at combined $L = 600$ fb^{-1}. The L15 $t\bar{t}h_{\rm SM} \to t\bar{t}4\ell$ rate is about a factor of 50 smaller at this mass implying 8 events. This seems too marginal to warrant further consideration. L10 would be still worse. The L11 and L16 ($W\ell\nu\ell\nu$ and $t\bar{t}\ell\nu\ell\nu$ final state channels) each have $\sigma BR(h_{\rm SM} \to \ell\nu\ell\nu) \sim 1.3$ fb. (No t or W branchings ratios are included; tagging with the two leptons from the $h_{\rm SM}$ decay is sufficient.) The $L = 600$ fb^{-1} event rates for each channel would thus be of order 800, *i.e.* larger than the L10 and L15 4ℓ event rates. But the inability to reconstruct the resonance mass in this channel would make extraction of a signal difficult. Separation of $Wh_{\rm SM}$ from $t\bar{t}h_{\rm SM}$ events could be performed as sketched earlier, but the input event rates would be lower due to the necessity of focusing on particular W and t decay final states. Still, further work on these $\ell\nu\ell\nu$ channels is clearly warranted, especially in light of the good results obtained in the inclusive $\ell\nu\ell\nu$ final state. Could the $\ell\nu 2j$ Higgs decay channel be used in $Wh_{\rm SM}$ and $t\bar{t}h_{\rm SM}$ associated production? For the moment, we adopt a pessimistic attitude. Clearly, given the importance of L11/L16 as a means of determining the $(WWh_{\rm SM})^2/(t\bar{t}h_{\rm SM})^2$ coupling-squared ratio, much more effort should be devoted in both the $\ell\nu\ell\nu$ and $\ell\nu 2j$ channels to determining if it will be possible to separately measure L11 and L16.

How about L5 and L6? Using a ratio of 1/5 for the WW/gg fusion production cross section ratio, we are left with about 80 events in the (L5) $WW \to h_{\rm SM} \to ZZ^\star \to 4\ell$ mode at $m_{h_{\rm SM}} = 150\,{\rm GeV}$; spectator jet tagging might allow a small background. If we assume 20% efficiency for double tagging adequate to effectively remove the gg fusion process (L2), we would be left with 16 events. While far from wonderful, this would allow in principle a $\lesssim \pm 25\%$ determination of the L5/L2 ratio implying an implicit determination of the L6/L5 would then yield $(WWh_{\rm SM})^2/(ZZh_{\rm SM})^2$, which could be combined with the L5/L2 result to give the very important set of relative weights: $(WWh_{\rm SM}) : (ZZh_{\rm SM}) : (t\bar{t}h_{\rm SM})$. If these relative weights agree with expectations for the $h_{\rm SM}$, it would be hard to imagine that the observed Higgs boson is not a SM-like Higgs. As noted, the ability to separate WW fusion events from gg fusion events with decent efficiency down at this low mass, using spectator jet tagging, will be critical for the above procedure.

M4

Let us now turn to the $155 \lesssim m_{h_{\rm SM}} \lesssim 2m_Z$ mass region. The most significant variation in this region arises due to the fact that as $h_{\rm SM} \to WW$ becomes kinematically allowed at $m_{h_{\rm SM}} \sim 160\,{\rm GeV}$, the $h_{\rm SM} \to ZZ^\star$ branching ratio dips, the dip being almost a factor of 4 at $m_{h_{\rm SM}} = 170\,{\rm GeV}$; see Table I. As a consequence, at $m_{h_{\rm SM}} = 170\,{\rm GeV}$ S/B (using ATLAS numbers) drops to 20/9.5 for $L = 100$ fb^{-1} compared to 69/10 at $m_{h_{\rm SM}} = 150\,{\rm GeV}$. Nonetheless, these S and B rates show that L2 can still be regarded as iron-clad throughout this region provided adequate L is accumulated. For $L = 600$ fb^{-1}, an accurate measurement of $(gg h_{\rm SM})^2 BR(h_{\rm SM} \to ZZ^\star)$ is clearly possible; results were already tabulated in Table V.

L3 is now an on-shell WW final state, and, according to the results summarized in Table VI, can be measured with good statistical accuracy in the $\ell\nu\ell\nu$ final state of the $h_{\rm SM} \to WW$ Higgs decay. The statistical accuracy for $(WWh_{\rm SM})^2/(ZZh_{\rm SM})^2$ deriving from L3/L2 is tabulated in Table VIII.

The fact that L3 provides a good signal is not really all that surprising. The cross section for L3 is about 16 pb. Neglecting the WW fusion inclusive contribution would mean that we could just collect events inclusively. Taking $BR(h_{\rm SM} \to WW) \sim 1$, $BR(W \to \ell\nu) \sim 2/9$, $BR(W \to 2j) \sim 2/3$ and $L = 600$ fb^{-1}, we get $\sim 5 \times 10^5$ events in the $\ell\nu\ell\nu$ channel and $\sim 3 \times 10^6$ events in the $\ell\nu 2j$ channel. Although the continuum WW and the $t\bar{t}$ backgrounds are large, there is lots of room for making cuts of the type considered in [14], which achieve $S/B = 1$ and $S/\sqrt{B} = 5 - 10$ in the M4 mass region for only $L = 5$ fb^{-1}. Thus, the error on the L3/L2 determination of $(WWh_{\rm SM})^2/(ZZh_{\rm SM})^2$ in the M4 mass region is dominated by that for the 4ℓ channel (tabulated in Table V).

Rates associated with measuring L5 are expected to be low given the small $BR(h_{\rm SM} \to ZZ^\star)$ in this mass region and the probably low efficiency for the double spectator tagging required to isolate the WW fusion process. We have made a rough estimate of what might be expected as follows. We take 1/5 as the ratio for the WW fusion production rate as compared to the gg fusion rate. We then assume a tagging efficiency (associated with eliminating the gg fusion signal) for both signal and background of order 20%. The result is that L5 errors would be about a factor of 5 larger than the L2 errors listed in Table V, implying at least $\pm 25\%$ statistical error for measuring the L5 rate. This in turn implies at least $\pm 25\%$ statistical error for measuring $(WWh_{\rm SM})^2/(gg h_{\rm SM})^2$ via L5/L2. While not particularly

detailed study should be performed to see if one could do better.

L6 would now be an on-shell final state, and might be measurable. The cross section for WW fusion is about 3 pb in this mass region. Assuming 20% efficiency for double spectator tagging, $BR(h_{\rm SM} \to WW) \sim 1$, $BR(W \to \ell\nu) \sim 2/9, BR(W \to 2j) \sim 2/3$ and $L = 600$ fb^{-1}, we get $\sim 2 \times 10^4$ events in the $\ell\nu\ell\nu$ channel and $\sim 1.2 \times 10^5$ events in the $\ell\nu 2j$ channel. It should be possible to get a decent measurement of L6 given the background reduction that would be obtained as part of the double-tagging procedure used to make gg fusion small. L6/L3 would determine $(WWh_{\rm SM})^2/(ggh_{\rm SM})^2$ and, thence, yield and implicit determination of $(WWh_{\rm SM})/(t\bar{t}h_{\rm SM})$.

We discard out-of-hand the L10 and L15 reactions given that $BR(h_{\rm SM} \to ZZ^\star)$ is in the dip region. The L11 and L16 reactions become on-shell decays, and probably deserve a close look, given that their ratio would yield the vital $WWh_{\rm SM}/t\bar{t}h_{\rm SM}$ ratio. We have not performed a study for this report. However, event rates are again encouraging. L11 has a cross section of about 0.3 pb and L16 is about 0.2 pb. Assuming 10% efficiency for tagging and isolating these processes from one another, $BR(h_{\rm SM} \to WW) \sim 1$, and the standard W decay branching ratios, we get $\sim 9 \times 10^2$ and $\sim 5 \times 10^3$ events in the $\ell\nu\ell\nu$ and $\ell\nu 2j$ channels, respectively (for $L = 600$ fb^{-1}). Given that backgrounds associated with these final states could be small because of our ability to tag these channels, the above event numbers might be sufficient to yield a reasonable determination of the L16/L11 ratio that would give a value for $(t\bar{t}h_{\rm SM})^2/(WWh_{\rm SM})^2$.

Table VIII: We tabulate the statistical errors at $m_{h_{\rm SM}} = 155, 170, 180$ GeV in the determination of $(WWh_{\rm SM})^2/(ZZh_{\rm SM})^2$ from L3/L2, assuming $L = 600$ fb^{-1} at the LHC.

Quantity	Errors		
Mass (GeV)	155	170	180
$(WWh_{\rm SM})^2/(ZZh_{\rm SM})^2$	$\pm 6\%$	$\pm 11\%$	$\pm 7\%$

M5

Finally we consider $m_{h_{\rm SM}} \gtrsim 2m_Z$. The first important remark is that $\Gamma^{\rm tot}_{h_{\rm SM}}$ becomes measurable in the 4ℓ channel once $\Gamma^{\rm tot}_{h_{\rm SM}} \gtrsim (1\% - 1.5\%) \times m_{h_{\rm SM}}$, which occurs starting at $m_{h_{\rm SM}} \sim 200$ GeV where $\Gamma^{\rm tot}_{h_{\rm SM}} \sim 2$ GeV. Quantitative estimates for the precision of the $\Gamma^{\rm tot}_{h_{\rm SM}}$ measurement will be discussed in Section G. At $m_{h_{\rm SM}} = 210$, 250, 300, and 400 GeV, rough percentage error expectations (assuming $L = 600$ fb^{-1} for ATLAS+CMS) for $\Gamma^{\rm tot}_{h_{\rm SM}}$ are $\pm 21\%$, $\pm 7\%$, $\pm 4\%$ and $\pm 3\%$, respectively.

Among the H1 to H6 modes, only H1 is gold-plated, and of course it alone provides very limited information about the actual Higgs properties. As described for the M4 mass region, the mode H2 has been studied for masses close to $2m_Z$ in the $\ell\nu\ell\nu$ final state in [13] and in the M4 mass region in [14]. These results indicate that reasonable to good accuracy for the H2/H1 $(WWh_{\rm SM})^2/(ZZh_{\rm SM})^2$, might be possible for Higgs masses not too far above $2m_Z$. One could also ask if it would be possible to separate out the WW final state in the $\ell\nu jj$ mode where a mass peak could be reconstructed (subject to the usual two-fold ambiguity procedures). Event rates would be quite significant, and a Monte Carlo study should be performed.

Processes H3 and H4 would have to be separated from H1 and H2 using spectator jet tagging to isolate the former WW fusion reactions. If this were possible, then H3/H1 and H4/H2 would both yield a determination of $(t\bar{t}h_{\rm SM})^2/(WWh_{\rm SM})^2$ under the assumption that the t-loop dominates the $(ggh_{\rm SM})$ coupling. However, the mass range for which separation of H3 and H4 would be possible is far from certain.[6]

Isolation of H4 is of particular importance given that $\Gamma^{\rm tot}_{h_{\rm SM}}$ becomes directly measurable in the 4ℓ final state once $m_{h_{\rm SM}} \gtrsim 2m_Z$. This is because the rate for H4 is proportional to $(WWh_{\rm SM})^2 BR(h_{\rm SM} \to WW)$. Multiplying by $\Gamma^{\rm tot}_{h_{\rm SM}}$ yields $(WWh_{\rm SM})^4$, which implies a very accurate determination of the $WWh_{\rm SM}$ coupling for even modest accuracy of the experimental inputs. Thus, further study of H4 for all values of $m_{h_{\rm SM}}$ above $2m_Z$ is a priority. If the $(WWh_{\rm SM})^2 : (ZZh_{\rm SM})^2 : (t\bar{t}h_{\rm SM})^2$ ratios could also be determined (using H1-H4 as outlined above), then the $(WWh_{\rm SM})^2$ magnitude would yield absolute values for $(ZZh_{\rm SM})^2$ and $(t\bar{t}h_{\rm SM})^2$ and, thence, a detailed test of the SM predictions.

We have not pursued the processes H5 and H6, as they will have lower rates. On the other hand, the backgrounds will be different, and one could imagine using them to confirm some of the results obtained from H1 through H4.

C. Measuring $\sigma BR(h_{\rm SM} \to c\bar{c}, b\bar{b}, WW^\star)$ using NLC and s-channel FMC data

We divide the discussion into:

- measurements that would be performed by running at $\sqrt{s} = 500$ GeV at the NLC (or in NLC-like running at the FMC) — the production modes of interest are $e^+e^- \to Zh_{\rm SM}$, $e^+e^- \to e^+e^-h_{\rm SM}$ (ZZ-fusion) and $e^+e^- \to \nu\bar{\nu}h_{\rm SM}$ (WW-fusion);[7]
- measurements performed in s-channel production at the FMC — the production mode being $\mu^+\mu^- \to h_{\rm SM}$.

In the first case, we presume that $L = 200$ fb^{-1} is available for the measurements at $\sqrt{s} = 500$ GeV. (Such operation at a FMC, would only be appropriate if the NLC has not been constructed or is not operating at expected instantaneous luminosity.) In the second case, we implicitly presume that the NLC

[6] A recent study [15] has shown that forward jet tagging allows isolation of H4 in the $\ell\nu jj$ final state for $m_{h_{\rm SM}} \gtrsim 600$ GeV (*i.e.* beyond the mass range being explicitly considered here), but suggests that the W+jets background is difficult to surmount for lower masses. However, strategies in the mass range down near $2m_Z$ could be quite different given the much larger signal rates.

[7] In the following, we will consistently use the notation $e^+e^-h_{\rm SM}$ and $\nu\bar{\nu}h_{\rm SM}$ for the ZZ fusion and WW fusion contributions to these final state channels only. The contributions to these same final states from $Zh_{\rm SM}$ with $Z \to e^+e^-$ and $Z \to \nu\bar{\nu}$, respectively, and interference at the amplitude level with the ZZ and WW fusion graphs is presumed excluded by appropriate cuts requiring that the e^+e^- or $\nu\bar{\nu}$ reconstructed mass not be near m_Z.

data collection would not be useful and devoting all the FMC luminosity to s-channel Higgs production would be entirely appropriate. The errors we quote in this second case will be those for only $L = 50\ \mathrm{fb}^{-1}$ at $\sqrt{s} = m_{h_{\rm SM}}$ (exactly). This is because the crucial measurement of $\Gamma^{\rm tot}_{h_{\rm SM}}$ by scanning the Higgs peak in the s-channel requires devoting significant luminosity to the wings of the peak (see later discussion).

1. *Measurements at* $\sqrt{s} = 500\,\mathrm{GeV}$

The accuracy with which cross section times branching ratio can be measured in various channels will prove to be vitally important in determining the branching ratios themselves and, ultimately, the total width and partial widths of the Higgs boson, which are its most fundamental properties. In addition, the ratios

$$\frac{\sigma BR(h_{\rm SM} \to c\bar{c})}{\sigma BR(h_{\rm SM} \to b\bar{b})}\,, \quad \frac{\sigma BR(h_{\rm SM} \to WW^\star)}{\sigma BR(h_{\rm SM} \to b\bar{b})} \tag{1}$$

will themselves be a sensitive probe of deviations from SM predictions to the extent that SM values for these branching ratios can be reliably computed (see later discussion). It should be noted that the $c\bar{c}$ and $WW^\star$ modes are complementary in that for $m_{h_{\rm SM}} \lesssim 130\,\mathrm{GeV}$ only the $c\bar{c}$ mode will have good measurement accuracy, while for $m_{h_{\rm SM}} \gtrsim 130\,\mathrm{GeV}$ accuracy in the $WW^\star$ mode will be best.

The h^0 of the MSSM provides a particularly useful testing ground for the accuracy with which the above ratios must be determined in order that such deviations be detectable. As m_{A^0} increases, the h^0 becomes increasingly SM-like. In typical GUT-unified versions of the MSSM, m_{A^0} values above 200 GeV are the norm and deviations of the h^0's couplings and branching ratios from those of the $h_{\rm SM}$ will only be detectable if the branching ratios can be determined with good accuracy. The survey of Ref. [1] and further work performed for this workshop [16] shows that the $c\bar{c}$, $b\bar{b}$ and $WW^\star$ partial widths and ratios of branching ratios provide sensitivity to h^0 vs. $h_{\rm SM}$ deviations out to higher values of m_{A^0} than any others. In particular, the $c\bar{c}/b\bar{b}$ and $WW^\star/b\bar{b}$ ratio deviations essentially depend only upon m_{A^0} and are quite insensitive to details of squark mixing and so forth. To illustrate, we present in Fig. 2 the ratio of the MSSM prediction to the SM prediction for these two ratios taking $m_{h^0} = 110\,\mathrm{GeV}$ (held fixed, implying variation of stop masses as m_{A^0} and $\tan\beta$ are changed) and assuming "maximal mixing" in the stop sector (as defined in Ref. [1]). Results are presented using contours in the $(m_{A^0}, \tan\beta)$ parameter space. Aside from an enlargement of the allowed parameter space region, the "no mixing" scenario contours are essentially the same. Results for larger m_{h^0} are very similar in the allowed portion of parameter space. We observe that it is necessary to detect deviations in the ratios at the level of 20% in order to have sensitivity up to $m_{A^0} \sim 400\,\mathrm{GeV}$. Of course, for a Higgs mass as small as $m_{h^0} = 110\,\mathrm{GeV}$, only the $c\bar{c}$ branching ratio has a chance of being measured with reasonable accuracy. Indeed, the $WW^\star$ branching ratio will inevitably be poorly measured for the h^0 of the MSSM if stop squark masses are $\lesssim 1\,\mathrm{TeV}$ im-

els the lightest Higgs can, however, be heavier and the $WW^\star$ branching ratio would then prove useful.

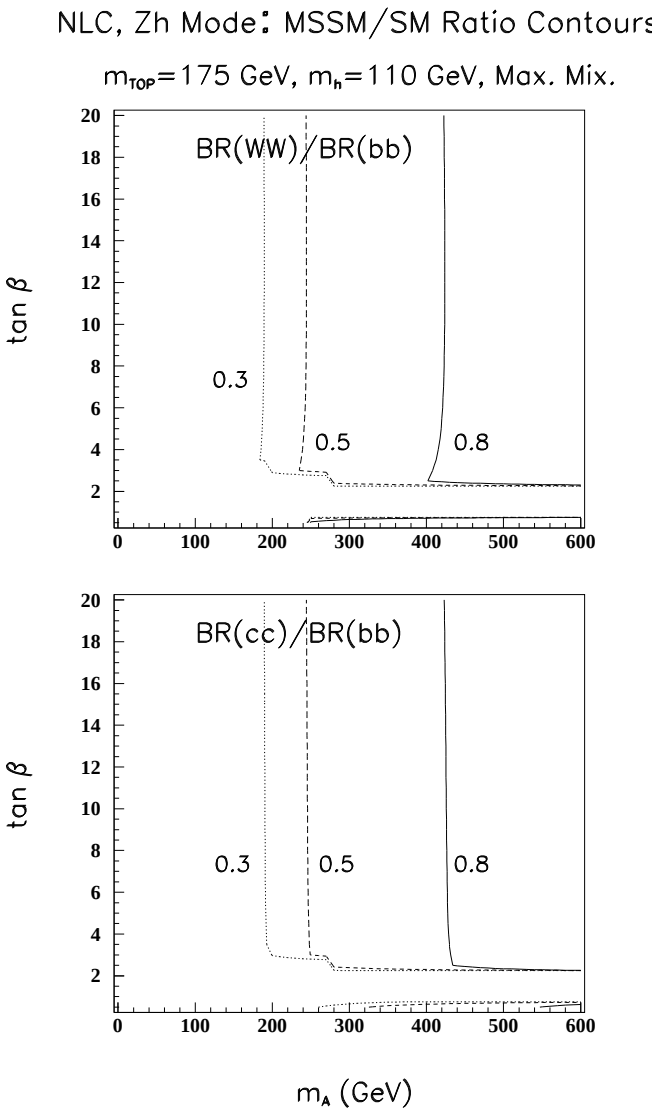

Figure 2: Constant value contours in $(m_{A^0}, \tan\beta)$ parameter space for the ratios $[WW^\star/b\bar{b}]_{h^0}/[WW^\star/b\bar{b}]_{h_{\rm SM}}$ and $[c\bar{c}/b\bar{b}]_{h^0}/[c\bar{c}/b\bar{b}]_{h_{\rm SM}}$. We assume "maximal-mixing" in the squark sector and present results for the case of fixed $m_{h^0} = 110\,\mathrm{GeV}$. The band extending out to large m_{A^0} at $\tan\beta \sim 2$ is where $m_{h^0} = 110\,\mathrm{GeV}$ is theoretically disallowed in the case of maximal mixing. For no mixing, see Ref. [1], the vertical contours are essentially identical — only the size of the disallowed band changes.

There are both experimental and theoretical sources of uncertainty for the branching ratio ratios of Eq. (1). We discuss first the systematic uncertainties that are present in the theoret-

with knowing the running b and c quark masses at the Higgs mass scale. These were recently reviewed [17] with rather optimistic conclusions. The values obtained in Ref. [18] from QCD sum rule calculations are $m_c(m_c) = 1.23^{+0.02}_{-0.04} \pm 0.06\,\mathrm{GeV}$ and $m_b(m_b) = 4.23^{+0.03}_{-0.04} \pm 0.04\,\mathrm{GeV}$, where the first error is that from $\alpha_s(m_Z) = 0.118 \pm 0.006$ and the second error is twice that claimed in [18]. With these inputs, one finds for $m_{h_{\mathrm{SM}}} \sim 100\,\mathrm{GeV}$ the result $m_c(m_{h_{\mathrm{SM}}}) = 0.62 \pm 0.05 \pm 0.02\,\mathrm{GeV}$, the first error being that from α_s uncertainties, including those deriving from the running. The uncertainty in $BR(h_{\mathrm{SM}} \to c\overline{c}) \propto m_c^2(m_{h_{\mathrm{SM}}})$ is then $\pm 15\%$. Analogously, the error for $BR(h_{\mathrm{SM}} \to b\overline{b})$ is about $\pm 4\%$. In the 10 years between now and operation of the NLC, it is reasonable to suppose that the α_s errors will be reduced to less than half the current value. The NLC itself will allow further improvement in the α_s determination [19]. Further improvement in the sum rule errors should also be possible, and fully competitive lattice calculation errors should be commonplace by the end of the century. Further, some of the uncertainties in the running α_s and other components of the theoretical calculations are common to the b and c channels, and will cancel out in the $c\overline{c}/b\overline{b}$ ratio of interest. In all, we find it not unreasonable to suppose that an accuracy of $\lesssim \pm 10\%$ can be achieved for the theoretical computations of the ratios of Eq. (1).

Early studies of the experimental accuracy with which the separate event rates for Zh_{SM} production with h_{SM} decaying to $b\overline{b}$, $c\overline{c}$ and $WW^\star$ could be measured are summarized in Ref. [1]; accuracies for the latter two were not encouraging. This was reexamined during the workshop [20].

We consider first $h_{\mathrm{SM}} \to b\overline{b}$ and $h_{\mathrm{SM}} \to c\overline{c}$. It is found that the separate $b\overline{b}$ and, especially, $c\overline{c}$ channel event rates can be measured in Zh_{SM} production with greater accuracy than previously estimated, provided one uses topological tagging techniques (as opposed to simple impact parameter tagging). Most importantly, the topological tagging allows a clean separation of the $c\overline{c}$ Higgs decay mode from the gg mode.[8] The purity of b and c topological single jet tagging as a function of the efficiency required is illustrated in Fig. 3, where the present performance of the SLD VXD3 upgrade pixel vertex detector is shown along with that predicted for a proposed pixel detector (NLC VTX) [23] in a typical NLC detector. This method allows for the reconstruction of a primary, secondary, and tertiary vertex to identify the presence of a b quark, only a primary and a secondary for a c quark, and tracks only coming from a primary in the case of a jet originating from a gluon.

The resulting ability to separate $b\overline{b}$, $c\overline{c}$ and gg, $q\overline{q}$ decays of the h_{SM} in Zh_{SM} events at $\sqrt{s} = 500\,\mathrm{GeV}$ was studied using simulations performed assuming the performance of the NLC detector [24] at the smeared four-vector level, signals with $m_{h_{\mathrm{SM}}} = 120\,\mathrm{GeV}$ and $130\,\mathrm{GeV}$, and considering the known Standard Model backgrounds. For determining $\sigma(Zh_{\mathrm{SM}})BR(h_{\mathrm{SM}} \to C)$ ($C = b\overline{b}$ or $c\overline{c}$), both $Z \to e^+e^-, \mu^+\mu^-$ and $Z \to jj$ decays (with full kinematically constrained fitting for both) are retained. The topological tagging works so well that $b\overline{b}$ events

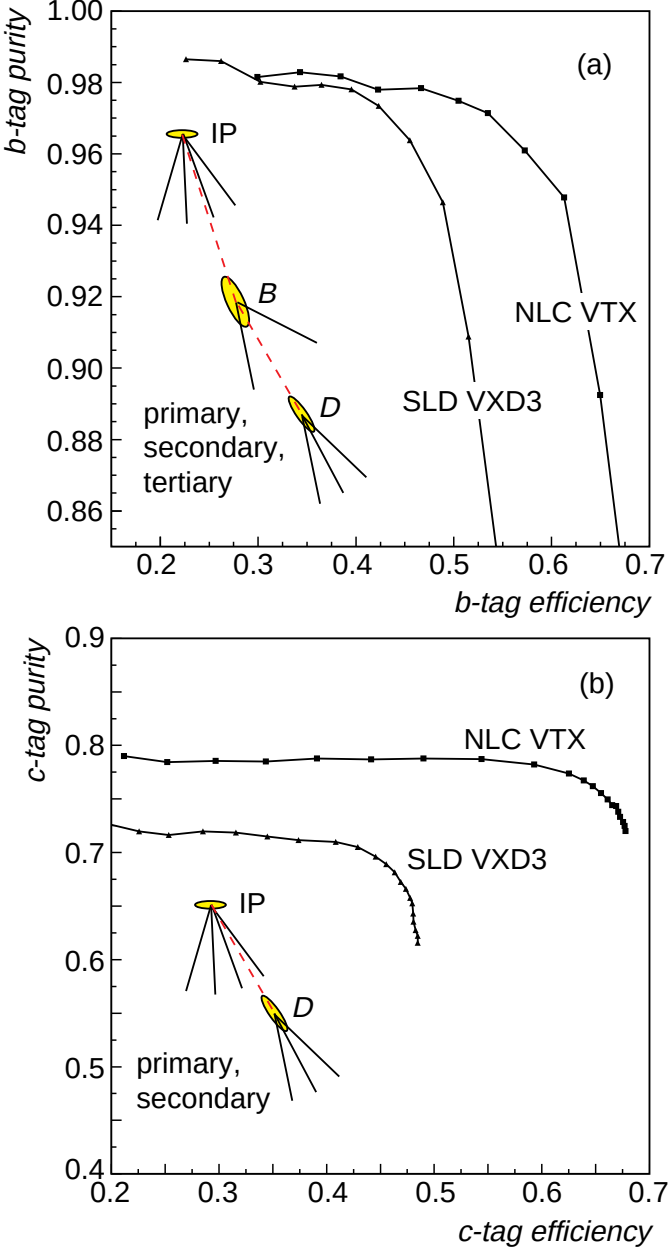

Figure 3: Purity vs. efficiency for b and c single jet tagging using the topological tagging techniques of Ref. [20].

can be identified with sufficient purity[9] by tagging just one (or both) of the b-jets. To isolate $c\overline{c}$ events with adequate purity, we require that both the c and the $\overline{c}$ be tagged. For tagging $h_{\mathrm{SM}} \to b\overline{b}$ events at $m_{h_{\mathrm{SM}}} = 120\,\mathrm{GeV}$ (for example), a sample

[8] The gg mode was simulated using the HAZA Monte Carlo generator [21] followed by default JETSET fragmentation [22].

[9] Here, and in the numbers quoted below, we refer to event, or decay-channel, purity (as opposed to single jet tagging purity as plotted in Fig. 3). Event/channel purity is defined as the number of events selected by the tagging procedure for a particular channel C that are truly from $h_{\mathrm{SM}} \to C$ decays divided by the total number so selected, including all h_{SM} decays with relative branching ratios as predicted in the SM.

one or both b-quarks with a purity of 95.4% (and efficiency for tagging c-quark decay events of 2.6%). For tagging c quark decay events, the operating point chosen resulted in an efficiency of 40% for tagging both the c and $\overline{c}$ quarks and a $c\overline{c}$ channel purity of 77.5% (and efficiencies of 11% for events where the $h_{\rm SM}$ decays to b-quarks and 0.2% for events where the $h_{\rm SM}$ decays to light quarks or gluons[10]).

These results represent a very substantial improvement over earlier expectations using impact parameter only. For Higgs masses below about 130 GeV, it will be possible [20] to measure $\sigma(Zh_{\rm SM})BR(h_{\rm SM} \to b\overline{b})$ with an error of $\sim \pm 2.5\% - \pm 3.5\%$ and $\sigma(Zh_{\rm SM})BR(h_{\rm SM} \to c\overline{c})$ to about $\pm 10\%$, for $L = 200$ fb^{-1}. This implies $\sim \pm 11\%$ error for $BR(h_{\rm SM} \to c\overline{c})/BR(h_{\rm SM} \to b\overline{b})$.

Although not specifically studied for this report, a crude estimate [25] suggests that the analogous procedure in the $e^+e^-h_{\rm SM}$ final state mode would yield a similar level of error for this ratio. (See the later $BR(h_{\rm SM} \to b\overline{b})$ discussion for comparative $Zh_{\rm SM}$ and $e^+e^-h_{\rm SM}$ errors in the $b\overline{b}$ decay mode.) The ratio could again be measured in the WW-fusion $\nu\overline{\nu}h_{\rm SM}$ final state. There, the error on $\sigma(\nu\overline{\nu}h_{\rm SM})BR(h_{\rm SM} \to b\overline{b})$ is expected to be in the $\pm 2.5\% - \pm 3.5\%$ range for $m_{h_{\rm SM}} \lesssim 140$ GeV as estimated in [1] and reconfirmed at this workshop. The $c\overline{c}$ final state has not been studied yet, but it would seem that accuracies in the $\pm 10\%$ vicinity for $\sigma(\nu\overline{\nu}h_{\rm SM})BR(h_{\rm SM} \to c\overline{c})$ are not out of the question. Combining [26] just the $Zh_{\rm SM}$ and $e^+e^-h_{\rm SM}$ modes, we could probably achieve $\sim \pm 7\% - \pm 8\%$ error for $c\overline{c}/b\overline{b}$. Including the $\nu\overline{\nu}h_{\rm SM}$ final state might allow us to reach $\lesssim \pm 7\%$. If we combine this error in quadrature with the earlier estimate of $\lesssim \pm 10\%$ for systematic error in the theoretical calculation of the $c\overline{c}/b\overline{b}$ ratio, we arrive at a net error of $\lesssim 12\%$. Fig. 2 shows that this would allow differentiation of the h^0 from the $h_{\rm SM}$ at the 2σ level out to $m_{A^0} \sim 450$ GeV. This is a very encouraging result. The dominance of the theoretical error in the above estimates indicates the high priority of obtaining theoretical predictions for $c\overline{c}/b\overline{b}$ that are as precise as possible. Overall, precision h^0 measurements at $\sqrt{s} = 500$ GeV with $L = 200$ fb^{-1} appear to have a good chance of probing the heavier Higgs mass scale (which is related to important SUSY-breaking parameters) even when the heavier Higgs bosons can not be (pair) produced without going to higher energy.

We now consider the $WW^\star$ mode, which would be relevant for a SM-like Higgs with mass above 130 GeV. Both $h_{\rm SM}$ production via WW fusion, $e^+e^- \to \nu\overline{\nu}h_{\rm SM}$, and $Zh_{\rm SM}$ production followed by $h_{\rm SM}$ decay into $WW^\star$ for heavier Higgs masses were simulated [27]. For $m_{h_{\rm SM}} = 150$ GeV, the cross-sections for these two production modes are roughly equal and it is advantageous to use both for more statistics. We shall see [26] that the measurement of $\sigma(WW \to h_{\rm SM})BR(h_{\rm SM} \to WW^\star)$ allows a direct probe of the $(WWh_{\rm SM})^2$ coupling and a determination of the total $h_{\rm SM}$ width. For the 2nd ratio of Eq. (1), it will also be important to compare rates for the $\nu\overline{\nu}b\overline{b}$ and $\nu\overline{\nu}WW^\star$ final states and rates for the $Zb\overline{b}$ and $ZWW^\star$ final states.

[10]Gluon splitting to heavy quarks is included in the Monte Carlo; at LEP energies the probabilities for $g \to c\overline{c}$ and $g \to b\overline{b}$ are of order 2.5% and 0.5%, respectively.

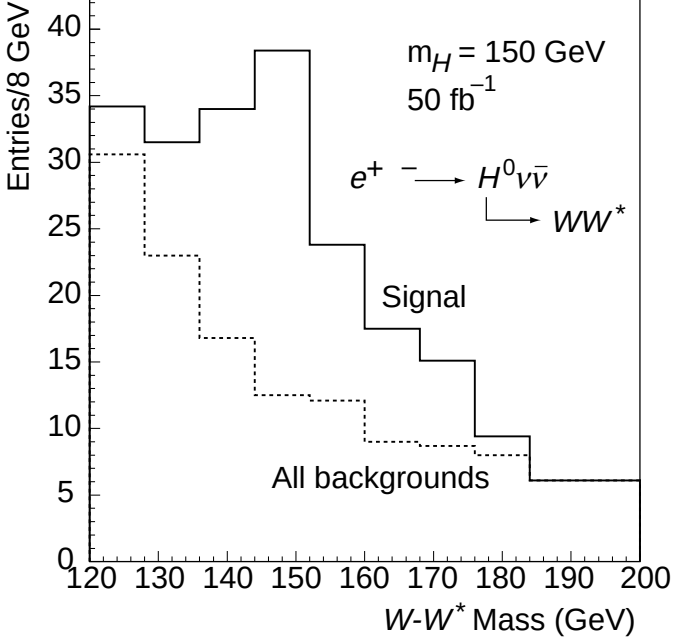

Figure 4: Signal and background rates for $L = 50$ fb^{-1} at $\sqrt{s} = 500$ GeV for $e^+e^- \to \nu\overline{\nu}WW^\star$ as a function of $WW^\star$ mass, taking $m_{h_{\rm SM}} = 150$ GeV.

For the case of $Zh_{\rm SM}$ production followed by $h_{\rm SM}$ decay into $WW^\star$, two topologies were examined: the first is the final state containing six jets — two from hadronic decay of the Z and two jets from each of the W bosons; the second final state considered is that with two leptons from the Z and four jets from the $WW^\star$. Simulations were performed at $\sqrt{s} = 500$ GeV assuming the performance of the NLC detector [24] at the smeared four-vector level, a signal with $m_{h_{\rm SM}} = 130 - 170$ GeV, and considering the known Standard Model backgrounds. After cuts demanding large visible energy, and that the event be well contained, a kinematic constrained fit was performed taking into account E_{cm}, m_Z, and one on-shell m_W after assigning the Z mass to the quark or lepton pair with invariant mass closest to and within 8 GeV of m_Z. Requiring the fit probability to be greater than 10% greatly reduced the background from WW, $t\bar{t}$ and light quarks. The purity is then enhanced further by employing the previously described topological quark tags as anti-tags on the jets assigned to the W bosons, i.e. requiring the jets fail the b and c topological tags. As an example, in $L = 50$ fb^{-1} of data with $m_{h_{\rm SM}} = 150$ GeV, 65 signal events survive on a background of 21 events, of which only 4.2 are from Higgs decays into heavy quarks and gluons. Extrapolating to $L = 200$ fb^{-1}, $S = 260$ with $B = 84$ implies $\sqrt{S+B}/S = 0.07$ for the indicated mass. The situation deteriorates considerably for $m_{h_{\rm SM}} = 130$ GeV with $S/B \approx 1.0$. For $L = 200$ fb^{-1} the statistical accuracy with which $\sigma(Zh_{\rm SM})BR(h_{\rm SM} \to WW^\star)$ can be measured is about

For $m_{h_{\rm SM}}$ above 150 GeV, the accuracy of the measurement improves over the $m_{h_{\rm SM}} = 150\,{\rm GeV}$ result, falling to a low of about $\pm 6\%$ at $m_{h_{\rm SM}} = 170\,{\rm GeV}$.

Of course, as the $WW^\star$ mode gets stronger, the $b\bar{b}$ mode weakens, see Table I. Thus, the $Zh_{\rm SM} \to Zb\bar{b}$ rate is measured with progressively poorer accuracy as $m_{h_{\rm SM}}$ increases. At $m_{h_{\rm SM}} \sim 150\,{\rm GeV}$, for example, we [26] estimate that the earlier $m_{h_{\rm SM}} \sim 110\,{\rm GeV}$ errors for $\sigma(Zh_{\rm SM})BR(h_{\rm SM} \to b\bar{b})$ will have increased by about a factor of two to $\sim \pm 6\%$, rising rapidly to $\sim \pm 28\%$ at $m_{h_{\rm SM}} = 170\,{\rm GeV}$. Combining [26] the $WW^\star$ and $b\bar{b}$ mode errors in the $Zh_{\rm SM}$ production mode, we find errors for $BR(h_{\rm SM} \to WW^\star)/BR(h_{\rm SM} \to b\bar{b})$ of roughly $\pm 22\%$, $\pm 11\%$, $\pm 9\%$ and $\sim \pm 28\%$ at $m_{h_{\rm SM}} = 130$, 140, 150 and 170 GeV, respectively.

For the case of $h_{\rm SM}$ production via WW fusion followed by the Higgs decaying into $WW^\star$, the final state is $\nu\bar{\nu}WW^\star$. Cuts are made demanding visible energy less than $0.5E_{cm}$, large missing mass, no isolated leptons, large missing transverse momentum, a large acoplanarity angle between the reconstructed W axes, and that the missing momentum vector does not point in the forward direction. These cuts reduce the dangerous $eeWW$, $\nu\bar{\nu}WW$, and $e\nu WZ$ backgrounds. The event is forced to be reconstructed into four jets, with two required to have invariant mass close to the W mass and the remaining two jets to have invariant mass well below the W mass (from the $W^\star$). The heavy quark topological tag is then again used as an anti-tag to increase the purity in the W sample. The visible mass of the entire event is then examined for peaking at the Higgs mass. A huge peak results at lower masses due to $e\nu W$ and $Z\nu\bar{\nu}$.

A typical result is that of Fig. 4 for $m_{h_{\rm SM}} = 150\,{\rm GeV}$, where $L = 50\ {\rm fb}^{-1}$ is assumed. In general, the statistical accuracy with which $\sigma(\nu\bar{\nu}h_{\rm SM})BR(h_{\rm SM} \to WW^\star)$ can be measured is estimated [26] to be very similar to that found for $\sigma(Zh_{\rm SM})BR(h_{\rm SM} \to WW^\star)$ above: for $L = 200\ {\rm fb}^{-1}$ the rough errors for the former are $\pm 22\%$, $\pm 10\%$, $\pm 8\%$ and $\pm 7\%$ for $m_{h_{\rm SM}} = 130$, 140, 150 and 170 GeV, respectively. At these same masses, the corresponding accuracy for $\sigma(\nu\bar{\nu}h_{\rm SM})BR(h_{\rm SM} \to b\bar{b})$ is $\sim \pm 3\%$, $\sim \pm 4\%$, $\sim \pm 7\%$ and $\gtrsim \pm 33\%$, respectively. At $m_{h_{\rm SM}} = 150\,{\rm GeV}$, the $WW^\star$ branching ratio is still more difficult to measure than $b\bar{b}$ because of the larger background and lower efficiency for isolating the final state. However, by $m_{h_{\rm SM}} = 170\,{\rm GeV}$ the $b\bar{b}$ branching ratio has become so small that errors in this channel rapidly increase. The above errors imply $\nu\bar{\nu}h_{\rm SM}$ channel errors for $BR(h_{\rm SM} \to WW^\star)/BR(h_{\rm SM} \to b\bar{b})$ of $\sim \pm 22\%$, $\sim \pm 11\%$, $\sim \pm 10\%$ or $\gtrsim \pm 33\%$ at $m_{h_{\rm SM}} = 130$, 140, 150 or 170 GeV, respectively.

Combining [26] the $Zh_{\rm SM}$ and $\nu\bar{\nu}h_{\rm SM}$ channel results, we obtain accuracies for $BR(WW^\star)/BR(b\bar{b})$ of roughly $\pm 16\%$, $\pm 8\%$ and $\pm 7\%$ for $WW^\star/b\bar{b}$ for $m_{h_{\rm SM}} = 130$, 140 and 150 GeV. At $m_{h_{\rm SM}} = 120\,{\rm GeV}$ and 170 GeV, we [26] estimate the errors to be $\sim \pm 23\%$ and $\sim \pm 21\%$, respectively. (We have not pursued the degree to which these errors would be further reduced by including the $e^+e^-h_{\rm SM}$ channel determination of this ratio.) Fig. 2 (which is fairly independent of parameter region) implies that a $\lesssim 10\%$ error, as achieved for $m_{h_{\rm SM}}$ in the $140 - 150\,{\rm GeV}$ mass range, would be a very useful level of accuracy in the MSSM should stop quark masses (contrary to expectations based on naturalness) be sufficiently above 1 TeV to make $m_{h^0} = 140 - 150\,{\rm GeV}$ possible. In the NMSSM, where the lightest higgs (denoted h_1) can have mass $m_{h_1} \sim 140 - 150\,{\rm GeV}$ and the second lightest (h_2) often has mass in the $m_{h_2} \sim 150 - 190\,{\rm GeV}$ range, even if stop masses are substantially below 1 TeV, deviations from SM expectations are typically even larger. This exemplifies the fact that the $WW^\star/b\bar{b}$ ratio will provide an extremely important probe of a non-minimal Higgs sector when both the $WW^\star$ and $b\bar{b}$ decays have significant branching ratio.

The NLC errors for the $(c\bar{c}h_{\rm SM})^2/(b\bar{b}h_{\rm SM})^2$ and $(WW^\star h_{\rm SM})^2/(b\bar{b}h_{\rm SM})^2$ coupling-squared ratios outlined above for $L = 200\ {\rm fb}^{-1}$ at $\sqrt{s} = 500\,{\rm GeV}$ are repeated in the NLC summary table, Table X.

2. Measuring $\sigma(\mu^+\mu^- \to h_{\rm SM})BR(h_{\rm SM} \to b\bar{b}, WW^\star, ZZ^\star)$ in s-channel FMC production

Table IX: Summary of approximate errors for $\sigma(\mu^+\mu^- \to h_{\rm SM})BR(h_{\rm SM} \to b\bar{b}, WW^\star, ZZ^\star)$, assuming $L = 50\ {\rm fb}^{-1}$ devoted to $\sqrt{s} = m_{h_{\rm SM}}$ and beam energy resolution of $R = 0.01\%$.

Channel	Errors				
$\mathbf{m_{h_{SM}}}$**(GeV)**	**80**	**90**	**100**	**110**	**120**
$b\bar{b}$	$\pm 0.2\%$	$\pm 1.6\%$	$\pm 0.4\%$	$\pm 0.3\%$	$\pm 0.3\%$
$WW^\star$	–	–	$\pm 3.5\%$	$\pm 1.5\%$	$\pm 0.9\%$
$ZZ^\star$	–	–	–	$\pm 34\%$	$\pm 6.2\%$
$\mathbf{m_{h_{SM}}}$**(GeV)**	**130**	**140**	**150**	**160**	**170**
$b\bar{b}$	$\pm 0.3\%$	$\pm 0.5\%$	$\pm 1.1\%$	$\pm 59\%$	–
$WW^\star$	$\pm 0.7\%$	$\pm 0.5\%$	$\pm 0.5\%$	$\pm 1.1\%$	$\pm 9.4\%$
$ZZ^\star$	$\pm 2.8\%$	$\pm 2.0\%$	$\pm 2.1\%$	$\pm 22\%$	$\pm 34\%$
$\mathbf{m_{h_{SM}}}$**(GeV)**	**180**	**190**	**200**	**210**	**220**
$WW^\star$	$\pm 18\%$	$\pm 38\%$	$\pm 58\%$	$\pm 79\%$	–
$ZZ^\star$	$\pm 25\%$	$\pm 27\%$	$\pm 35\%$	$\pm 45\%$	$\pm 56\%$

The accuracies expected for these measurements were determined in Ref. [3] under the assumption that the relevant detector challenges associated with detecting and tagging final states in the potentially harsh FMC environment can be met. As explained in the introduction to this section, if $L = 200\ {\rm fb}^{-1}$ is used so as to optimize the Higgs peak scan determination of $\Gamma^{\rm tot}_{h_{\rm SM}}$, then the equivalent $\sqrt{s} = m_{h_{\rm SM}}$ Higgs peak luminosity accumulated for measuring $\sigma(\mu^+\mu^- \to h_{\rm SM})BR(h_{\rm SM} \to X)$ in various channels is of order $L = 50\ {\rm fb}^{-1}$. The associated errors expected for $\sigma(\mu^+\mu^- \to h_{\rm SM})BR(h_{\rm SM} \to b\bar{b}, WW^\star, ZZ^\star)$ are summarized as a function of $m_{h_{\rm SM}}$ in Table IX. As is apparent from the table, the errors are remarkably small for $m_{h_{\rm SM}} \lesssim 150\,{\rm GeV}$. As already stated, detector performance in the FMC environment will be critical to whether

ample, to achieve the good b-tagging efficiencies and purities employed in obtaining the NLC detector errors given in this report, a relatively clean environment is required and it must be possible to get as close as 1.5 cm to the beam. FMC detectors discussed to date do not allow for instrumentation this close to the beam. More generally, in all the channels it is quite possible that the FMC errors will in practice be at least in the few per cent range. This, however, would still constitute an extremely valuable level of precision.

For later purposes, it is important to understand the relation between $\sigma(\mu^+\mu^- \to h_{\rm SM})$ and the $\Gamma(h_{\rm SM} \to \mu^+\mu^-)$ partial width (which is directly proportional to the $(\mu^+\mu^- h_{\rm SM})^2$ coupling-squared). Very generally, the average cross section for production of any Higgs boson in the s-channel, $\overline{\sigma}_h$, is obtained by convoluting the standard Breit-Wigner shape for the Higgs resonance with a Gaussian distribution in $\sqrt{s}$ of width $\sigma_{\sqrt{s}}$. For a distribution centered at $\sqrt{s} = m_h$, $\overline{\sigma}_h$ is given by $\overline{\sigma}_h \sim 4\pi m_h^{-2} BR(h \to \mu^+\mu^-)$ if $\sigma_{\sqrt{s}} \ll \Gamma_h$ and by $\overline{\sigma}_h \sim 2\pi^2 m_h^{-2}\Gamma(h \to \mu^+\mu^-)/(\sqrt{2\pi}\sigma_{\sqrt{s}})$ if $\sigma_{\sqrt{s}} \gg \Gamma_h$. To get near maximal $\overline{\sigma}_h$ and to have sensitivity to Γ_h via scanning in $\sqrt{s}$ (see later subsection) it is important that $\sigma_{\sqrt{s}}$ be no larger than $2-3\times\Gamma_h$. Fig. 1 shows that $\Gamma_h < 1-10\,$MeV is typical of the $h_{\rm SM}$ for $m_{h_{\rm SM}} \lesssim 140\,$GeV. Using the parameterization $\sigma_{\sqrt{s}} \simeq 7\,{\rm MeV}\left(\frac{R}{0.01\%}\right)\left(\frac{\sqrt{s}}{100\,{\rm GeV}}\right)$ for $\sigma_{\sqrt{s}}$ in terms of the beam energy resolution, R, we see that very excellent resolution $R \sim 0.01\%$ typically yields $\sigma_{\sqrt{s}} \sim 2-3\times\Gamma^{\rm tot}_{h_{\rm SM}}$ when $m_{h_{\rm SM}} \lesssim 140\,$GeV. In this mass region, $\overline{\sigma}_{h_{\rm SM}}$ is then roughly proportional to $\Gamma(h_{\rm SM} \to \mu^+\mu^-)/\sigma_{\sqrt{s}}$ with small corrections sensitive to Γ_h. Thus, a measurement of $\overline{\sigma}_{h_{\rm SM}} BR(hsm \to X)$ in the $m_{h_{\rm SM}} \lesssim 140\,$GeV mass region can be readily converted to a determination of $\Gamma(h_{\rm SM} \to \mu^+\mu^-)BR(h_{\rm SM} \to X)$ provided that $\Gamma^{\rm tot}_{h_{\rm SM}}$ is measured with good accuracy (given that $\sigma_{\sqrt{s}}$ will be accurately known). As reviewed in a later subsection, one finds that (with $R = 0.01\%$) very good precision for $\Gamma^{\rm tot}_{h_{\rm SM}}$ is possible in $\mu^+\mu^- \to h_{\rm SM}$ collisions by employing a simple scan of the Higgs resonance peak.

D. Measuring $\sigma BR(h_{\rm SM} \to \gamma\gamma)$ at the NLC [28]

We will later review why a determination of $BR(h_{\rm SM} \to \gamma\gamma)$ is the only means for extracting $\Gamma^{\rm tot}_{h_{\rm SM}}$ in the $m_{h_{\rm SM}} \lesssim 130\,$GeV mass range. Of course, $BR(h_{\rm SM} \to \gamma\gamma)$ and especially $\Gamma(h_{\rm SM} \to \gamma\gamma)$ are of special interest themselves in that the $\gamma\gamma h_{\rm SM}$ coupling is sensitive to one-loop graphs involving arbitrarily heavy states (that get their mass from the $h_{\rm SM}$ sector vev — to be contrasted with, for example, heavy SUSY partner states which decouple since they get mass from explicit SUSY breaking).

At the NLC, the only means of getting at $BR(h_{\rm SM} \to \gamma\gamma)$ is to first measure $\sigma BR(h_{\rm SM} \to \gamma\gamma)$ in all accessible production modes, and then divide out by the σ's as computed using other data. One finds that the errors in the σ's are small so that the net error for $BR(h_{\rm SM} \to \gamma\gamma)$ is essentially that obtained by combining the statistical errors for the available σBR measurements. The $\sigma BR(h_{\rm SM} \to \gamma\gamma)$ errors have been studied Ref. [28]. The error for $\sigma(Zh_{\rm SM})BR(h_{\rm SM} \to \gamma\gamma)$ is minimized for a given total luminosity L by running at a $\sqrt{s}$ value that is near the maximum of the $Zh_{\rm SM}$ cross section, roughly $\sqrt{s} \sim m_{h_{\rm SM}} + m_Z +$ a few GeV; precise optimal $\sqrt{s}_{\rm opt}$ values are given in Ref. [28]. The error for $\sigma(\nu\overline{\nu}h_{\rm SM})BR(h_{\rm SM} \to \gamma\gamma)$ at given L is minimized by operating at the highest available $\sqrt{s}$; this maximizes the WW-fusion cross section. The errors in $\sigma(Zh_{\rm SM})BR(h_{\rm SM} \to \gamma\gamma)$ for $L = 200\ {\rm fb}^{-1}$ accumulated at $\sqrt{s} = \sqrt{s}_{\rm opt}$ and in $\sigma(\nu\overline{\nu}h_{\rm SM})BR(h_{\rm SM} \to \gamma\gamma)$ for $L = 200\ {\rm fb}^{-1}$ accumulated at $\sqrt{s} = 500\,{\rm GeV}$ are plotted as a function of $m_{h_{\rm SM}}$ in the first two windows of Fig. 5. The effective $\sigma BR(h_{\rm SM} \to \gamma\gamma)$ error obtained by combining the statistics for the $Zh_{\rm SM}$ and WW-fusion modes assuming $L = 200\ {\rm fb}^{-1}$ is accumulated at $\sqrt{s} = 500\,{\rm GeV}$ is plotted in the third window of Fig. 5. The effective $\sigma BR(h_{\rm SM} \to \gamma\gamma)$ error for $L = 200\ {\rm fb}^{-1}$ at $\sqrt{s} = \sqrt{s}_{\rm opt}$ is essentially the same as for the $Zh_{\rm SM}$ mode alone, the WW-fusion contribution to the statistics being unimportant at these low $\sqrt{s}$ values.

Results are presented for four different electromagnetic calorimeter resolutions: I corresponds to the very excellent resolution of the CMS calorimeter [10]. II and III are somewhat optimistic limits of the resolutions currently planned for the NLC detectors [24]; and IV is the resolution planned for the JLC detector [29]. (For details and references, see Ref. [28].)

It is important to compare the $\sigma BR(h_{\rm SM} \to \gamma\gamma)$ error found using the $Zh_{\rm SM}$ mode statistics for $L = 200\ {\rm fb}^{-1}$ at $\sqrt{s} = \sqrt{s}_{\rm opt}$ to the error found by combining WW-fusion and $Zh_{\rm SM}$ statistics for $L = 200\ {\rm fb}^{-1}$ at $\sqrt{s} = 500\,{\rm GeV}$ (window 1 vs. window 3 of Fig. 5). We find that in resolution cases II-IV (I) the $Zh_{\rm SM}$, $\sqrt{s} = \sqrt{s}_{\rm opt}$ measurement yields smaller errors for $70 \lesssim m_{h_{\rm SM}} \lesssim 100\,{\rm GeV}$ ($70 \lesssim m_{h_{\rm SM}} \lesssim 120\,{\rm GeV}$). The $Zh_{\rm SM}$ mode at $\sqrt{s} = \sqrt{s}_{\rm opt}$ is most superior to the combined WW-fusion plus $Zh_{\rm SM}$, $\sqrt{s} = 500\,{\rm GeV}$ error if $m_{h_{\rm SM}} = 70\,{\rm GeV}$: for excellent calorimeter resolution case I ('standard' resolution cases II/III), $Zh_{\rm SM}$ at $\sqrt{s} = \sqrt{s}_{\rm opt}$ yields an error of $\pm 27\%$ ($\pm 40\%$) vs. combined WW-fusion plus $Zh_{\rm SM}$, $\sqrt{s} = 500\,{\rm GeV}$ error of $\pm 40\%$ ($\pm 53\%$). However, the above $Zh_{\rm SM}|_{\sqrt{s}=\sqrt{s}_{\rm opt}}$ advantage would be lost if the instantaneous luminosity ($\mathcal{L}$) at $\sqrt{s}_{\rm opt} \sim 165\,{\rm GeV}$ is more than a factor of 2.2 (1.8) below that at $\sqrt{s} = 500\,{\rm GeV}$ in resolution case I (cases II/III). If the interaction region is designed for maximal $\mathcal{L}$ at $\sqrt{s} = 500\,{\rm GeV}$, $\mathcal{L}$ at $\sqrt{s} = \sqrt{s}_{\rm opt}$ would decrease by an even larger factor since $\mathcal{L} \propto (\sqrt{s}/500\,{\rm GeV})^2$ [30] as the energy is lowered; for any $m_{h_{\rm SM}}$ the best results would be obtained by running at $\sqrt{s} = 500\,{\rm GeV}$. Although it would not be all that expensive to build new quads *etc.* suited to a lower $\sqrt{s}$ [30], any significant associated loss in running time would quickly offset the potential benefits. Further, lower energy operation might decrease sensitivity to other types of new physics. If $m_{h_{\rm SM}}$ is known ahead of time (from LEP2 or LHC) to be below 100 GeV (120 GeV) or so, for which focusing on $Zh_{\rm SM}$ production at $\sqrt{s} = \sqrt{s}_{\rm opt}$ would be appropriate in resolution cases II-IV (I), then an interaction region with maximal $\mathcal{L}$ at $\sqrt{s} = \sqrt{s}_{\rm opt}$ could be included in the design from the beginning.

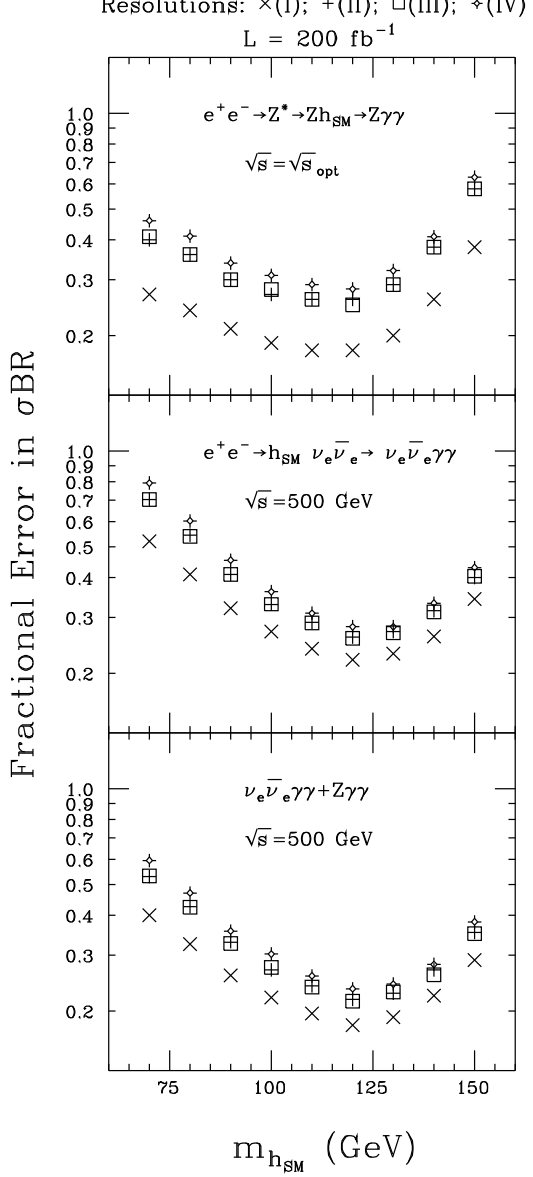

Figure 5: The fractional error in the measurement of $\sigma(\nu_e\bar{\nu}_e h_{\rm SM})BR(h_{\rm SM}\to\gamma\gamma)$ [$\sigma(Zh_{\rm SM})BR(h_{\rm SM}\to\gamma\gamma)$] as a function of $m_{h_{\rm SM}}$ assuming $L=200$ fb^{-1} is accumulated at $\sqrt{s}=500\,{\rm GeV}$ [$\sqrt{s}=\sqrt{s}_{\rm opt}$]. Also shown is the fractional $\sigma BR(h_{\rm SM}\to\gamma\gamma)$ error obtained by combining $Zh_{\rm SM}$ and $\nu_e\overline{\nu}_e h_{\rm SM}$ channels for $L=200$ fb^{-1} at $\sqrt{s}=500\,{\rm GeV}$. Results for the four electromagnetic calorimeter resolutions described in the text are given.

Clearly, the most likely situation is that $L=200$ fb^{-1} is accumulated at $\sqrt{s}=500\,{\rm GeV}$ and that the calorimeter is at the optimistic end of current plans for the NLC detector (cases II and III). After combining the statistics for the WW-fusion and $Zh_{\rm SM}$ modes, the errors in $\sigma BR(h_{\rm SM}\to\gamma\gamma)$ range from $\sim\pm22\%$ at $m_{h_{\rm SM}}=120\,{\rm GeV}$ to $\sim\pm35\%$ ($\sim\pm53\%$) at $m_{h_{\rm SM}}=$ region, the errors are smallest and lie in the $\pm22\%-\pm27\%$ range.

We note that it is also possible to consider measuring $\sigma BR(h_{\rm SM}\to\gamma\gamma)$ in the $e^+e^-\to e^+e^-h_{\rm SM}$ (ZZ-fusion) production mode. A study of this case [31] shows, however, that the errors will be much worse than found for either $Zh_{\rm SM}$ production or WW-fusion production. For instance, compared to the $Zh_{\rm SM}$ channel, where all Z decay modes can be included, [11] the $e^+e^-h_{\rm SM}$ rate with $M_{e^+e^-}\not\sim m_Z$ is substantially smaller.

Let us now turn to the errors that can be expected for the coupling-squared ratio $(\gamma\gamma h_{\rm SM})^2/(b\bar{b}h_{\rm SM})^2$. We have already tabulated in Tables III and IV the errors expected from LHC data for $m_{h_{\rm SM}}\le 130\,{\rm GeV}$; the LHC error varies from $\pm17\%$ to $\pm25\%$ as $m_{h_{\rm SM}}$ goes from 90 GeV to 130 GeV. Above $m_{h_{\rm SM}}=130\,{\rm GeV}$, the LHC error for the ratio is expected to be quite large. At the NLC, $(\gamma\gamma h_{\rm SM})^2/(b\bar{b}h_{\rm SM})^2$ can be computed in the $Zh_{\rm SM}$ and WW-fusion production modes (treated separately) as $\sigma BR(h_{\rm SM}\to\gamma\gamma)/\sigma BR(h_{\rm SM}\to b\bar{b})$; the numerator and denominator in this latter ratio can be obtained (assuming reasonable knowledge of efficiencies) from measured event rates. We will presume that all NLC measurements are performed by accumulating $L=200$ fb^{-1} at $\sqrt{s}=500\,{\rm GeV}$. The $L=200$ fb^{-1}, $\sqrt{s}=500\,{\rm GeV}$ errors for the denominator in the $Zh_{\rm SM}$ and WW-fusion production modes have been given in the previous section. The WW-fusion numerator errors are those given in the 2nd window of Fig. 5. The $Zh_{\rm SM}$ numerator errors have not been separately plotted, but are those implicit in the 3rd window of Fig. 5. The $Zh_{\rm SM}$ and WW-fusion determinations of $(\gamma\gamma h_{\rm SM})^2/(b\bar{b}h_{\rm SM})^2$ are statistically independent and can be combined to get a net error. The resulting net NLC-only error is not terribly good; at $m_{h_{\rm SM}}=80$, 100, 110, 120, 130, 140, 150 GeV the errors for $(\gamma\gamma h_{\rm SM})^2/(b\bar{b}h_{\rm SM})^2$ are $\pm42\%$, $\pm27\%$, $\pm24\%$, $\pm22\%$, $\pm23\%$, $\pm26\%$, $\pm35\%$, respectively. For the lower $m_{h_{\rm SM}}$ values the LHC does better. If we combine the LHC and NLC measurements, the errors for $(\gamma\gamma h_{\rm SM})^2/(b\bar{b}h_{\rm SM})^2$ at the above $m_{h_{\rm SM}}$ values are $\pm16\%$, $\pm14\%$, $\pm15\%$, $\pm16\%$, $\pm17\%$, $\pm26\%$, $\pm35\%$, respectively. The NLC-only errors are repeated later in the NLC summary table, Table X.

Finally, we note that in later discussions we show that the large errors for the $\gamma\gamma$ final state will dominate in computing some important quantities that potentially allow discrimination between the SM Higgs boson and a SM-like Higgs boson of an extended model.

E. Determining the $ZZh_{\rm SM}$ coupling at the NLC

Determination of the $(ZZh_{\rm SM})^2$ coupling-squared is possible in two modes. These are (using e^+e^- collision notation):

- $e^+e^-\to Zh_{\rm SM}$, where $Z\to\ell^+\ell^-$ ($\ell=e,\mu$);
- $e^+e^-\to e^+e^-h_{\rm SM}$ (via ZZ-fusion) [25].

[11] This is possible since we can constrain the recoil mass, constructed from $\sqrt{s}$ and the momenta of the two photons from $h_{\rm SM}\to\gamma\gamma$ decay, to be close to m_Z.

nary. It is convenient to separate $Zh_{\rm SM}$ and ZZ-fusion for the purposes of discussion even though in the $e^+e^-h_{\rm SM}$ final state there is some interference between the ZZ-fusion and $Zh_{\rm SM}$ diagrams. Experimentally this separation is easily accomplished by an appropriate cut on the e^+e^- pair mass.[12]

In both cases, the $h_{\rm SM}$ is inclusively isolated by examining the recoil mass spectrum computed using the incoming e^+e^- momentum and the momenta of the outgoing leptons. In the $Zh_{\rm SM}$ case, only $\ell = e, \mu$ in the Z decay are considered (τ's and jets are excluded) since it is essential that the recoil mass peak be as narrow as possible in order that only a small mass window need be kept, thereby making backgrounds very small. Clearly, excellent momentum resolution for electrons and muons will be essential, especially for Higgs masses in the vicinity of m_Z.[13]

Exactly how good the momentum resolution should be in order to eliminate backgrounds is an important question; it is currently being pursued. The study of Ref. [32] obtains good results in the $Zh_{\rm SM}$ case only if the "super" performance of the JLC-I detector [29] is assumed. Current generic NLC detector designs will not be quite so good, but appear to be adequate. As an example, using four-vectors smeared according to the performance of a typical NLC detector [24], the recoil mass resolution using electrons and muons has been found [33] to be approximately 3.5 GeV as shown in Fig. 6(a) where a reasonable mass window results in about 20% background for $m_{h_{\rm SM}} = 130\,{\rm GeV}$ and obviously degrading for smaller masses and improving for higher masses. (As described later, running at $\sqrt{s} \sim 300\,{\rm GeV}$, *i.e.* well below $\sqrt{s} = 500\,{\rm GeV}$, is critical for such good recoil mass resolution.) It is interesting to note that the current performance goals of this detector give a similar mass resolution of 3.9 GeV from the invariant jet-jet mass of tagged b-quark jets following kinematically-constrained fitting – indicating a good match of momentum and energy resolution. Our error estimates below will assume momentum resolution such that the recoil mass peak is sufficiently narrow that backgrounds are small and can be neglected in the limit of large luminosity. Preliminary results for the backgrounds are at the $B \sim 0.2S$ level, for which the errors computed below with $B = 0$ would be only slightly increased. Since, as we shall see, the recoil mass peak cross section errors sometimes dominate the errors in extracting branching ratios, it is quite crucial that the final detector design be adequate to achieve a small background under the recoil mass peak.

The relative value of the two production modes depends upon many factors, but in particular it depends on how the available instantaneous luminosity varies with $\sqrt{s}$. For an interaction region configuration/design optimized for maximal luminosity at

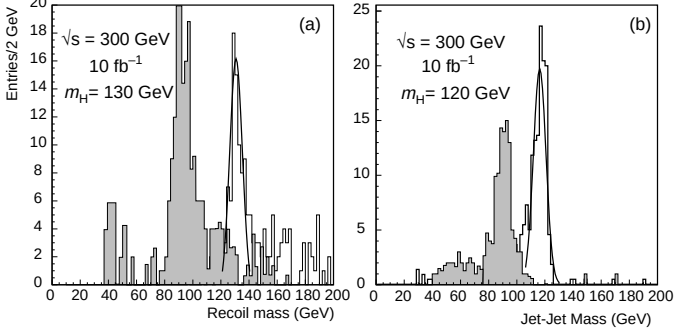

Figure 6: Higgs mass resolution determined using a typical NLC detector [24] using (a) the recoil mass against a pair of electrons or muons from Z decay and (b) from the jet-jet invariant mass of tagged b-quark jets after kinematically-constrained fitting.

$\sqrt{s_0}$, $\mathcal{L}$ falls as $[\sqrt{s}/\sqrt{s_0}]^2$ [30] as one moves to energies lower than $\sqrt{s_0}$. This is an issue since $\sigma(Zh_{\rm SM})$ is maximal at $\sqrt{s} \sim m_Z + m_{h_{\rm SM}} + 10$ or 20 GeV, whereas $\sigma(e^+e^-h_{\rm SM})$ increases monotonically with energy. For the moment, let us assume that the final focus is designed to maximize $\mathcal{L}$ at $\sqrt{s} = 500\,{\rm GeV}$. In Fig. 7, we plot $\sigma(Zh_{\rm SM})BR(Z \to \ell^-\ell^+)$ ($\ell = e, \mu$, no cuts) and $\sigma(e^+e^-h_{\rm SM})$ (with a $\theta > 10^\circ$ cut[14] on the angles of the final state e^+ and e^-) as a function of $m_{h_{\rm SM}}$ for $\sqrt{s} = 500\,{\rm GeV}$. We observe a cross-over such that, for $m_{h_{\rm SM}} \lesssim 200\,{\rm GeV}$, a higher raw event rate for the recoil spectrum is obtained using ZZ fusion.

For an integrated luminosity of $L = 200\ {\rm fb}^{-1}$ and an overall efficiency of 30% for the cuts required to make the background small, the error $1/\sqrt{S}$ in the $\sigma(Zh_{\rm SM})BR(Z \to \ell^-\ell^+)$ ($\ell = e, \mu$) measurement would range from 6.5% to 8% as $m_{h_{\rm SM}}$ ranges from 60 to 200 GeV, growing to 11% by $m_{h_{\rm SM}} = 300\,{\rm GeV}$. Errors in this measurement of similar magnitude can also be achieved for $L \sim 30 - 50\ {\rm fb}^{-1}$ if $\sqrt{s}$ is adjusted to be near the value for which $\sigma(Zh_{\rm SM})$ is maximal [32]. However, depending upon $m_{h_{\rm SM}}$, accumulating this much L at lower energy often takes more than the ~ 4 years required for $L = 200\ {\rm fb}^{-1}$ at $\sqrt{s} = 500\,{\rm GeV}$ unless the final focus is optimized for the lower $\sqrt{s}$ value. For the $\sigma(e^+e^-h_{\rm SM})$ measurement, assuming cut efficiency of 40% relative to the cross section plotted in Fig. 7 (we have already included the $\theta > 10^\circ$ calorimetry cut) and $L = 200\ {\rm fb}^{-1}$, we find errors that range from 4% to 8% to 14% as $m_{h_{\rm SM}}$ goes from 60 to 200 to 300 GeV. Combining [26, 25] the $\sqrt{s} = 500\,{\rm GeV}$ errors for the two processes gives an error on the $(ZZh_{\rm SM})^2$ coupling-squared that ranges from $\sim 3\%$ to $\sim 6\%$ to $\sim 9\%$ for $m_{h_{\rm SM}} = 60$, 200, and 300 GeV, respectively. These errors are at least as good as those found for $L = 200\ {\rm fb}^{-1}$ using the

[12] Whenever ZZ-fusion dominates the $Z^\star$ diagrams, such a cut requiring $M_{e^+e^-} \not\sim m_Z$ usually improves $S/\sqrt{B}$ and reduces the $\sqrt{S+B}/S$ error.

[13] In order to inclusively sum over all $h_{\rm SM}$ decays, it is important to avoid making any use of $h_{\rm SM}$ decay products in reconstructing the Higgs mass peak. Thus, a 4-C fit using the energies and angles of the jets from Higgs decay and leptons from Z decay should not be employed; kinematic fits (involving fewer than 4 constraints) considering the leptons from Z decay and the knowledge of $E_{\rm cm}$ could however still be employed. In any case, such fits yield a jet-jet mass resolution that is no better than (worse than) that for the recoil mass for NLC (super-JLC) momentum resolution.

[14] Assuming coverage down to such angles is optimistic, but not unrealistic. In particular, it may be possible to employ a pixel vertexing device with a first layer at radius of ~ 1.5 cm followed by next-generation tracking devices to avoid the superconducting quads inside the detector.

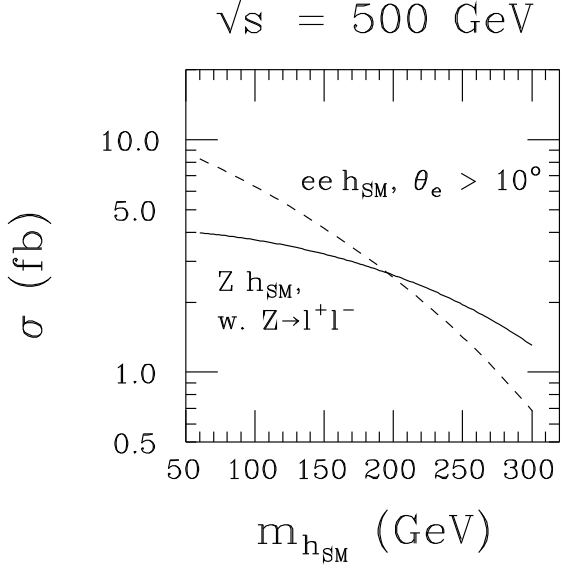

Figure 7: $\sigma(Zh_{\rm SM})BR(Z \to \ell^-\ell^+)$ ($\ell = e, \mu$, no cuts) and $\sigma(e^+e^-h_{\rm SM})$ (with a cut of $\theta > 10^\circ$ on the e^+ and e^- in the final state) as a function of $m_{h_{\rm SM}}$ for $\sqrt{s} = 500\,{\rm GeV}$. From Ref. [25].

$Zh_{\rm SM}$ mode alone at the optimal $\sqrt{s}$. Thus, for determining the $(ZZh_{\rm SM})^2$ coupling-squared via the recoil mass procedure there does not appear to be any advantage to lowering the machine energy even if the final focus *etc.* is reconfigured so as to maintain the same instantaneous luminosity.

F. Determining $h_{\rm SM}$ branching ratios and the $WWh_{\rm SM}$ coupling at the NLC

A determination of $BR(h_{\rm SM} \to X)$ requires measuring $\sigma(h_{\rm SM})BR(h_{\rm SM} \to X)$ and $\sigma(h_{\rm SM})$ for some particular production mode, and then computing

$$BR(h_{\rm SM} \to X) = \frac{\sigma(h_{\rm SM})BR(h_{\rm SM} \to X)}{\sigma(h_{\rm SM})}\,. \qquad (2)$$

In e^+e^- collisions, the $e^+e^- \to Zh_{\rm SM}$ and $e^+e^- \to e^+e^-h_{\rm SM}$ (ZZ-fusion) modes just discussed are the only ones for which the absolute magnitude of $\sigma(h_{\rm SM})$ can be measured, inclusively summing over all final states X. The WW-fusion $e^+e^- \to \nu\overline{\nu}h_{\rm SM}$ cross section must be determined by the procedure of first measuring $\sigma BR(h_{\rm SM} \to X)$ in some mode X and then dividing by $BR(h_{\rm SM} \to X)$ as determined from the ZZ-fusion or $Zh_{\rm SM}$ channels.

1. $BR(h_{\rm SM} \to b\overline{b})$ and $BR(h_{\rm SM} \to c\overline{c})$

By running at $\sqrt{s} = 500\,{\rm GeV}$ and accumulating $L = 200\ {\rm fb}^{-1}$, we found earlier that by using topological tagging a roughly $\pm 2.5\% - \pm 3.5\%$ determination of $\sigma(Zh_{\rm SM})BR(h_{\rm SM} \to b\overline{b})$ is possible for $m_{h_{\rm SM}} \lesssim 140\,{\rm GeV}$ mass. Error on $\sigma(Zh_{\rm SM})$ (just discussed) is in the $\pm 6.5\% - \pm 7\%$ in the $m_{h_{\rm SM}} \lesssim 140\,{\rm GeV}$ mass region, rising to $\sim \pm 7.5\%$ for $m_{h_{\rm SM}} \sim 150\,{\rm GeV}$. From Eq. (2) the error in $BR(h_{\rm SM} \to b\overline{b})$ will then be in the $\pm 7\% - \pm 8\%$ range for $m_{h_{\rm SM}} \lesssim 140\,{\rm GeV}$, rising to $\sim \pm 10\%$ at $m_{h_{\rm SM}} \sim 150\,{\rm GeV}$.

The error for the $\sigma(e^+e^-h_{\rm SM})BR(h_{\rm SM} \to b\overline{b})$ measurement has not been studied in detail, but can be estimated as follows. We assume that an event identification efficiency (which should include the efficiency for b-tagging) of 40% is adequate to make backgrounds small. The number of events (S) is then computed by multiplying $\sigma(e^+e^-h_{\rm SM})$ in Fig. 7 by $0.4BR(h_{\rm SM} \to b\overline{b})L$ using $BR(h_{\rm SM} \to b\overline{b})$ as tabulated in Table I and $L = 200\ {\rm fb}^{-1}$. The measurement fractional error is then estimated as $1/\sqrt{S}$. This yields [25] an error in $\sigma(e^+e^-h_{\rm SM})BR(h_{\rm SM} \to b\overline{b})$ ranging from $\pm 4.5\%$ to $\pm 14\%$ as $m_{h_{\rm SM}}$ varies from $\lesssim 110\,{\rm GeV}$ to $\sim 150\,{\rm GeV}$; for higher $m_{h_{\rm SM}}$ values the error deteriorates rapidly. [15] Recalling the previously estimated error in the $\sigma(e^+e^-h_{\rm SM})$ rate, which ranges from $\pm 4\%$ to $\pm 6\%$ in the $m_{h_{\rm SM}} = 110$ to $150\,{\rm GeV}$ mass region, the resulting error [25] on $BR(h_{\rm SM} \to b\overline{b})$ as computed from Eq. (2) in the $e^+e^-h_{\rm SM}$ final state is then in the $\pm 6\% - \pm 8\%$ range for $m_{h_{\rm SM}} \lesssim 140\,{\rm GeV}$, rising to $\sim \pm 15\%$ for $m_{h_{\rm SM}} \sim 150\,{\rm GeV}$.

By combining [26, 25] the $Zh_{\rm SM}$ and $e^+e^-h_{\rm SM}$ determinations, we find that $BR(h_{\rm SM} \to b\overline{b})$ can be measured with an accuracy of about $\pm 5\% - \pm 6\%$ in the $m_{h_{\rm SM}} \lesssim 140\,{\rm GeV}$ range, rising to $\sim \pm 9\%$ for $m_{h_{\rm SM}} \sim 150\,{\rm GeV}$.

For $BR(h_{\rm SM} \to c\overline{c})$, we recall that by using topological tagging it is estimated that the error for $\sigma(Zh_{\rm SM})BR(h_{\rm SM} \to c\overline{c})$ will be of order $\pm 10\%$ in the $m_{h_{\rm SM}} \leq 130\,{\rm GeV}$ mass region. Using $\pm 7\%$ for the $\sigma(Zh_{\rm SM})$ error in this mass region implies an error for $BR(h_{\rm SM} \to c\overline{c})$ of order $\pm 12\%$. Above, we found that in the $b\overline{b}$ channel the $e^+e^-h_{\rm SM}$ production mode might yield errors that are comparable to the $Zh_{\rm SM}$ mode. A similar result is expected to apply to the $c\overline{c}$ mode [25], implying that the $BR(h_{\rm SM} \to c\overline{c})$ error would be brought down to $\sim \pm 9\%$. This same level of error would be achieved if we computed $BR(h_{\rm SM} \to c\overline{c}) = [(c\overline{c}h_{\rm SM})^2/(b\overline{b}h_{\rm SM})^2]BR(h_{\rm SM} \to b\overline{b})$ and used the $(c\overline{c}h_{\rm SM})^2/(b\overline{b}h_{\rm SM})^2$ errors given in Table X. Aside from the $\nu\overline{\nu}h_{\rm SM}$ component in determining the $c\overline{c}$ to $b\overline{b}$ ratio, these two techniques are not statistically independent. It is not clear which would have smaller systematic error. Presumably, one would pursue both techniques to cross-check and possibly combine the techniques taking into account the statistical correlations.

2. $BR(h_{\rm SM} \to WW^\star)$

The possible procedures are [26]:

- Measure $\sigma(Zh_{\rm SM})BR(h_{\rm SM} \to WW^\star)$ and $\sigma(Zh_{\rm SM})$ and compute $BR(h_{\rm SM} \to WW^\star)$ by dividing. As discussed earlier, errors in $\sigma(Zh_{\rm SM})BR(h_{\rm SM} \to WW^\star)$ are roughly $\pm 22\%$, $\pm 10\%$ and $\pm 7\%$ for $m_{h_{\rm SM}} = 130$, 140

[15] These errors must be confirmed by a more complete simulation to verify the level of efficiency, including b-tagging, that could be retained and still have small backgrounds for this channel.

detection) ranges (see earlier) from $\sim \pm 4\%$ to $\sim \pm 6\%$ in this mass range. The resulting $BR(h_{\rm SM} \to WW^\star)$ error would be roughly $\pm 22\%$, $\pm 11\%$, $\pm 9\%$ for $m_{h_{\rm SM}} = 130$, 140 and 150 GeV, respectively. At $m_{h_{\rm SM}} = 200, 300\,{\rm GeV}$ accuracies for $BR(h_{\rm SM} \to WW^\star)$ of $\sim \pm 12\%$ and $\sim \pm 17\%$ are predicted by extrapolation based on event rate and branching ratio changes.[16]

- Measure $\sigma(e^+e^- h_{\rm SM})BR(h_{\rm SM} \to WW^\star)$ and $\sigma(e^+e^- h_{\rm SM})$ (the ZZ-fusion processes) and again compute $BR(h_{\rm SM} \to WW^\star)$ by dividing [25]. In the $130 - 200\,{\rm GeV}$ mass region, we have already seen that the $\sigma(e^+e^- h_{\rm SM})$ measurement will be comparable (perhaps slightly superior) in accuracy to the $\sigma(Zh_{\rm SM})$ measurement. A first estimate indicates that the accuracy of the $\sigma(e^+e^- h_{\rm SM})BR(h_{\rm SM} \to WW^\star)$ measurement will also be comparable to that for $\sigma(Zh_{\rm SM})BR(h_{\rm SM} \to WW^\star)$. For example, at $m_{h_{\rm SM}} = 150\,{\rm GeV}$ Fig. 7 gives $\sigma(e^+e^- h_{\rm SM}) \sim 4$ fb and from Table I we find $BR(h_{\rm SM} \to W^+W^-) \sim 0.7$. If the efficiency for tagging the $WW^\star$ final state and requiring the recoil mass to be close to the known value of $m_{h_{\rm SM}}$ is, say, 40%, then we would have $S = 224$ signal events with relatively small background (due to our ability to always require recoil mass $\sim m_{h_{\rm SM}}$[17] in this production mode). The resulting error for $\sigma(Zh_{\rm SM})BR(h_{\rm SM} \to WW^\star)$ is $\sim \pm 7\%$. Thus, errors on $BR(h_{\rm SM} \to WW^\star)$ in the $e^+e^- h_{\rm SM}$ production channel will be close to those in the $Zh_{\rm SM}$ channel for $m_{h_{\rm SM}}$ in the $130 - 200\,{\rm GeV}$ mass range.

  At $m_{h_{\rm SM}} = 300\,{\rm GeV}$, $\sigma(e^+e^- h_{\rm SM})$ is smaller than $\sigma(Zh_{\rm SM})$ (see Fig. 7). After including efficiency we found in the previous subsection that the error on $\sigma(e^+e^- h_{\rm SM})$ will be about $\pm 14\%$ (vs. $\pm 11\%$ for $\sigma(Zh_{\rm SM})$). Similarly, the error on $\sigma(e^+e^- h_{\rm SM})BR(h_{\rm SM} \to WW^\star)$ will be larger than for $\sigma(Zh_{\rm SM})BR(h_{\rm SM} \to WW^\star)$. At $m_{h_{\rm SM}} = 300\,{\rm GeV}$, we find (by extrapolation, subject to footnote caveats) error on the former of about $\pm 18\%$ (vs. $\sim \pm 12\%$ for the latter); combining with the $\pm 14\%$ error on $\sigma(e^+e^- h_{\rm SM})$ yields error for $BR(h_{\rm SM} \to WW^\star)$ of order $\pm 23\%$ at this mass for the $e^+e^- h_{\rm SM}$ channel.

If we combine [26, 25] the above two determinations, the overall $BR(h_{\rm SM} \to WW^\star)$ error would be reduced to the roughly $\pm 16\%$, $\pm 8\%$, $\pm 6\%$ level for $m_{h_{\rm SM}} = 130$, 140 and 150 GeV, and even somewhat smaller at $m_{h_{\rm SM}} = 170\,{\rm GeV}$. Above 170 GeV, the accuracy of the determination slowly declines to about $\pm 8\%$ at $m_{h_{\rm SM}} = 200\,{\rm GeV}$ and $\pm 14\%$ at $m_{h_{\rm SM}} = 300\,{\rm GeV}$.

[16] We have assumed that the background scales with the signal rate. A full simulation would be required to verify the extrapolation assumptions.

[17] Typically, the recoil mass resolution is better in the $Zh_{\rm SM}$ ($Z \to e^+e^-, \mu^+\mu^-$) channel than in the $e^+e^- h_{\rm SM}$ channel once the Z mass is used in a kinematically constrained fit. However, all that is needed for the statistical estimates given here to apply is that the recoil mass resolution in $e^+e^- h_{\rm SM}$ events be sufficient that the background in the peak region be small; this should be the case given that the e^+e^- momenta would be quite well-measured.

The goal will be to determine $\sigma(\nu\overline{\nu} h_{\rm SM})$ which is proportional to the the $(WWh_{\rm SM})^2$ coupling-squared. The best procedure [26] depends upon $m_{h_{\rm SM}}$:

- If $m_{h_{\rm SM}} \lesssim 140\,{\rm GeV}$, then good accuracy is attained by measuring $\sigma(\nu\overline{\nu} h_{\rm SM})BR(h_{\rm SM} \to b\overline{b})$ and then dividing by $BR(h_{\rm SM} \to b\overline{b})$. For $L = 200$ fb^{-1} and $m_{h_{\rm SM}} \lesssim 140\,{\rm GeV}$, the measurement error for the former is $\sim \pm 2.5\% - \pm 3.5\%$ (as stated earlier), and that for the latter $b\overline{b}$ branching ratio is $\pm 5\% - \pm 6\%$ (as stated above). The net error in $(WWh_{\rm SM})^2$ obtained in this way is of order $\pm 6\%$ for $m_{h_{\rm SM}} \lesssim 140\,{\rm GeV}$. By $m_{h_{\rm SM}} = 150\,{\rm GeV}$, the accuracy of the $b\overline{b}$ mode determination of $(WWh_{\rm SM})^2$ has worsened to about $\pm 11\%$, coming from $\sim \pm 6\%$ for $\sigma(\nu\overline{\nu} h_{\rm SM})BR(h_{\rm SM} \to b\overline{b})$ and $\sim \pm 9\%$ for $BR(h_{\rm SM} \to b\overline{b})$; see earlier subsections.

- If $m_{h_{\rm SM}} \gtrsim 150\,{\rm GeV}$, then good accuracy is achieved by measuring $\sigma(\nu\overline{\nu} h_{\rm SM})BR(h_{\rm SM} \to WW^\star)$ (in WW-fusion) and dividing by $BR(h_{\rm SM} \to WW^\star)$ (see earlier subsection) to get $\sigma(\nu\overline{\nu} h_{\rm SM})$. Explicitly, we estimated above that an error on $BR(h_{\rm SM} \to WW^\star)$ at the $\sim \pm 8\%, \pm 6\%, \pm 8\%, \pm 14\%$ level could eventually be achieved for $m_{h_{\rm SM}} \sim 140, 150, 200, 300\,{\rm GeV}$. Earlier, we saw that the error in $\sigma(\nu\overline{\nu} h_{\rm SM})BR(h_{\rm SM} \to WW^\star)$ is estimated to be $\pm 10\%, \pm 8\%, \pm$ at $m_{h_{\rm SM}} = 140, 150\,{\rm GeV}$. Extrapolating to $200, 300\,{\rm GeV}$,[18] we estimate errors of $\pm 10\%, \pm 20\%$, respectively. Combining, we find that the error on the $(WWh_{\rm SM})^2$ coupling-squared from the $WW^\star$ final state determination would be about $\pm 13\%$, $\pm 10\%$, $\pm 13\%$, $\pm 24\%$ at $m_{h_{\rm SM}} \sim 140$, 150, 200, 300 GeV, respectively. The error at $m_{h_{\rm SM}} = 170\,{\rm GeV}$ would be slightly smaller than that at $m_{h_{\rm SM}} = 150\,{\rm GeV}$. The $m_{h_{\rm SM}} = 140\,{\rm GeV}$ result is poorer than that obtained in the $b\overline{b}$ mode, but by $m_{h_{\rm SM}} = 150\,{\rm GeV}$ the $WW^\star$ mode determination has become comparable, and for higher masses is distinctly superior.

If we combine the $b\overline{b}$ and $WW^\star$ mode determinations, we get an error for $(WWh_{\rm SM})^2$ of order $\pm 5\%$ for $m_{h_{\rm SM}} \lesssim 140\,{\rm GeV}$, worsening to about $\pm 8\%$ for $m_{h_{\rm SM}} \gtrsim 150\,{\rm GeV}$. For 170 GeV and above the error is simply that found in the $WW^\star$ mode, *e.g.* $\pm 13\%, \pm 24\%$ at $m_{h_{\rm SM}} = 200, 300\,{\rm GeV}$, respectively.

It is, of course, of great interest to test the custodial SU(2) symmetry prediction for the coupling-squared ratio $(WWh_{\rm SM})^2/(ZZh_{\rm SM})^2$. In an earlier subsection we estimated the error on $(ZZh_{\rm SM})^2$ for $m_{h_{\rm SM}} \lesssim 60 - 200\,{\rm GeV}$ to be $\sim \pm 4\% - \pm 6\%$, rising to $\sim \pm 9\%$ at $m_{h_{\rm SM}} = 300\,{\rm GeV}$. Combining with the above results for the $(WWh_{\rm SM})^2$ errors, we estimate errors for $(WWh_{\rm SM})^2/(ZZh_{\rm SM})^2$ of order $\pm 7\%$ for $m_{h_{\rm SM}} \lesssim 140\,{\rm GeV}$, $\pm 10\%$ for $m_{h_{\rm SM}} \sim 150\,{\rm GeV}$, rising slowly to $\sim \pm 14\%$ for $m_{h_{\rm SM}} = 200\,{\rm GeV}$, reaching $\sim \pm 25\%$ at $m_{h_{\rm SM}} = 300\,{\rm GeV}$.

[18] We re-emphasize the fact that simulations at 200 and 300 GeV are needed to check our extrapolations.

We focus on $m_{h_{\rm SM}} \lesssim 130\,{\rm GeV}$. Only two ways to get a handle on $BR(h_{\rm SM} \to \gamma\gamma)$ have been demonstrated to be viable.

- The first involves measuring $\sigma(pp \to Wh_{\rm SM})BR(h_{\rm SM} \to \gamma\gamma)$ and $\sigma(pp \to t\bar{t}h_{\rm SM})BR(h_{\rm SM} \to \gamma\gamma)$ at the LHC. As outlined earlier, each can be determined to about $\pm 15\%$ for $m_{h_{\rm SM}}$ in the range $90 - 130\,{\rm GeV}$. Although not explicitly simulated in the ATLAS and CMS studies, we assume this same error applies at $80\,{\rm GeV}$. These measurements can be employed in two ways.

  – In the first approach one also measures $\sigma(pp \to t\bar{t}h_{\rm SM})BR(h_{\rm SM} \to b\bar{b})$ at the LHC and then computes $BR(h_{\rm SM} \to \gamma\gamma)$ as

$$BR(h_{\rm SM} \to \gamma\gamma) = BR(h_{\rm SM} \to b\bar{b}) \times \frac{[\sigma(pp \to t\bar{t}h_{\rm SM})BR(h_{\rm SM} \to \gamma\gamma)]}{[\sigma(pp \to t\bar{t}h_{\rm SM})BR(h_{\rm SM} \to b\bar{b})]} \qquad (3)$$

  using $BR(h_{\rm SM} \to b\bar{b})$ determined at the NLC as described earlier. Since the error for $BR(h_{\rm SM} \to b\bar{b})$ will be of order $\pm 4\% - \pm 5\%$ (for $L = 200\,{\rm fb}^{-1}$ at the NLC), the error in the determination of $BR(h_{\rm SM} \to \gamma\gamma)$ is dominated by that for the $\gamma\gamma/b\bar{b}$ ratio (see Tables III and IV), and will range from about $\pm 18\%$ to $\pm 26\%$ over the $80 - 130\,{\rm GeV}$ mass range.

  – In the second approach, one uses only $\sigma(pp \to Wh_{\rm SM})BR(h_{\rm SM} \to \gamma\gamma)$ from the LHC, and then divides by the computed $\sigma(pp \to Wh_{\rm SM})$ cross section. In the $m_{h_{\rm SM}} \lesssim 130\,{\rm GeV}$ mass region, the cross section is best computed using the $(WWh_{\rm SM})^2$ coupling-squared determination from the NLC which, as noted earlier, has an error of order $\pm 6\%$ for this mass region. Including systematics, the error in $\sigma(pp \to Wh_{\rm SM})$ is then likely to be of order $\pm 10\%$. Combining with the $\sim \pm 15\%$ error for $\sigma(pp \to Wh_{\rm SM})BR(h_{\rm SM} \to \gamma\gamma)$ yields an error of $\sim \pm 18\%$ in the determination of $BR(h_{\rm SM} \to \gamma\gamma)$ in the $m_{h_{\rm SM}} = 80 - 130\,{\rm GeV}$ region.

  To the extent that determinations from these two ways of getting at $BR(h_{\rm SM} \to \gamma\gamma)$ are statistically independent, they can be combined to yield statistical accuracy of $\lesssim \pm 16\%$ in the $m_{h_{\rm SM}} \lesssim 130\,{\rm GeV}$ range. A rough guess based on simulations performed at lower masses is that at $m_{h_{\rm SM}} = 140\,{\rm GeV}$ this error would deteriorate to about $\pm 25\%$. We also assume very large error for $m_{h_{\rm SM}} \geq 150\,{\rm GeV}$.

- The second technique is that explored in Ref. [28], using the $\sigma BR(h_{\rm SM} \to \gamma\gamma)$ measurements at the NLC discussed earlier. These lead to two possible techniques for getting $BR(h_{\rm SM} \to \gamma\gamma)$.

  – Measure $\sigma(e^+e^- \to Zh_{\rm SM})BR(h_{\rm SM} \to \gamma\gamma)$ and compute $BR(h_{\rm SM} \to \gamma\gamma)$ as

$$\frac{[\sigma(Zh_{\rm SM})BR(h_{\rm SM} \to \gamma\gamma)]}{\sigma(Zh_{\rm SM})}\,; \qquad (4)$$

  – Measure $\sigma(e^+e^- \to \nu\bar{\nu}h_{\rm SM})BR(h_{\rm SM} \to b\bar{b})$ (both being WW-fusion processes) and compute $BR(h_{\rm SM} \to \gamma\gamma)$ as

$$\frac{[\sigma(\nu\bar{\nu}h_{\rm SM})BR(h_{\rm SM} \to \gamma\gamma)]BR(h_{\rm SM} \to b\bar{b})}{[\sigma(\nu\bar{\nu}h_{\rm SM})BR(h_{\rm SM} \to b\bar{b})]}\,. \qquad (5)$$

  The $e^+e^-h_{\rm SM}$ final state from ZZ-fusion is a third alternative, but does not yield errors competitive with the above two techniques [31] because of a smaller signal relative to background.

At the NLC, the errors in the $BR(h_{\rm SM} \to \gamma\gamma)$ determinations are completely dominated by the $\sigma BR(h_{\rm SM} \to \gamma\gamma)$ errors, which we have discussed earlier; see Fig. 5. Assuming running at $\sqrt{s} = 500\,{\rm GeV}$, we found that the smallest σBR error was achieved in the WW-fusion mode. However, a useful level of error was also achieved in the $Zh_{\rm SM}$ mode when running at this energy. The errors expected for $BR(h_{\rm SM} \to \gamma\gamma)$ by combining the determinations of Eqs. (4) and (5) are essentially the same as the combined $\sigma BR(h_{\rm SM} \to \gamma\gamma)$ error plotted in the 3rd window of Fig. 5. For a calorimeter at the optimistic end of current plans for the NLC detector, the net error is predicted to range from $\sim \pm 22\%$ at $m_{h_{\rm SM}} = 120\,{\rm GeV}$ to $\sim \pm 35\%$ ($\sim \pm 53\%$) at $m_{h_{\rm SM}} = 150\,{\rm GeV}$ ($70\,{\rm GeV}$).

Of course, the NLC and LHC determinations can be combined to give sometimes substantially smaller error than achieved at either machine alone. The errors for $BR(h_{\rm SM} \to \gamma\gamma)$ obtained by combining LHC and NLC data will be tabulated later in Table X.

Although one of the big motivations for measuring $BR(h_{\rm SM} \to \gamma\gamma)$ at the NLC is its crucial role in determining $\Gamma^{\rm tot}_{h_{\rm SM}}$ (to be outlined later), whereas $\Gamma^{\rm tot}_{h_{\rm SM}}$ can be directly measured at the FMC by scanning (see next subsection), a measurement of $BR(h_{\rm SM} \to \gamma\gamma)$ would ultimately also be of interest at the FMC, especially if there is no NLC.[19] The possibility of measuring the branching ratio using FMC data at $\sqrt{s} = m_{h_{\rm SM}}$ was examined [31]; for a SM-like Higgs boson, S/B turns out to be much too small for this to succeed. Thus, at the FMC, $BR(h_{\rm SM} \to \gamma\gamma)$ would have to be determined following the same non-s-channel procedures as for the NLC.

G. Determining $\Gamma^{\rm tot}_{h_{\rm SM}}$ and $h_{\rm SM}$ partial widths

The most fundamental properties of the Higgs boson are its mass, its total width and its partial widths. Discussion of the mass determination will be left till the next subsection. The total Higgs width, while certainly important in its own right, becomes doubly so since it is required in order to compute many important partial widths. The partial widths, being directly proportional to the underlying couplings, provide the most direct means of verifying that the observed Higgs boson is or is not the $h_{\rm SM}$. Branching ratios, being the ratio of a partial width to the total width can not be unambiguously interpreted. In contrast, a

[19] In particular, since a $\gamma\gamma$ collider is not possible at the FMC [3], if there is no NLC then the very interesting partial width $\Gamma(h_{\rm SM} \to \gamma\gamma)$ can only be obtained in the form $\Gamma^{\rm tot}_{h_{\rm SM}} BR(h_{\rm SM} \to \gamma\gamma)$.

squared which, in turn, is directly determined in the SM or any extension thereof without reference to mass scales for possibly unexpected (*e.g.* SUSY) decays. Any deviations of partial widths from SM predictions can be directly compared to predictions of alternative models such as the MSSM, the NMSSM, or the general 2HDM. The more accurately the total width and the various branching ratios can be measured, the greater the sensitivity to such deviations and the greater our ability to recognize and constrain the alternative model.

For $m_{h_{\rm SM}} \lesssim 2m_W$, $\Gamma^{\rm tot}_{h_{\rm SM}}$ is too small to be reconstructed in the final state; indirect determination of $\Gamma^{\rm tot}_{h_{\rm SM}}$ is necessary. We note that the $m_{h_{\rm SM}} \lesssim 2m_W$ mass range is that which would be relevant for the SM-like Higgs boson of the MSSM. For larger $m_{h_{\rm SM}}$, direct final state reconstruction of $\Gamma^{\rm tot}_{h_{\rm SM}}$ starts to become possible; the mass above which reasonable error on $\Gamma^{\rm tot}_{h_{\rm SM}}$ is obtained depends upon detector and machine characteristics. The possibilities are reviewed below.

1. *Determining* $\Gamma^{\rm tot}_{h_{\rm SM}}$

There are only two basic possibilities for determining $\Gamma^{\rm tot}_{h_{\rm SM}}$ in the $m_{h_{\rm SM}} \lesssim 2m_W$ mass range in which $\Gamma^{\rm tot}_{h_{\rm SM}}$ is too small to be reconstructed in the final state.

- The first is to employ FMC $\mu^+\mu^-$ collisions at $\sqrt{s} \sim m_{h_{\rm SM}}$ and directly measure $\Gamma^{\rm tot}_{h_{\rm SM}}$ by scanning. In this case, the FMC determination of $\Gamma^{\rm tot}_{h_{\rm SM}}$ can be used to compute the partial width for any channel with a branching ratio measured at the NLC:

$$\Gamma(h_{\rm SM} \to X) = \Gamma^{\rm tot}_{h_{\rm SM}} BR(h_{\rm SM} \to X)\,. \qquad (6)$$

- If there is no muon collider, then $\Gamma^{\rm tot}_{h_{\rm SM}}$ must be determined indirectly using a multiple step process; the best process depends upon the Higgs mass. $\Gamma^{\rm tot}_{h_{\rm SM}}$ is ultimately computed as:

$$\Gamma^{\rm tot}_{h_{\rm SM}} = \frac{\Gamma(h_{\rm SM} \to X)}{BR(h_{\rm SM} \to X)}\,, \qquad (7)$$

  where $X = \gamma\gamma$ ($WW^\star$) gives the best error for $m_{h_{\rm SM}} \lesssim 130\,{\rm GeV}$ ($\gtrsim 140\,{\rm GeV}$). In this case, $\Gamma^{\rm tot}_{h_{\rm SM}}$ can be used to compute partial widths via Eq. (6) only for channels other than those used in the determination of $\Gamma^{\rm tot}_{h_{\rm SM}}$ via Eq. (7).

In what follows we outline the errors anticipated in the ultimate determination of $\Gamma^{\rm tot}_{h_{\rm SM}}$ in the $m_{h_{\rm SM}} \lesssim 2m_W$ mass region, and then discuss implications for the errors in partial widths, both with and without combining NLC and FMC data. We also discuss the determination of $\Gamma^{\rm tot}_{h_{\rm SM}}$ by final state mass peak reconstruction in the mass range $m_{h_{\rm SM}} \gtrsim 2m_W$.

FMC-scan determination of $\Gamma^{\rm tot}_{h_{\rm SM}}$

Only the $\mu^+\mu^-$ collider can have the extremely precise energy resolution and energy setting capable of measuring $\Gamma^{\rm tot}_{h_{\rm SM}}$ by scanning [3]. The amount of integrated luminosity required for a $\pm 33\%$ determination of $\Gamma^{\rm tot}_{h_{\rm SM}}$ using a 3-point scan with 0.01% case is if $m_{h_{\rm SM}} \sim m_Z$, implying a large Z background to $h_{\rm SM}$ production in the s-channel. The accuracy of the $\Gamma^{\rm tot}_{h_{\rm SM}}$ determination scales as $1/\sqrt{L}$.

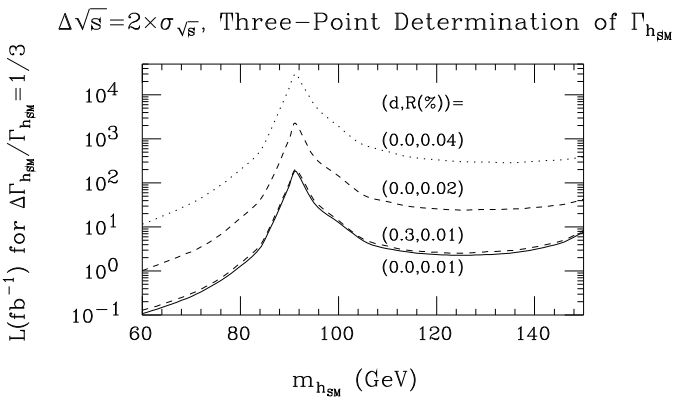

Figure 8: Luminosity required for a $\Delta\Gamma^{\rm tot}_{h_{\rm SM}}/\Gamma^{\rm tot}_{h_{\rm SM}} = 1/3$ measurement in the $b\bar{b}$ final state using the 3-point technique described in [3]. Results for resolutions of $R = 0.01\%, 0.02\%$ and 0.04% are shown for $d = 0$, where $d = |\sqrt{s_0} - m_{h_{\rm SM}}|/\sigma_{\sqrt{s}}$. Here, $\sqrt{s_0}$ is the location of the central energy setting in the 3-point scan and $\sigma_{\sqrt{s}}$ is the resolution in $\sqrt{s}$ for a given value of R. The result for $d = 0.3$ and $R = 0.01\%$ illustrates how insensitive the total luminosity required is to the accuracy of the central setting.

We assume that since the mass of the Higgs boson will be relatively precisely known from the LHC (see next subsection) the FMC would be designed to have optimal luminosity at $\sqrt{s} \sim m_{h_{\rm SM}}$, so that accumulation of $L = 200$ fb^{-1} for scanning the Higgs peak would be possible. It is important to note that in the 3-point scan procedure of Ref. [3] most (5/6) of the luminosity is devoted to the wings of the Higgs peak; only 1/6 of the total L is accumulated at $\sqrt{s} = m_{h_{\rm SM}}$ (exactly). Very roughly the total number of Higgs events from the wing measurements is equivalent to $\sim 0.3L$ on the peak, but S/B is smaller on the wings. Overall, if luminosity L is devoted to the scan procedure, the errors that can be achieved for rate measurements in specific channels are roughly equivalent to what would be achieved if $0.25L$ was devoted to $\sqrt{s} = m_{h_{\rm SM}}$ running. Since it is not useful to sacrifice accuracy in the $\Gamma^{\rm tot}_{h_{\rm SM}}$ measurement in order to devote more luminosity to the peak, in Table IX we quoted measurement errors for specific channels obtained for $L = 50$ fb^{-1} at $\sqrt{s} = m_{h_{\rm SM}}$. These same channel errors will be used in subsequent calculations.

Fig. 8 implies that integrated luminosity of $L = 200$ fb^{-1} would yield a $\pm 2.6\%$, $\pm 32\%$, $\pm 3.6\%$, $\pm 6.5\%$ determination of $\Gamma^{\rm tot}_{h_{\rm SM}}$ at $m_{h_{\rm SM}} = 80\,{\rm GeV}$, m_Z, $120\,{\rm GeV}$, $150\,{\rm GeV}$, respectively. A complete listing of errors appears (later) in Table XI. In the $m_{h_{\rm SM}} \sim m_Z$ worst case, the s-channel FMC accuracy will turn out to be worse than can be attained at the NLC. However, for most masses, the s-channel FMC accuracy would be

to precision tests of the Higgs sector.

Indirect determination of $\Gamma^{\rm tot}_{h_{\rm SM}}$

If there is no $\mu^+\mu^-$ collider, then $\Gamma^{\rm tot}_{h_{\rm SM}}$ must be determined indirectly. The best procedure for doing so depends upon the Higgs mass. If $m_{h_{\rm SM}} \lesssim 130\,{\rm GeV}$, then one must make use of $\gamma\gamma$ Higgs decays. If $m_{h_{\rm SM}} \gtrsim 140\,{\rm GeV}$, $WW^\star$ Higgs decays will be most useful. In both cases, we ultimately employ Eq. (7) to obtain $\Gamma^{\rm tot}_{h_{\rm SM}}$.

Since the $\Gamma(h_{\rm SM}\to\gamma\gamma)$ partial width plays a crucial role in the $m_{h_{\rm SM}} \lesssim 130\,{\rm GeV}$ procedure, it is convenient to discuss it first. The study of $\gamma\gamma \to h_{\rm SM} \to b\bar b$ at the NLC is performed by tuning the beam energy so that the $\gamma\gamma$ luminosity peak at $\sim 0.8\sqrt{s}$ coincides with $m_{h_{\rm SM}}$ [34, 35]. The statistical accuracy that could be achieved for $\Gamma(h_{\rm SM}\to\gamma\gamma)BR(h_{\rm SM}\to b\bar b)$ was estimated in Ref. [35]. Systematic errors have now been evaluated and the effects of gluon radiation and ZZ backgrounds have been included [36]. Suppressing the dangerous $c\bar c g$ backgrounds reduces the signal by only a factor of two. The net error on $\Gamma(h_{\rm SM}\to\gamma\gamma)BR(h_{\rm SM}\to b\bar b)$ for $L = 50\ {\rm fb}^{-1}$ is illustrated in Fig. 9. For $L = 200\ {\rm fb}^{-1}$, the error would be only half as large as shown, but since the luminosity employed in this measurement would be lost to normal running to get the branching ratios *etc.*, we consider only the $L = 50\ {\rm fb}^{-1}$ errors. Thus, the error in the $m_{h_{\rm SM}} \lesssim 120\,{\rm GeV}$ mass region will be in the 8%-10% range, rising to 15% by $m_{h_{\rm SM}} = 140\,{\rm GeV}$ and peaking at 30% at $m_{h_{\rm SM}} = 150\,{\rm GeV}$, as illustrated in Fig. 9. To get the accuracy in the $\Gamma(h_{\rm SM}\to\gamma\gamma)$ partial width itself, we recall that $BR(h_{\rm SM}\to b\bar b)$ is measured with accuracy of $\pm5\% - \pm6\%$ for $m_{h_{\rm SM}} \lesssim 140\,{\rm GeV}$, rising to $\pm9\%$ at $m_{h_{\rm SM}} \sim 150\,{\rm GeV}$. The result is $\Gamma(h_{\rm SM}\to\gamma\gamma)$ error of order $\pm12\%$ for $m_{h_{\rm SM}} \lesssim 120\,{\rm GeV}$, rising to $\sim \pm17\%$ at $m_{h_{\rm SM}} \sim 140\,{\rm GeV}$ and $\sim \pm31\%$ at $m_{h_{\rm SM}} \sim 150\,{\rm GeV}$.

We now give the procedures for determining $\Gamma^{\rm tot}_{h_{\rm SM}}$.

- For $m_{h_{\rm SM}} \lesssim 130\,{\rm GeV}$ (*i.e.* in the MSSM m_{h^0} range), the only known procedure for determining $\Gamma^{\rm tot}_{h_{\rm SM}}$ is that outlined in Ref. [1]. NLC data is required.
  - As described above, measure $\Gamma(h_{\rm SM}\to\gamma\gamma)BR(h_{\rm SM}\to b\bar b)$ and then compute $\Gamma(h_{\rm SM}\to\gamma\gamma)$ by dividing by the value of $BR(h_{\rm SM}\to b\bar b)$.
  - Compute $\Gamma^{\rm tot}_{h_{\rm SM}} = \Gamma(h_{\rm SM}\to\gamma\gamma)/BR(h_{\rm SM}\to\gamma\gamma)$, using the $BR(h_{\rm SM}\to\gamma\gamma)$ determination(s) described earlier.

  The accuracies of the various measurements involved are a crucial issue. The results obtained in earlier sections appear in Table X. Using the determination of $BR(h_{\rm SM}\to\gamma\gamma)$ based on combining NLC and LHC data, we find an error on $\Gamma^{\rm tot}_{h_{\rm SM}}$ of $\sim \pm18-19\%$ for $m_{h_{\rm SM}} = 80-120\,{\rm GeV}$ and $\sim\ \pm20\%$ for $m_{h_{\rm SM}} = 130\,{\rm GeV}$. At $m_{h_{\rm SM}} = 140, 150\,{\rm GeV}$, errors on $BR(h_{\rm SM}\to\gamma\gamma)$ and $\Gamma(h_{\rm SM}\to\gamma\gamma)$ increase and the $\Gamma^{\rm tot}_{h_{\rm SM}}$ error would be $\sim\ \pm25\%, \sim \pm46\%$, respectively.

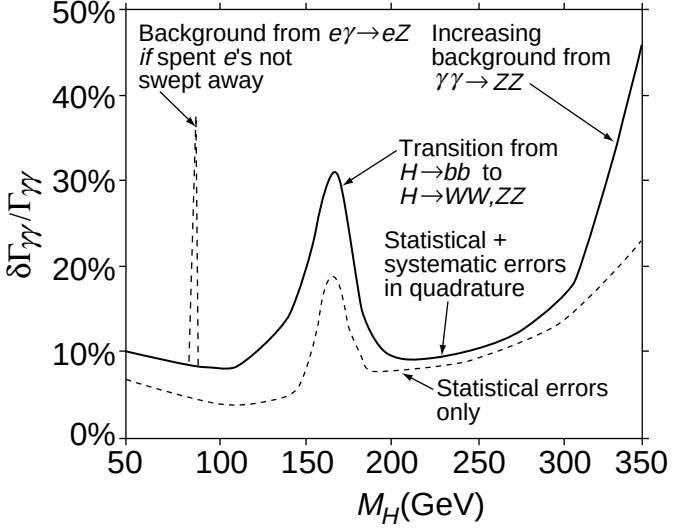

Figure 9: Accuracy (including systematic as well as statistical errors) with which $\Gamma(h_{\rm SM}\to\gamma\gamma)BR(h_{\rm SM}\to b\bar b\ {\rm or} WW, ZZ)$ can be measured at the NLC $\gamma\gamma$ collider with integrated luminosity of $L = 50\ {\rm fb}^{-1}$ [36].

- For $m_{h_{\rm SM}} \gtrsim 130\,{\rm GeV}$, a second possible procedure based on $h_{\rm SM}\to WW^\star$ decays emerges. Use $(WWh_{\rm SM})^2$ to compute $\Gamma(h_{\rm SM}\to WW^\star)$ and then compute $\Gamma^{\rm tot}_{h_{\rm SM}} = \Gamma(h_{\rm SM}\to WW^\star)/BR(h_{\rm SM}\to WW^\star)$. [20] The required errors were obtained in earlier sections and are tabulated in Table X. We find an error for $\Gamma^{\rm tot}_{h_{\rm SM}}$ of about $\pm17\%$ at $m_{h_{\rm SM}} = 130\,{\rm GeV}$, falling to $\pm10\% - \pm11\%$ for $m_{h_{\rm SM}}$ in the $150-170\,{\rm GeV}$ range. This latter is certainly much better than the $\sim\ \pm46\%$ achieved in the $\gamma\gamma$ channel at $m_{h_{\rm SM}} \sim 150\,{\rm GeV}$ using NLC $\gamma\gamma$ collider data and the (NLC+LHC) determination of $BR(h_{\rm SM}\to\gamma\gamma)$. For $m_{h_{\rm SM}} \sim 130\,{\rm GeV}$, the $\pm17\%$ achieved in the present $WW^\star$ technique is still superior to the $\pm20\%$ for the $\gamma\gamma$ technique. Combining the determinations made via the two techniques at $m_{h_{\rm SM}} = 130\,{\rm GeV}$, we would get an error on $\Gamma^{\rm tot}_{h_{\rm SM}}$ of order $\pm13\%$. For $m_{h_{\rm SM}} \lesssim 120\,{\rm GeV}$, the $\gamma\gamma$ technique determination of $\Gamma^{\rm tot}_{h_{\rm SM}}$ is substantially superior to what can be achieved via the $WW^\star$ technique, primarily because $BR(h_{\rm SM}\to WW^\star)$ is very poorly determined.

In Table X, we tabulate the errors for $\Gamma^{\rm tot}_{h_{\rm SM}}$ obtained by using both the $\gamma\gamma$ and the $WW^\star$ techniques, and including the (NLC+LHC) determination of $BR(h_{\rm SM}\to\gamma\gamma)$ in the former.

As apparent from Tables XI and X, for $m_{h_{\rm SM}} \lesssim 130\,{\rm GeV}$ (and $m_{h_{\rm SM}} \not\sim m_Z$) the FMC-scan determination of $\Gamma^{\rm tot}_{h_{\rm SM}}$ is very much superior to the NLC determination. The superiority is still significant at $m_{h_{\rm SM}} = 140\,{\rm GeV}$ while errors are similar at $m_{h_{\rm SM}} = 150\,{\rm GeV}$. At $m_{h_{\rm SM}} = 150\,{\rm GeV}$, combining

[20] Of course, keeping only the $WW^\star$ mode, this latter procedure can be viewed as a computation of $\Gamma^{\rm tot}_{h_{\rm SM}} \propto \sigma(\nu\bar\nu h_{\rm SM})/[BR(h_{\rm SM}\to WW^\star)]^2$.

accuracy for $\Gamma^{\rm tot}_{h_{\rm SM}}$, yielding a combined error of $\sim \pm 5.4\%$ (vs. $\pm 6.5\%$ for the FMC-scan alone). This would be beneficial for computing partial widths (other than that for the $WW^\star$ channel used in the NLC determination of $\Gamma^{\rm tot}_{h_{\rm SM}}$ at this mass). For $m_{h_{\rm SM}} \gtrsim 160\,{\rm GeV}$, FMC s-channel detection of the $h_{\rm SM}$ becomes difficult, and only the NLC allows a reasonable determination of $\Gamma^{\rm tot}_{h_{\rm SM}}$.

Final-state mass peak determination of $\Gamma^{\rm tot}_{h_{\rm SM}}$: NLC

Of course, once $m_{h_{\rm SM}} \gtrsim 2m_W$, $\Gamma^{\rm tot}_{h_{\rm SM}}$ is large enough that measurement directly from the shape of the mass peak becomes conceivable. The precise sensitivity depends upon detector characteristics and other details. We [26] will illustrate results for $Zh_{\rm SM}$ production in five cases. In the first four cases, we demand that $Z \to e^+e^-, \mu^+\mu^-$ and reconstruct the Higgs peak via the recoil mass. The momenta of the muons are measured by the tracking component of the detector. The momenta of the electrons are measured by both the tracker and the electromagnetic calorimeter — since these are not statistically independent of one another, we use the measurement having the smaller error. The e^+e^- and $\mu^+\mu^-$ final states are treated separately, and at the end their errors are statistically combined. Four different combinations of tracking and calorimetry are considered. In the fifth case, we allow the Z to decay to either $e^+e^-, \mu^+\mu^-$ or $q\overline{q}$, and reconstruct the Higgs resonance peak using the $b\overline{b}$ or W^+W^- Higgs decay products. The five cases are specified in detail as follows:

1. We assume super-JLC tracking [29], implying $\Delta p/p = 5 \times 10^{-5} p(\,{\rm GeV}) \oplus 0.001$, and slightly better than 'standard' NLC detector [24] calorimetry of $\Delta E/E = 0.12/\sqrt{E(\,{\rm GeV})} \oplus 0.005$. In this case, the best electron momentum measurement is almost always from the tracking, so that the natural event-by-event resolution ($\Gamma_{\rm R}$) in the e^+e^- and $\mu^+\mu^-$ channels is the same. One finds that $\Gamma_{\rm R}$ can be as small as $0.3\,{\rm GeV}$ or so when $\sqrt{s} = m_Z + m_{h_{\rm SM}} + \sim 20\,{\rm GeV}$ and the e's/μ's are not terribly energetic but that $\Gamma_{\rm R}$ deteriorates considerably if the machine is run at $\sqrt{s} = 500\,{\rm GeV}$ because of the much larger energies of the leptons, implying larger tracking errors. We assume a systematic error in our knowledge of $\Gamma_{\rm R}$ in the e^+e^- and $\mu^+\mu^-$ channels of 10%.

2. The assumptions for this case are exactly the same as for the first case, except that we allow for a much larger systematic error of 50%, as could be relevant when $\Gamma_{\rm R}$ is so small.

3. We assume the 'standard' NLC detector tracking [24], implying $\Delta p/p = 5 \times 10^{-4} p(\,{\rm GeV}) \oplus 0.0015/\sqrt{p(\,{\rm GeV})}$, and electromagnetic calorimetry unchanged at $\Delta E/E = 0.12/\sqrt{E(\,{\rm GeV})} \oplus 0.005$. In this case, the best electron momentum measurement is always from the calorimetry, especially when $m_{h_{\rm SM}}$ is small and one runs at the higher $\sqrt{s} = 500\,{\rm GeV}$. Thus, the natural resolution $\Gamma_{\rm R}$ in the e^+e^- and $\mu^+\mu^-$ channels is the same. One finds that $\Gamma_{\rm R}$ can be as small as $0.3\,{\rm GeV}$ or so when $\sqrt{s} = m_Z + m_{h_{\rm SM}} + \sim 20\,{\rm GeV}$ and the e's/μ's are not terribly energetic but that $\Gamma_{\rm R}$ deteriorates considerably if the machine is run at $\sqrt{s} = 500\,{\rm GeV}$ because of the much larger energies of the leptons, implying larger tracking errors. We assume a systematic error in our knowledge of $\Gamma_{\rm R}$ in the e^+e^- and $\mu^+\mu^-$ channels of 10%.

4. We assume the same 'standard' NLC tracking as in the 3rd case, but adopt a CMS [10] type electromagnetic calorimeter, specified by $\Delta E/E = 0.02/\sqrt{E(\,{\rm GeV})} \oplus 0.005 \oplus 0.2/E(\,{\rm GeV})$. The electron resolution improves still further and the e^+e^- channel yields much smaller resolution and errors than the $\mu^+\mu^-$ channel. Systematic error of 10% for $\Gamma_{\rm R}$ is assumed.

5. The resolution $\Gamma_{\rm R}$ for the Higgs mass peak in the $b\overline{b}$ and W^+W^- final states (we weight according to branching ratio) has been studied systematically as a function of $m_{h_{\rm SM}}$. The result for the NLC detector specified in Ref. [24] can be parameterized as $\Gamma_{\rm R} = 4.86 - 0.019 m_{h_{\rm SM}} + 0.964 \cdot 10^{-4} m^2_{h_{\rm SM}} - 0.103 \cdot 10^{-6} m^3_{h_{\rm SM}}$. Typically $\Gamma_{\rm R}$ is of order $4\,{\rm GeV}$, as illustrated in Fig. 6. Systematic error of 10% for $\Gamma_{\rm R}$ is assumed.

Sensitivity to Higgs widths becomes possible when $\Gamma^{\rm tot}_{h_{\rm SM}}$ is not too much smaller than $\Gamma_{\rm R}$; some benchmarks are (see Fig. 1) $\Gamma^{\rm tot}_{h_{\rm SM}} \sim 17\,{\rm MeV}, 32\,{\rm MeV}, 400\,{\rm MeV}, 1\,{\rm GeV}, 4\,{\rm GeV}, 10\,{\rm GeV}$ for $m_{h_{\rm SM}} \sim 150, 155, 170, 190, 245, 300\,{\rm GeV}$, respectively. Results for recoil mass $\Gamma_{\rm R}$'s are potentially sensitive to beamstrahlung, bremsstrahlung and beam energy smearing. We shall assume that these effects are small. The JLC studies of Ref. [32] show that they are clearly so if one has small 0.4% full width beam energy spread and runs at $\sqrt{s} \sim m_Z + m_{h_{\rm SM}} + 20\,{\rm GeV}$.

In order to compute the error in the $\Gamma^{\rm tot}_{h_{\rm SM}}$ measurement given a value for the event-by-event resolution $\Gamma_{\rm R}$, one proceeds as follows. The convolution of the Higgs gaussian and the resolution gaussian yields a gaussian of effective width $\Gamma_{\rm eff} = \sqrt{[\Gamma^{\rm tot}_{h_{\rm SM}}]^2 + [\Gamma_{\rm R}]^2}$. Assuming small background, the statistical accuracy with which $\Gamma_{\rm eff}$ can be measured is $\Delta\Gamma^{\rm stat}_{\rm eff} = \Gamma_{\rm eff}/\sqrt{2N}$ where N is the number of events in the Higgs mass peak. The systematic error in $\Gamma_{\rm eff}$ coming from the systematic uncertainty $\Delta\Gamma^{\rm sys}_{\rm R}$ in $\Gamma_{\rm R}$ is $\Delta\Gamma^{\rm sys}_{\rm eff} = \Delta\Gamma^{\rm sys}_{\rm R}\Gamma_{\rm R}/\Gamma_{\rm eff}$. Adding in quadrature, we have a total $\Delta\Gamma_{\rm eff} = \sqrt{[\Delta\Gamma^{\rm stat}_{\rm eff}]^2 + [\Delta\Gamma^{\rm sys}_{\rm eff}]^2}$. The relationship between this and the $\Delta\Gamma^{\rm tot}_{h_{\rm SM}}$ error in $\Gamma^{\rm tot}_{h_{\rm SM}}$ is: $\Delta\Gamma^{\rm tot}_{h_{\rm SM}} = [\Gamma_{\rm eff}/\Gamma^{\rm tot}_{h_{\rm SM}}]\Delta\Gamma_{\rm eff}$. (For very small $\Gamma^{\rm tot}_{h_{\rm SM}}$, this error becomes ill-defined and it is $[\Gamma^{\rm tot}_{h_{\rm SM}}]^2$ that is more appropriately studied; however, for masses such that $\Gamma^{\rm tot}_{h_{\rm SM}}$ is, indeed, resolvable, the result obtained by the above procedure is valid.)

The implications of the event-by-event mass resolutions in the five cases will now be described [26]. We assume integrated luminosity of $L = 200\ {\rm fb}^{-1}$ at the energies $\sqrt{s} = m_Z + m_{h_{\rm SM}} + 20\,{\rm GeV}$ and $\sqrt{s} = 500\,{\rm GeV}$. An overall detection and acceptance efficiency of 60% is employed. $BR(Z \to e^+e^-) = BR(Z \to \mu^+\mu^-) = 0.0336$ is employed in cases 1-4 and $BR(Z \to e^+e^- + \mu^+\mu^- + q\overline{q}) = 0.7672$ is employed in case 5. The resulting percentage errors in $\Gamma^{\rm tot}_{h_{\rm SM}}$ as a function of Higgs mass are plotted in Fig. 10.

We see from the figure that a reasonable accuracy of *e.g.* $\pm 20\%$ for $\Gamma^{\rm tot}_{h_{\rm SM}}$ is achieved in cases 1,2,3,4,5 at $m_{h_{\rm SM}} \sim 163, 165, 187, 170, 235\,{\rm GeV}$ assuming $\sqrt{s} = m_Z + m_{h_{\rm SM}} + 20\,{\rm GeV}$ and at $m_{h_{\rm SM}} \sim 178, 189, 218, 192, 235\,{\rm GeV}$ assuming

which $\Gamma^{\rm tot}_{h_{\rm SM}}$ becomes of order $\Gamma_{\rm R}$, as one might naively anticipate. We see immediately the importance of optimizing luminosity for $\sqrt{s} = m_Z + m_{h_{\rm SM}} + 20\,{\rm GeV}$ and also having either excellent tracking or excellent calorimetry if the Higgs mass happens to be in the $\sim 160\,{\rm GeV}$ to $\sim 190\,{\rm GeV}$ range. For $m_{h_{\rm SM}} = 190 - 220\,{\rm GeV}$, running at $\sqrt{s} = 500\,{\rm GeV}$ would allow a 20% measurement of $\Gamma^{\rm tot}_{h_{\rm SM}}$ if we have excellent tracking or excellent calorimetry. However, if we only have the 'standard' tracking and calorimetry of case 3, then a 20% measurement in the $m_{h_{\rm SM}} = 190 - 220\,{\rm GeV}$ range would require optimizing luminosity at the lower $\sqrt{s} = m_Z + m_{h_{\rm SM}} + 20\,{\rm GeV}$ energy. The case 5 results show that the increased statistics from being able to include $q\overline{q}$ as well as $e^+e^-, \mu^+\mu^-$ decays of the Z when using the Higgs decay final state to reconstruct the mass peak becomes important for $m_{h_{\rm SM}} \gtrsim 270\,{\rm GeV}$.

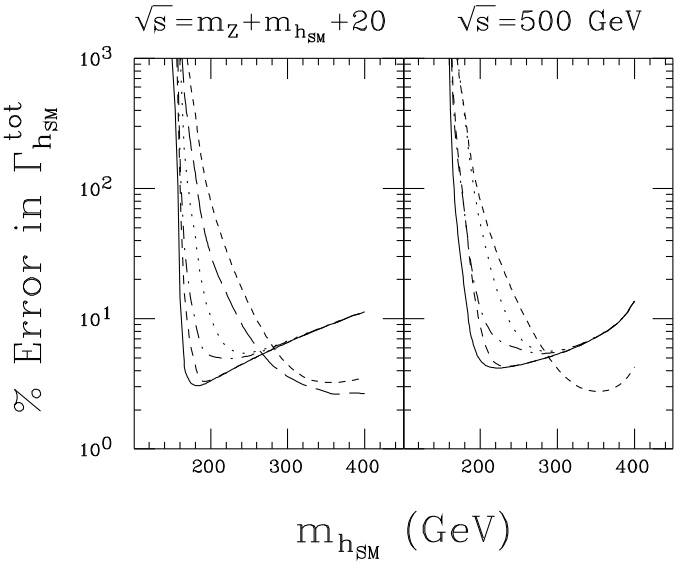

Figure 10: Accuracy (including systematic as well as statistical errors) with which $\Gamma^{\rm tot}_{h_{\rm SM}}$ can be *directly* measured for $\sqrt{s} = m_Z + m_{h_{\rm SM}} + 20\,{\rm GeV}$ and $\sqrt{s} = 500\,{\rm GeV}$ with luminosity times efficiency of $L = 120\ {\rm fb}^{-1}$ using the $Zh_{\rm SM}$ production mode at the NLC [26]. Results are given for the five cases described in the text: 1=solid; 2=regular dashes; 3=dots; 4=dot dashes; 5=short dashes. Bremsstrahlung, beamstrahlung, and beam energy smearing are assumed unimportant compared to the contributions of tracking and calorimetry to $\Gamma_{\rm R}$. Also shown in the first window (very long dashes) are estimated errors for $\Gamma^{\rm tot}_{h_{\rm SM}}$ using the $ZZ^{(*)} \to 4\ell$ mode with $L = 600\ {\rm fb}^{-1}$ for ATLAS+CMS at the LHC.

If the errors for the direct measurement of $\Gamma^{\rm tot}_{h_{\rm SM}}$ are compared with those for the indirect determination assuming $\sqrt{s} = 500\,{\rm GeV}$, we see that super-JLC tracking resolution of cases 1 or 2 would make the direct measurement errors competitive with those from the indirect determination for $m_{h_{\rm SM}} \gtrsim 180\,{\rm GeV}$. The total error on $\Gamma^{\rm tot}_{h_{\rm SM}}$ would be significantly improved by the $180 - 190\,{\rm GeV}$ range: combined error would be of order $\pm 10\%, \pm 6\%, \pm 4.6\%$ at $m_{h_{\rm SM}} = 180, 190, 200\,{\rm GeV}$, respectively. Below this mass range, the indirect determination is much the better, while above this mass range the direct determination has by far the smaller error. The mass range of the cross over would move to lower masses for running at $\sqrt{s} = m_Z + m_{h_{\rm SM}} + 20\,{\rm GeV}$. In either case, we would obtain a very important improvement over indirect determination errors in a mass region where $\Gamma^{\rm tot}_{h_{\rm SM}}$ cannot be precisely measured via s-channel scanning at the FMC. The above should be contrasted with the situation for the 'standard' tracking/calorimetry of case 3, where we are left with a $m_{h_{\rm SM}}$ region in which neither direct nor indirect errors are good, the direct measurement errors only becoming competitive with indirect errors for $m_{h_{\rm SM}} \gtrsim 250\,{\rm GeV}$.

Final-state mass peak determination of $\Gamma^{\rm tot}_{h_{\rm SM}}$: LHC

Measurement of $\Gamma^{\rm tot}_{h_{\rm SM}}$ in the $gg \to h_{\rm SM} \to ZZ^{(*)} \to 4\ell$ mode at the LHC will also be possible. For our estimates we have taken a 4ℓ resolution of $\Gamma_{\rm R} = 1.25\% m_{h_{\rm SM}}$, which approximates the ATLAS resolutions quoted in Table 29 of Ref. [12] in the $m_{h_{\rm SM}} \leq 180\,{\rm GeV}$ mass region. The $L = 100\ {\rm fb}^{-1}$ event rates from Table 29 ($m_{h_{\rm SM}} \leq 180\,{\rm GeV}$) and Table 38 ($m_{h_{\rm SM}} \geq 200\,{\rm GeV}$) appearing in Ref. [12] have been rescaled to $L = 600\ {\rm fb}^{-1}$ (assuming CMS and ATLAS will have similar resolution) and a systematic error of $\pm 10\%$ for $\Gamma_{\rm R}$ is incorporated in quadrature. The background rate given in Tables 29 and (especially) 38 is always small compared to the signal rate and can be neglected in computing the error in $\Gamma^{\rm tot}_{h_{\rm SM}}$. Following the same error estimation procedures as outlined in the NLC subsection, we arrive at the results plotted as the long dashes in the first window of Fig. 10. The expected error for $\Gamma^{\rm tot}_{h_{\rm SM}}$ has a similar mass dependence to that obtained via hadronic final state reconstruction at the NLC, but is uniformly smaller for the assumed integrated luminosity. The excellent 4ℓ mass resolution expected for ATLAS and CMS is crucial for this favorable result. If both LHC and NLC results are available, then it will be useful to combine results to improve the error. Even so, error for $\Gamma^{\rm tot}_{h_{\rm SM}}$ below 20% using reconstruction of the $h_{\rm SM}$ resonance peak in decay final states only becomes possible once $m_{h_{\rm SM}} \gtrsim 210\,{\rm GeV}$.

2. *Partial widths using* $\Gamma^{\rm tot}_{h_{\rm SM}}$

In this section, we focus on results obtained using NLC data, FMC data, or a combination thereof. (It is important to recall our convention that the notation NLC means $\sqrt{s} = 500\,{\rm GeV}$ running in e^+e^- or $\mu^+\mu^-$ collisions, while FMC refers explicitly to s-channel Higgs production in $\mu^+\mu^-$ collisions.) Due to lack of time, LHC data has generally not been incorporated. The only exception is that the error on $BR(h_{\rm SM} \to \gamma\gamma)$ is estimated after including the (NLC+LHC) determination. This is particularly crucial in obtaining a reasonable error for the indirect determination of $\Gamma^{\rm tot}_{h_{\rm SM}}$ when $m_{h_{\rm SM}} \lesssim 130\,{\rm GeV}$.

$(WWh_{\rm SM})^2$ and $(\gamma\gamma h_{\rm SM})^2$ couplings-squared are possible in $\sqrt{s} = 500\,{\rm GeV}$ NLC running without employing $\Gamma^{\rm tot}_{h_{\rm SM}}$. However, determination of $(b\overline{b}h_{\rm SM})^2$ is only possible by determining $\Gamma^{\rm tot}_{h_{\rm SM}}$ and then employing Eq. (6). This procedure can also be used for $(c\overline{c}h_{\rm SM})^2$, but it turns out that it is statistically better to compute $(c\overline{c}h_{\rm SM})^2$ using $(b\overline{b}h_{\rm SM})^2$ and the experimental determination of their ratio (described earlier). Finally, by using the FMC-scan determination of $\Gamma^{\rm tot}_{h_{\rm SM}}$ and Eq. (6), we can obtain determinations of $(WWh_{\rm SM})^2$ and $(\gamma\gamma h_{\rm SM})^2$ from $BR(h_{\rm SM} \to WW^\star)$ and $BR(h_{\rm SM} \to \gamma\gamma)$ (as measured in $\sqrt{s} = 500\,{\rm GeV}$ running), respectively, which are independent of the NLC determinations of these same quantities made directly without use of $\Gamma^{\rm tot}_{h_{\rm SM}}$.

Given a determination of $\Gamma^{\rm tot}_{h_{\rm SM}}$, we can employ Eq. (6) and the determination of $BR(h_{\rm SM} \to b\overline{b})$ (which has reasonable accuracy for $m_{h_{\rm SM}} \lesssim 150\,{\rm GeV}$) to determine $\Gamma(h_{\rm SM} \to b\overline{b})$ (equivalent to determining the $(b\overline{b}h_{\rm SM})^2$ squared coupling). The expected $(b\overline{b}h_{\rm SM})^2$ errors using the indirect $\Gamma^{\rm tot}_{h_{\rm SM}}$-determination errors are listed in Table X. They are not especially good, primarily because of the large $\Gamma^{\rm tot}_{h_{\rm SM}}$ errors. The $(c\overline{c}h_{\rm SM})^2$ coupling-squared can be computed either from $(b\overline{b}h_{\rm SM})^2$ and the $(c\overline{c}h_{\rm SM})^2/(b\overline{b}h_{\rm SM})^2$ measurement or from $BR(h_{\rm SM} \to c\overline{c})$ and Eq. (6). Either way, the errors are ultimately dominated by those for $\Gamma^{\rm tot}_{h_{\rm SM}}$. Thus, using NLC data only, the $(c\overline{c}h_{\rm SM})^2$ errors will be essentially the same as those for $(b\overline{b}h_{\rm SM})^2$.

The $(b\overline{b}h_{\rm SM})^2$ errors are greatly improved for $m_{h_{\rm SM}} \lesssim 140\,{\rm GeV}$ by using the FMC-scan determination of $\Gamma^{\rm tot}_{h_{\rm SM}}$ in conjunction with the $\sqrt{s} = 500\,{\rm GeV}$, $L = 200\,{\rm fb}^{-1}$ $BR(h_{\rm SM} \to b\overline{b})$ errors [37]. Combining the FMC-scan determination of $\Gamma^{\rm tot}_{h_{\rm SM}}$ with the indirect NLC determination of $\Gamma^{\rm tot}_{h_{\rm SM}}$ to minimize the $\Gamma^{\rm tot}_{h_{\rm SM}}$ error and then computing $\Gamma(h_{\rm SM} \to b\overline{b})$ yields the errors $(b\overline{b}h_{\rm SM})^2|_{\rm NLC+FMC}$ tabulated in Table XII. The corresponding $(c\overline{c}h_{\rm SM})^2$ errors as computed from $(b\overline{b}h_{\rm SM})^2$ and the $(c\overline{c}h_{\rm SM})^2/(b\overline{b}h_{\rm SM})^2$ ratio using the errors for the latter tabulated in Table X are also listed. These are slightly superior to those obtained if $(c\overline{c}h_{\rm SM})^2$ is computed via Eq. (6) using the combined NLC+FMC $\Gamma^{\rm tot}_{h_{\rm SM}}$ determination.

$(\mu^+\mu^- h_{\rm SM})^2$: NLC+FMC data

The very small errors for the FMC s-channel measurements of $\sigma(\mu^+\mu^- \to h_{\rm SM})BR(h_{\rm SM} \to b\overline{b}, WW^\star, ZZ^\star)$ [3] are summarized in Table IX.[21] As noted in the associated discussion, a measurement of $\sigma(\mu^+\mu^- \to h_{\rm SM})BR(h_{\rm SM} \to X)$ is readily converted to an equally accurate determination of $\Gamma(h_{\rm SM} \to \mu^+\mu^-)BR(h_{\rm SM} \to X)$. Given these measurements, there are four independent ways of combining NLC data with the s-channel FMC data to determine $\Gamma(h_{\rm SM} \to \mu^+\mu^-)$ [37].

1) compute $\Gamma(h_{\rm SM} \to \mu^+\mu^-) = [\Gamma(h_{\rm SM} \to \mu^+\mu^-)BR(h_{\rm SM} \to b\overline{b})]_{\rm FMC}/BR(h_{\rm SM} \to b\overline{b})_{\rm NLC}$;

2) compute $\Gamma(h_{\rm SM} \to \mu^+\mu^-) = [\Gamma(h_{\rm SM} \to \mu^+\mu^-)BR(h_{\rm SM} \to WW^\star)]_{\rm FMC}/BR(h_{\rm SM} \to WW^\star)_{\rm NLC}$;

3) compute $\Gamma(h_{\rm SM} \to \mu^+\mu^-) = [\Gamma(h_{\rm SM} \to \mu^+\mu^-)BR(h_{\rm SM} \to ZZ^\star)]_{\rm FMC}\Gamma^{\rm tot}_{h_{\rm SM}}/\Gamma(h_{\rm SM} \to ZZ^\star)_{\rm NLC}$, where the combined direct FMC plus indirect NLC determination of $\Gamma^{\rm tot}_{h_{\rm SM}}$ can be used since the NLC $(ZZ^\star h_{\rm SM})^2$ determination was not used in the indirect NLC determination of $\Gamma^{\rm tot}_{h_{\rm SM}}$;

4) compute $\Gamma(h_{\rm SM} \to \mu^+\mu^-) = [\Gamma(h_{\rm SM} \to \mu^+\mu^-)BR(h_{\rm SM} \to WW^\star)\Gamma^{\rm tot}_{h_{\rm SM}}]_{\rm FMC}/\Gamma(h_{\rm SM} \to$ mined at the FMC since $(WW^\star h_{\rm SM})^2$ is used in the NLC indirect determination of $\Gamma^{\rm tot}_{h_{\rm SM}}$.

The resulting (very small) errors for $(\mu^+\mu^- h_{\rm SM})^2$ obtained by combining determinations from all four techniques are labelled $(\mu^+\mu^- h_{\rm SM})^2|_{\rm NLC+FMC}$ and tabulated in Table XII.

$(WWh_{\rm SM})^2$ and $(\gamma\gamma h_{\rm SM})^2$: NLC+FMC data

In Table X we summarized the errors for the $(WWh_{\rm SM})^2$ coupling squared coming from determining the $\nu\overline{\nu}h_{\rm SM}$ cross section from $\sqrt{s} = 500\,{\rm GeV}$ running at the NLC. We [37] can obtain a second independent determination of $(WWh_{\rm SM})^2$ by taking $BR(h_{\rm SM} \to WW^\star)$ (as determined in $Zh_{\rm SM}$ and $e^+e^-h_{\rm SM}$ production at the NLC) and multiplying by $\Gamma^{\rm tot}_{h_{\rm SM}}$ as determined by s-channel scanning at the FMC — the NLC $\Gamma^{\rm tot}_{h_{\rm SM}}$ determination employs the $WW^\star$ branching ratio in the relevant mass region and cannot be used as part of a statistically independent determination. These errors are summarized in Table XII using the notation $(WWh_{\rm SM})^2|_{\rm FMC}$. If we combine the two different determinations, then we get the errors denoted $(WWh_{\rm SM})^2|_{\rm NLC+FMC}$. (Results are not quoted for $m_{h_{\rm SM}} \leq 130\,{\rm GeV}$, for which $BR(h_{\rm SM} \to WW^\star)$ is too poorly measured for this procedure to yield any improvement over the errors of Table X.)

Also given in Table X were the errors for $(\gamma\gamma h_{\rm SM})^2$ coming from combining NLC $\gamma\gamma$ collider data with $b\overline{b}$ and $WW^\star$ branching ratios as measured at the NLC. In close analogy to the $WW^\star$ procedure given above, we [37] can obtain a second independent determination of $(\gamma\gamma h_{\rm SM})^2$ by taking $BR(h_{\rm SM} \to \gamma\gamma)$ (as determined using LHC and $\nu\overline{\nu}h_{\rm SM}$ NLC data) and multiplying by $\Gamma^{\rm tot}_{h_{\rm SM}}$ as determined by s-channel scanning at the FMC — the NLC $\Gamma^{\rm tot}_{h_{\rm SM}}$ determination employs the $\gamma\gamma$ branching ratio in the relevant mass region and cannot be used as part of a statistically independent determination. The resulting errors are summarized in Table XII using the notation $(\gamma\gamma h_{\rm SM})^2|_{\rm FMC}$. If we combine the two different determinations, then we get the errors denoted $(\gamma\gamma h_{\rm SM})^2|_{\rm NLC+FMC}$.

One last point concerning $\Gamma(h_{\rm SM} \to \gamma\gamma)$ is worth noting. At the FMC, a $\gamma\gamma$ collider is not possible [3], Only the $(\gamma\gamma h_{\rm SM})^2_{\rm FMC}$ determination of this potentially very revealing coupling would be available.

3. *Summary Tables*

We present in Tables X, XI, and XII a final summary of the errors that can be achieved for fundamental $h_{\rm SM}$ properties (other than the mass) in three different situations:

- $L = 200\,{\rm fb}^{-1}$ devoted to $\sqrt{s} = 500\,{\rm GeV}$ running at the NLC supplemented with $L = 50\,{\rm fb}^{-1}$ of $\gamma\gamma$ collider data at $\sqrt{s} \sim m_{h_{\rm SM}}/0.8$ and the (LHC+NLC) determination of $BR(h_{\rm SM} \to \gamma\gamma)$;
- A total $L = 200\,{\rm fb}^{-1}$ of luminosity devoted to scanning the Higgs peak to determine $\Gamma^{\rm tot}_{h_{\rm SM}}$ — as explained earlier, specific channel rate errors are equivalent to those that would be obtained by devoting $L = 50\,{\rm fb}^{-1}$ to the Higgs peak at $\sqrt{s} = m_{h_{\rm SM}}$;

[21] Recall that the FMC s-channel errors quoted are for $L = 50\,{\rm fb}^{-1}$, the amount of luminosity exactly on the $\sqrt{s} = m_{h_{\rm SM}}$ Higgs peak that is roughly equivalent to the on-peak and off-peak luminosity accumulated in performing the scan determination of $\Gamma^{\rm tot}_{h_{\rm SM}}$.

Table X: Summary of approximate errors for branching ratios, coupling-squared ratios, and couplings-squared as determined using $L = 200\ \mathrm{fb}^{-1}$ of data accumulated in $\sqrt{s} = 500\,\mathrm{GeV}$ running at the NLC. For $BR(h_{\rm SM} \to \gamma\gamma)$, but *not* $(\gamma\gamma h_{\rm SM})^2/(b\bar{b}h_{\rm SM})^2$, we have combined the NLC $\sqrt{s} = 500\,\mathrm{GeV}$ results with results obtained using LHC data; the net accuracy so obtained for $BR(h_{\rm SM} \to \gamma\gamma)$ is also reflected in the errors quoted for the determination of $\Gamma^{\rm tot}_{h_{\rm SM}}$ following the indirect procedure. The errors for $\Gamma(h_{\rm SM} \to \gamma\gamma)$ quoted are for $L = 50\ \mathrm{fb}^{-1}$ accumulated in $\gamma\gamma$ collider running at $\sqrt{s} \sim m_{h_{\rm SM}}/0.8$, and are those employed in the indirect $\Gamma^{\rm tot}_{h_{\rm SM}}$ determination. A $-$ indicates large error and a ? indicates either that a reliable simulation or estimate is not yet available or that the indicated number is a very rough estimate.

Quantity	Errors			
$\mathbf{m_{h_{SM}}}$**(GeV)**	**80**	**100**	**110**	**120**
$(c\bar{c}h_{\rm SM})^2/(b\bar{b}h_{\rm SM})^2$	$\sim \pm 7\%$			
$(WWh_{\rm SM})^2/(b\bar{b}h_{\rm SM})^2$	$-$	$-$	$-$	$\pm 23\%$
$(\gamma\gamma h_{\rm SM})^2/(b\bar{b}h_{\rm SM})^2$	$\pm 42\%$	$\pm 27\%$	$\pm 24\%$	$\pm 22\%$
$(ZZh_{\rm SM})^2$	$\pm 3\% - \pm 4\%$			
$BR(h_{\rm SM} \to b\bar{b})$	$\pm 5\%$			
$BR(h_{\rm SM} \to c\bar{c})$	$\sim \pm 9\%$			
$BR(h_{\rm SM} \to WW^\star)$	$-$			
$(WWh_{\rm SM})^2$	$\pm 5\%$			
$(ZZh_{\rm SM})^2/(WWh_{\rm SM})^2$	$\pm 6\% - \pm 7\%$			
$BR(h_{\rm SM} \to \gamma\gamma)$	$\pm 15\%$	$\pm 14\%$	$\pm 13\%$	$\pm 13\%$
$(\gamma\gamma h_{\rm SM})^2$	$\sim \pm 12\%$			
$\Gamma^{\rm tot}_{h_{\rm SM}}$ (indirect)	$\pm 19\%$	$\pm 18\%$	$\pm 18\%$	$\pm 18\%$
$(b\bar{b}h_{\rm SM})^2$	$\pm 20\%$	$\pm 19\%$	$\pm 18\%$	$\pm 18\%$
$\mathbf{m_{h_{SM}}}$**(GeV)**	**130**	**140**	**150**	**170**
$(c\bar{c}h_{\rm SM})^2/(b\bar{b}h_{\rm SM})^2$	$\pm 7\%$	?		
$(WWh_{\rm SM})^2/(b\bar{b}h_{\rm SM})^2$	$\pm 16\%$	$\pm 8\%$	$\pm 7\%$	$\pm 16\%$
$(\gamma\gamma h_{\rm SM})^2/(b\bar{b}h_{\rm SM})^2$	$\pm 23\%$	$\pm 26\%$	$\pm 35\%$	$-$
$(ZZh_{\rm SM})^2$	$\pm 4\%$			
$BR(h_{\rm SM} \to b\bar{b})$	$\pm 6\%$		$\pm 9\%$	$\sim 20\%$?
$BR(h_{\rm SM} \to c\bar{c})$	$\sim \pm 9\%$	?		
$BR(h_{\rm SM} \to WW^\star)$	$\pm 16\%$	$\pm 8\%$	$\pm 6\%$	$\pm 5\%$
$(WWh_{\rm SM})^2$	$\pm 5\%$	$\pm 5\%$	$\pm 8\%$	$\pm 10\%$
$(ZZh_{\rm SM})^2/(WWh_{\rm SM})^2$	$\pm 7\%$	$\pm 7\%$	$\pm 9\%$	$\pm 11\%$
$BR(h_{\rm SM} \to \gamma\gamma)$	$\pm 13\%$	$\pm 18\%$?	$\pm 35\%$	$-$
$(\gamma\gamma h_{\rm SM})^2$	$\pm 15\%$	$\pm 17\%$	$\pm 31\%$	$-$
$\Gamma^{\rm tot}_{h_{\rm SM}}$ (indirect)	$\pm 13\%$	$\pm 9\%$	$\pm 10\%$	$\pm 11\%$
$(b\bar{b}h_{\rm SM})^2$	$\pm 14\%$	$\pm 11\%$	$\pm 13\%$	$\pm 23\%$
$\mathbf{m_{h_{SM}}}$**(GeV)**	**180**	**190**	**200**	**300**
$(ZZh_{\rm SM})^2$	$\pm 4\% - \pm 5\%$		$\pm 6\%$	$\pm 9\%$
$(WWh_{\rm SM})^2$	$\pm 11\%$	$\pm 12\%$	$\pm 13\%$	$\pm 24\%$
$(ZZh_{\rm SM})^2/(WWh_{\rm SM})^2$	$\pm 12\%$	$\pm 13\%$	$\pm 14\%$	$\pm 25\%$
$BR(h_{\rm SM} \to WW)$	$\pm 6\%$	$\pm 7\%$	$\pm 8\%$	$\pm 14\%$?
$(\gamma\gamma h_{\rm SM})^2$	$\pm 13\%$	$\pm 12\%$	$\pm 12\%$	$\pm 22\%$
$\Gamma^{\rm tot}_{h_{\rm SM}}$ (indirect)	$\pm 13\%$	$\pm 14\%$	$\pm 15\%$	$\pm 28\%$

- combining the above two sets of data.

The results we have obtained depend strongly on detector parameters and analysis techniques and in some cases (those marked by a ?) were obtained by extrapolation rather than full simulation. Nonetheless, these results should serve as an illustration of what might ultimately be achievable on the basis of NLC $\sqrt{s} = 500\,\mathrm{GeV}$ running and/or FMC s-channel data. Results for FMC s-channel errors assume very excellent 0.01% beam energy resolution and the ability to measure the beam energy with precision on the order of 1 part in 10^6. Due to lack of time, except for the determination of $BR(h_{\rm SM} \to \gamma\gamma)$ and implications for $\Gamma^{\rm tot}_{h_{\rm SM}}$, we have not explored the undoubted benefits that would result from combining NLC/FMC data with LHC data. Such a study is in progress.

Of course, it should not be forgotten that the $\sqrt{s} = 500\,\mathrm{GeV}$ data could also be obtained by running an FMC with a final ring optimized for this energy. (Confirmation that the FMC can achieve the same precisions as the NLC when run at $\sqrt{s} = 500\,\mathrm{GeV}$ must await a full machine and detector design; it could

Table XI: Summary of approximate errors for coupling-squared ratios and $\Gamma^{\rm tot}_{h_{\rm SM}}$ in the case of s-channel Higgs production at the FMC, assuming $L = 200\ \mathrm{fb}^{-1}$ total scan luminosity (which for rate measurements in specific channels is roughly equivalent to $L = 50\ \mathrm{fb}^{-1}$ at the $\sqrt{s} = m_{h_{\rm SM}}$ peak). Beam resolution of $R = 0.01\%$ is assumed. A $-$ indicates large error and a ? indicates either that a reliable simulation or estimate is not yet available or that the indicated number is a very rough estimate.

Quantity	Errors			
$\mathbf{m_{h_{SM}}}$**(GeV)**	**80**	m_Z	**100**	**110**
$(WW^\star h_{\rm SM})^2/(b\bar{b}h_{\rm SM})^2$	$-$	$-$	$\pm 3.5\%$	$\pm 1.6\%$
$(ZZ^\star h_{\rm SM})^2/(b\bar{b}h_{\rm SM})^2$	$-$	$-$	$-$	$\pm 34\%$
$(ZZ^\star h_{\rm SM})^2/(WW^\star h_{\rm SM})^2$	$-$	$-$	$-$	$\pm 34\%$
$\Gamma^{\rm tot}_{h_{\rm SM}}$	$\pm 2.6\%$	$\pm 32\%$	$\pm 8.3\%$	$\pm 4.2\%$
$\mathbf{m_{h_{SM}}}$**(GeV)**	**120**	**130**	**140**	**150**
$(WW^\star h_{\rm SM})^2/(b\bar{b}h_{\rm SM})^2$	$\pm 1\%$	$\pm 0.7\%$	$\pm 0.7\%$	$\pm 1\%$
$(ZZ^\star h_{\rm SM})^2/(b\bar{b}h_{\rm SM})^2$	$\pm 6\%$	$\pm 3\%$	$\pm 2\%$	$\pm 2\%$
$(ZZ^\star h_{\rm SM})^2/(WW^\star h_{\rm SM})^2$	$\pm 6\%$	$\pm 3\%$	$\pm 2\%$	$\pm 2\%$
$\Gamma^{\rm tot}_{h_{\rm SM}}$	$\pm 3.6\%$	$\pm 3.6\%$	$\pm 4.1\%$	$\pm 6.5\%$

Table XII: Summary of approximate errors for branching ratios, coupling-squared ratios and couplings-squared obtained by combining the results of Tables X and XI. See text for further discussion. A $-$ indicates large error and a ? indicates either that a reliable simulation or estimate is not yet available or that the indicated number is a very rough estimate.

Quantity	Errors			
$\mathbf{m_{h_{SM}}}$**(GeV)**	**80**	**100**	**110**	**120**
$(b\bar{b}h_{\rm SM})^2\vert_{\rm NLC+FMC}$	$\pm 6\%$	$\pm 9\%$	$\pm 7\%$	$\pm 6\%$
$(c\bar{c}h_{\rm SM})^2\vert_{\rm NLC+FMC}$	$\pm 9\%$	$\pm 11\%$	$\pm 10\%$	$\pm 9\%$
$(\mu^+\mu^- h_{\rm SM})^2\vert_{\rm NLC+FMC}$	$\pm 5\%$	$\pm 5\%$	$\pm 4\%$	$\pm 4\%$
$(\gamma\gamma h_{\rm SM})^2\vert_{\rm FMC}$	$\pm 15\%$	$\pm 16\%$	$\pm 14\%$	$\pm 13\%$
$(\gamma\gamma h_{\rm SM})^2\vert_{\rm NLC+FMC}$	$\pm 9\%$	$\pm 10\%$	$\pm 9\%$	$\pm 9\%$
$\mathbf{m_{h_{SM}}}$**(GeV)**	**130**	**140**	**150**	**170**
$(b\bar{b}h_{\rm SM})^2\vert_{\rm NLC+FMC}$	$\pm 7\%$	$\pm 7\%$	$\pm 10\%$	$\pm 23\%$
$(c\bar{c}h_{\rm SM})^2\vert_{\rm NLC+FMC}$	$\pm 10\%$	?		
$(\mu^+\mu^- h_{\rm SM})^2\vert_{\rm NLC+FMC}$	$\pm 3\%$	$\pm 3\%$	$\pm 4\%$	$\pm 10\%$
$(WW^\star h_{\rm SM})^2\vert_{\rm FMC}$	$\pm 16\%$	$\pm 9\%$	$\pm 9\%$	$-$
$(WW^\star h_{\rm SM})^2\vert_{\rm NLC+FMC}$	$\pm 5\%$	$\pm 4\%$	$\pm 6\%$	$\pm 10\%$
$(\gamma\gamma h_{\rm SM})^2\vert_{\rm FMC}$	$\pm 14\%$	$\pm 18\%$	$\pm 36\%$	$-$
$(\gamma\gamma h_{\rm SM})^2\vert_{\rm NLC+FMC}$	$\pm 10\%$	$\pm 13\%$	$\pm 23\%$	$-$

nificantly from those employed in the $\sqrt{s}=500\,\mathrm{GeV}$ studies reported here.) However, it should be apparent from comparing Tables X, XI and XII that if there is a SM-like Higgs boson in the $m_{h_{\rm SM}}\lesssim 2m_W$ mass region (as expected in supersymmetric models) then it is very advantageous to have $L=200~\mathrm{fb}^{-1}$ of data from both $\sqrt{s}=500\,\mathrm{GeV}$ running and from an FMC s-channel scan of the Higgs resonance. Thus, the importance of obtaining a full complement of Higgs boson data on a reasonable time scale argues for having either an NLC plus a FMC or two FMC's. A single FMC with two final rings — one optimized for $\sqrt{s}=m_{h_{\rm SM}}$ and one for $\sqrt{s}=500\,\mathrm{GeV}$ — would suffice, but take twice as long (8 years at $L_{\rm year}=50~\mathrm{fb}^{-1}$) to accumulate the necessary data.

H. Measuring $m_{h_{\rm SM}}$ at TeV33, LHC and NLC

In our discussion, we will focus on the $m_{h_{\rm SM}}\leq 2m_W$ mass region, but give some results for higher masses. In the $m_{h_{\rm SM}}\leq 2m_W$ region, measurement of the Higgs boson mass at the LHC and/or NLC will be of great practical importance for the FMC since it will enable a scan of the Higgs resonance peak with minimal luminosity wasted on locating the center of the peak. Ultimately the accuracy of the Higgs mass measurement will impact precision tests of loop corrections, both in the SM and in extended models such as the MSSM. For example, in the minimal supersymmetric standard model, the prediction for the mass of the light SM-like h^0 to one loop is [1]:

$$m_{h^0}^2 = \frac{1}{2}\left[m_{A^0}^2+m_Z^2-\left\{(m_{A^0}^2+m_Z^2)^2 -4m_{A^0}^2 m_Z^2\cos^2 2\beta\right\}^{1/2}\right]+\Delta m_{h^0}^2\,, \quad (8)$$

where $\Delta m_{h^0}^2=3g^2m_t^4\ln\left(m_{\widetilde t}^2/m_t^2\right)/[8\pi^2m_W^2]$. Here, $m_{\widetilde t}$ is the top-squark mass and we have simplified by neglecting top-squark mixing and non-degeneracy. From Eq. (8), one can compute dm_{h^0}/dm_{A^0}, $dm_{h^0}/d\tan\beta$, dm_{h^0}/dm_t, and $dm_{h^0}/dm_{\widetilde t}$ for a given choice of input parameters. These derivatives determine the sensitivity of these parameters to the error in m_{h^0}. For example, for $m_{A^0}=200\,\mathrm{GeV}$, $m_{\widetilde t}=260\,\mathrm{GeV}$, $\tan\beta=14$ and $m_t=175\,\mathrm{GeV}$, for which $m_{h^0}=100\,\mathrm{GeV}$, we find that a $\pm 100\,\mathrm{MeV}$ measurement of m_{h^0} (a precision that should be easily achieved, as discussed below) would translate into constraints (for variations of one variable at a time) on m_{A^0}, $\tan\beta$, m_t and $m_{\widetilde t}$ of about $\pm 37\,\mathrm{GeV}$, ± 0.7, $\pm 670\,\mathrm{MeV}$ and $\pm 1\,\mathrm{GeV}$, respectively. Since m_t will be known to much better accuracy than this and (for such low m_{A^0}) the A^0 would be observed and its mass measured with reasonable accuracy, the determination of m_{h^0} would be used as a joint constraint on $m_{\widetilde t}$ and $\tan\beta$. More generally, squark mixing parameters should be included in the analysis. The challenge will be to compute higher loop corrections to m_{h^0} to the $\pm 100\,\mathrm{MeV}$ level.

Determination of $m_{h_{\rm SM}}$ will proceed by examining a peaked mass distribution constructed using the measured momenta of particles appearing in the final state. At TeV33 and the LHC, these will be the particles into which the Higgs boson decays. At the NLC, we may employ the $Z\to\ell^+\ell^-$ decay products and reconstruct the recoil mass peak or we may directly reconstruct the Higgs mass from its decay products, as outlined in the discussion associated with determining $\Gamma_{h_{\rm SM}}^{\rm tot}$. The accuracy of the Higgs boson mass determination will depend upon the technique/channel, the detector performance and the signal and background statistics.

If the background under the peak is small, then the accuracy of the mass measurement is given by $\Delta m_h\sim\Gamma_{\rm R}/\sqrt{S}$, where $\Gamma_{\rm R}$ is the natural (Gaussian) mass resolution of the reconstruction and S is the total number of events in the mass peak.[22] The background at the NLC is generally sufficiently small that this is a good approximation. At the LHC, the background level is small (after cuts) in the 4ℓ final state of $h_{\rm SM}\to ZZ^{(*)}$ decay. But, in the inclusive production 2γ final state mode the background is much larger than the signal and in the associated $Wh_{\rm SM}+t\bar t h_{\rm SM}\to\ell\nu 2\gamma X$ modes the background and signal event rates are approximately equal (after cuts). If we assume that the background is constant under the Higgs peak, that the signal peak is Gaussian with width $\Gamma_{\rm R}$, and that we examine the portion of the mass peak lying between $m_h-n\Gamma_{\rm R}$ and $m_h+n\Gamma_{\rm R}$, then one can demonstrate that the statistical error in m_h is

$$\Delta m_h^{\rm stat}=\frac{\Gamma_{\rm R}}{\sqrt{S}}\left[c(n)+\frac{n^2B}{3S}\right]\,, \quad (9)$$

where $c(n)\equiv\int_{-n}^{+n}dx\,x^2\exp[-x^2/2]/\int_{-n}^{+n}dx\,\exp[-x^2/2]$ and S and B are the total number of signal and background events contained in the above-specified interval. In our TeV33 and LHC estimates, we will employ $n=2$, for which $c(n)=0.774$. All signal and background rates from tables given in the various TeV33 and LHC studies will be scaled (using Gaussian shape for the signal peak and assuming a flat background) to the above value of n.

LEP2, TeV33 and LHC

The first measurement of $m_{h_{\rm SM}}$ will probably take place at LEP2, the Tevatron, or the LHC. At LEP2, the accuracy will be limited by statistics. For example, at $\sqrt{s}=192\,\mathrm{GeV}$ and with $L=150~\mathrm{pb}^{-1}$ for each of the four experiments and summing over all channels, the number of signal and background events will be roughly $S,B=250,100$ at $m_{h_{\rm SM}}=80\,\mathrm{GeV}$ and $S,B=180,150$ at $m_{h_{\rm SM}}=91\,\mathrm{GeV}$ in a $n=2$ interval [38]. A conservative expectation for the resolution in all channels is $\Gamma_{\rm R}\sim 3\,\mathrm{GeV}$ [38]. Using Eq. (9), these event numbers lead to $\Delta m_{h_{\rm SM}}\sim 250,400\,\mathrm{MeV}$ at $m_{h_{\rm SM}}=80,91\,\mathrm{GeV}$, respectively.

At the Tevatron, the primary discovery mode is $Wh_{\rm SM}$ with $h_{\rm SM}\to b\bar b$. We give $\Delta m_{h_{\rm SM}}$ estimates for TeV33. A detailed study of the accuracy with which $m_{h_{\rm SM}}$ can be determined at Tev33 has not been performed, but we have estimated the error from the mass plots and statistics of Ref. [4]. Examining Fig. 1 of Ref. [4] and comparing to the mass bins quoted in the Table I caption of Ref. [4] one concludes that $\Gamma_{\rm R}\sim 10.0,12.5,13.8,16.3\,\mathrm{GeV}$ at $m_{h_{\rm SM}}=60,80,100,120\,\mathrm{GeV}$,

[22] As always, our notation is that ΔX represents the absolute magnitude of the 1σ error on the quantity X; that is the 1σ limits on X are $X\pm\Delta X$.

to $n \sim 1.2$. Rescaling the $L = 10$ fb^{-1} final S and B values of Table IV [4] to $n = 2$ and to an ultimate integrated luminosity of $L = 60$ fb^{-1} (3 years for two detectors) implies statistical errors of $\Delta m_{h_{\rm SM}}^{\rm stat} = 0.61, 0.96, 1.5, 2.7\,{\rm GeV}$ at $m_{h_{\rm SM}} = 60, 80, 100, 120\,{\rm GeV}$, respectively. Allowing for systematic effects at the level of $\Delta m_h^{\rm syst} = 0.01 m_h$, added in quadrature, already increases these errors to $\Delta m_{h_{\rm SM}}^{\rm tot} = 0.85, 1.3, 1.8, 2.9\,{\rm GeV}$, respectively. It is clearly crucial that systematic effects be well controlled.

At the LHC, the excellent $\gamma\gamma$ mass resolution planned by both the ATLAS and CMS detectors implies that the best mass measurement in the $m_{h_{\rm SM}} \lesssim 150\,{\rm GeV}$ range will come from detection modes in which $h_{\rm SM} \to \gamma\gamma$; the production modes for which detection in the $\gamma\gamma$ final state is possible are $gg \to h_{\rm SM}$ inclusive and $Wh_{\rm SM}, t\bar{t}h_{\rm SM}$ associated production. ATLAS $M_{\gamma\gamma}$ resolutions from Table 21 of Ref. [12] are $\Gamma_{\rm R} = 1.07, 1.16, 1.25, 1.30, 1.34, 1.43, 1.52\,{\rm GeV}$ at $m_{h_{\rm SM}} = 60, 90, 100, 110, 120, 130, 150\,{\rm GeV}$, respectively. The $M_{\gamma\gamma}$ resolution currently claimed by CMS is of order $\Gamma_{\rm R} =\sim 0.7\% m_{h_{\rm SM}}$ at high luminosity.

ATLAS inclusive signal and background rates for $n = 1.4$, $L = 100$ fb^{-1} appear in Table 21 of [12]. We have rescaled these to $n = 2$ and $L = 300$ fb^{-1}. CMS inclusive signal rates have been estimated for $L = 100$ fb^{-1} and $n = 2$ by counting events in the peaks of Fig. 12.3 of Ref. [10]: the $L = 100$ fb^{-1}, $n = 2$ estimates are $S = 1275, 1700, 1840, 650$ at $m_{h_{\rm SM}} = 90, 110, 130, 150\,{\rm GeV}$, respectively. The corresponding background rates have been computed using the $S/\sqrt{B}$ values from Fig. 12.5 of [10] (after appropriate rescalings to account for the fact that the plotted $S/\sqrt{B}$ values are those for $n \sim 1.2$, *i.e.* for keeping about 75% of the signal peak): the $n = 1.2$ values are $S/\sqrt{B} = 6.5, 10, 13, 8$ at $m_{h_{\rm SM}} = 90, 110, 130, 150\,{\rm GeV}$, respectively. The resulting S and B for $L = 100$ fb^{-1} are multiplied by a factor of 3 to get $L = 300$ fb^{-1} rates. The combined $Wh_{\rm SM}, t\bar{t}h_{\rm SM}$ event rates in the $h_{\rm SM} \to \gamma\gamma$ final state for ATLAS at $L = 100$ fb^{-1} were taken from Table 11.8 of Ref. [9], namely $S = B = 15$ for $m_{h_{\rm SM}} = 80, 100, 120\,{\rm GeV}$. We assume these rates correspond to a bin of size $n = 2$. CMS signal and background rates for the associated production modes were obtained from the $L = 165$ fb^{-1}, $n = 2$ Table 12.3 of Ref. [10]. The associated production S and B rates for both ATLAS and CMS are rescaled to $L = 300$ fb^{-1}. The statistical error in $m_{h_{\rm SM}}$ is then computed from Eq. (9) for ATLAS/inclusive ATLAS/associated, CMS/inclusive and CMS/associated, separately. The net error $\Delta m_{h_{\rm SM}}$ for each detector is then computed by combining the associated and inclusive results and then adding in a systematic error (in quadrature) given by $\Delta m_{h_{\rm SM}}^{\rm syst} = 0.001 m_{h_{\rm SM}}$ (the ATLAS estimate). Finally, the net error is computed by combining the ATLAS and CMS net errors.

The result is that $\Delta m_{h_{\rm SM}} \sim 90 - 110$ MeV for $m_{h_{\rm SM}} \lesssim 130\,{\rm GeV}$ with $\Delta m_{h_{\rm SM}} \sim 150$ MeV for $m_{h_{\rm SM}} = 150\,{\rm GeV}$. For example, at $m_{h_{\rm SM}} = 100\,{\rm GeV}$, we obtained the following

$$\Delta m_{h_{\rm SM}} = \begin{cases} \text{ATLAS/inclusive} & 204\,{\rm MeV} \\ \text{ATLAS/associated} & 270\,{\rm MeV} \\ \text{ATLAS/stat+syst} & 191\,{\rm MeV} \\ \text{CMS/inclusive} & 65\,{\rm MeV} \\ \text{CMS/associated} & 85\,{\rm MeV} \\ \text{CMS/stat+syst} & 111\,{\rm MeV} \\ \text{Total} & 96\,{\rm MeV} \end{cases} \quad (10)$$

As one cross check on this computation, we [8] took the S and B numbers for $L = 300$ fb^{-1} at $m_{h_{\rm SM}} = 100\,{\rm GeV}$, for inclusive and associated production separately, from ATLAS and then generated 100 experiments throwing S and B according to Gaussian/Poisson statistics. The background subtraction was then made to get the signal peak, and the rms of the peak position for the 100 experiments was computed. $\Delta m_{h_{\rm SM}}^{\rm stat}$ was found to be 230 MeV for inclusive production and 246 MeV for associated production. Combining these with a 100 MeV systematic error gives $\Delta m_{h_{\rm SM}}^{\rm tot} \sim 200\,{\rm MeV}$. All these results are very similar to the above-quoted ATLAS numbers. CMS statistical errors are smaller by virtue of the better resolution; in fact, the assumed 0.1% systematic uncertainty dominates the CMS statistical plus systematic error.

For $m_{h_{\rm SM}} \gtrsim 130\,{\rm GeV}$, $m_{h_{\rm SM}}$ can also be determined using the inclusive $h_{\rm SM} \to ZZ^{(*)} \to 4\ell$ final state. Our inputs from Ref. [12] are the same as in the discussion of the 4ℓ-mode determination of $\Gamma_{h_{\rm SM}}^{\rm tot}$. For $m_{h_{\rm SM}} \leq 180\,{\rm GeV}$, we employ the $L = 100$ fb^{-1} signal and background rates of Table 29 and the corresponding value of $n = 2$ (for which $c(n) = 0.774$) in Eq. (9). For $m_{h_{\rm SM}} \geq 200\,{\rm GeV}$, we employ the $L = 100$ fb^{-1} signal and background rates of Table 38 which effectively correspond to $n = 1.65$ [23] for which $c(n) = 0.626$. All rates are scaled to $L = 600$ fb^{-1}. Further, we include in quadrature a 1 per mil systematic uncertainty in the overall mass scale. The resulting error for $m_{h_{\rm SM}}$ is in the range $\Delta m_{h_{\rm SM}} \sim 60 - 120\,{\rm MeV}$ for $140 \leq m_{h_{\rm SM}} \leq 400\,{\rm GeV}$, except at $m_{h_{\rm SM}} \sim 170\,{\rm GeV}$ where $\Delta m_{h_{\rm SM}} \sim 270\,{\rm MeV}$. For $m_{h_{\rm SM}} \geq 200\,{\rm GeV}$, it is possible that smaller error could be obtained for less stringent cuts (implying larger signal rates, but also larger background) than those employed in Table 38. We have not pursued this possibility.

The improvement in $\Delta m_{h_{\rm SM}}$ obtained by combining the $\gamma\gamma$ and 4ℓ mode determinations of $m_{h_{\rm SM}}$ is small since only the $\gamma\gamma$ (4ℓ) mode gives small errors for $m_{h_{\rm SM}} \lesssim 130\,{\rm GeV}$ ($\gtrsim 140\,{\rm GeV}$).

NLC

At the NLC, we [26] consider the same five cases discussed earlier with regard to directly determining $\Gamma_{h_{\rm SM}}^{\rm tot}$ from the Higgs mass peak in the $Zh_{\rm SM}$ production mode. The resulting errors for $m_{h_{\rm SM}}$ are plotted in Fig. 11. (Cases 1 and 2 are indistinguishable, the systematic error in $\Gamma_{\rm R}$ not having significant influence on $\Delta m_{h_{\rm SM}}$.) The results for $\Delta m_{h_{\rm SM}}$ in case 5 (in which the Higgs peak is reconstructed from the $h_{\rm SM} \to$

[23] The table caption states that the accepted mass interval includes 90% of the events, which for a Gaussian shape would imply $n \sim 1.65$.

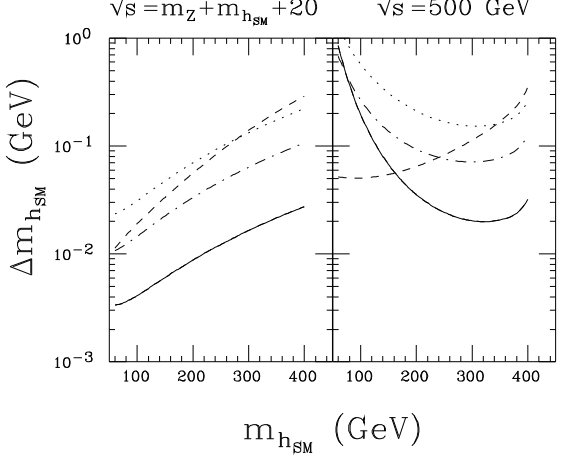

Figure 11: The error $\Delta m_{h_{\rm SM}}$ for measurements at $\sqrt{s} = m_Z + m_{h_{\rm SM}} + 20\,{\rm GeV}$ and $\sqrt{s} = 500\,{\rm GeV}$ with luminosity times efficiency of $L = 120\ {\rm fb}^{-1}$ using the $Zh_{\rm SM}$ production mode at the NLC [26]. Results are given for the five cases described in association with directly measuring $\Gamma^{\rm tot}_{h_{\rm SM}}$ — see Fig. 10; 1=2=solid; 3=dots; 4=dot dashes; 5=short dashes. Bremsstrahlung, beamstrahlung, and beam energy smearing are assumed unimportant compared to the contributions of tracking and calorimetry to $\Gamma_{\rm R}$.

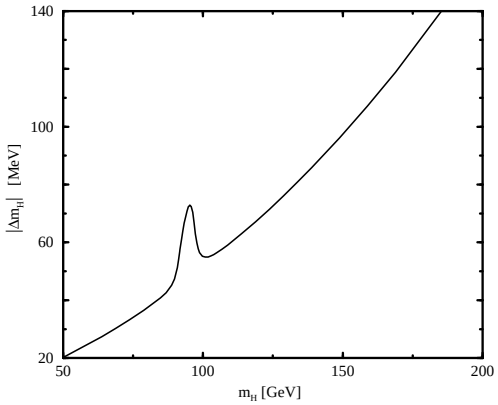

Figure 12: The precision $\Delta m_{h_{\rm SM}}$ attainable from a 50 ${\rm fb}^{-1}$ measurement of the $Zb\bar{b}$ cross section at $\sqrt{s} = m_Z + m_{h_{\rm SM}} + 0.5\,{\rm GeV}$ as a function of $m_{h_{\rm SM}}$, including b-tagging and cuts. Bremsstrahlung, beamstrahlung, and beam energy smearing are neglected. A precise measurement of the cross section well above threshold is presumed available. Results from Ref. [39].

$b\bar{b}, W^+W^-$ final states assuming hadronic calorimetry as defined in Ref. [24]) are probably too optimistic when $m_{h_{\rm SM}}$ is near m_Z, given that we have not included backgrounds in the estimates. Backgrounds should be small in cases 1-4 since we demand quite precise reconstruction of $Z \to e^+e^-, \mu^+\mu^-$ in the $Zh_{\rm SM}$ final state, implying that the only background would be from ZZ production where one of the Z's decays leptonically. (For a sample plot showing the small expected background level, see Fig. 2 of Ref. [32].) Fig. 11 shows that distinctly greater accuracy at the NLC is possible than by using the $\gamma\gamma$ mode at the LHC, provided NLC systematic errors are not substantial. In all cases, for $m_{h_{\rm SM}} \lesssim 300\,{\rm GeV}$ running at $\sqrt{s} = 500\,{\rm GeV}$ yields much larger $\Delta m_{h_{\rm SM}}$ than running at $\sqrt{s} \sim m_Z + m_{h_{\rm SM}} + 20\,{\rm GeV}$.

Another technique that is available at the NLC is to employ a threshold measurement of the $Zh_{\rm SM}$ cross section [39]. The procedure makes use of the fact that both $m_{h_{\rm SM}}$ and the $\sqrt{s} = 500\,{\rm GeV}$ cross section for $e^+e^- \to Zh_{\rm SM}$ (with $h_{\rm SM} \to b\bar{b}$) will be well-measured after a number of years of NLC running. One then re-configures the collider for maximal luminosity just above the threshold energy $\sqrt{s} = m_Z + m_{h_{\rm SM}}$, and expends $L = 50\ {\rm fb}^{-1}$ at $\sqrt{s} = m_Z + m_{h_{\rm SM}} + 0.5\,{\rm GeV}$, *i.e.* on the steeply rising portion of the threshold curve for the $Zh_{\rm SM}$ cross section. The ratio of the cross section at $\sqrt{s} = m_Z + m_{h_{\rm SM}} + 0.5\,{\rm GeV}$ to that at $\sqrt{s} = 500\,{\rm GeV}$ is insensitive to systematic effects and yields a rather precise $m_{h_{\rm SM}}$ determination. The expected precision for the Higgs mass after including appropriate cuts to reduce backgrounds, but before including the effects of bremsstrahlung, beamstrahlung and beam energy smearing, is given in Fig. 12 for an integrated luminosity of 50 ${\rm fb}^{-1}$. (We deem it unlikely that more than $L = 50\ {\rm fb}^{-1}$ would be devoted to this special purpose energy.) The precision degrades as $m_{h_{\rm SM}}$ increases because the signal cross section is smaller. The background from the Z-peak reduces the precision for $m_{h_{\rm SM}} \sim m_Z$. Bremsstrahlung, beamstrahlung and beam energy smearing yield a reduction in sensitivity of 15% at a muon collider and 35% at an e^+e^- collider. Comparing to the errors that one would have for $L = 50\ {\rm fb}^{-1}$ at $\sqrt{s} \sim m_Z + m_{h_{\rm SM}} + 20\,{\rm GeV}$ from Higgs peak reconstruction in the $Zh_{\rm SM}$ mode (which are a factor of 2 larger than the $L = 200\ {\rm fb}^{-1}$ errors plotted in Fig. 11), we see that the threshold measurement errors would be quite competitive for $m_{h_{\rm SM}} \not\sim m_Z$ unless the detector has either excellent CMS-style calorimetry (case 4) or super-JLC type tracking (case 1) for the recoil mass reconstruction.

FMC

The ultimate in $m_{h_{\rm SM}}$ accuracy is that which can be achieved at a muon collider by scanning the Higgs mass peak in the s-channel. The scan was described earlier. For $L = 200\ {\rm fb}^{-1}$ devoted to the scan and a beam energy resolution of 0.01%, one finds [3] $\Delta m_{h_{\rm SM}} = 0.007, 0.025, 0.35, 0.10, 0.060, 0.20, 0.49\,{\rm MeV}$ for $m_{h_{\rm SM}} = 60, 80, 90, 100, 120, 140, 150\,{\rm GeV}$, respectively.

Summary

A summary of the accuracies possible for $m_{h_{\rm SM}}$ at the various machines using the techniques described is given for $m_{h_{\rm SM}} \leq 300\,{\rm GeV}$ in Table XIII.

Table XIII: Summary of approximate errors, $\Delta m_{h_{\rm SM}}$, for $m_{h_{\rm SM}} \leq 300\,{\rm GeV}$. LEP2 errors are for $L = 600\ {\rm pb}^{-1}$. Tev33 errors are for $L = 60\ {\rm fb}^{-1}$. LHC errors are for $L = 600\ {\rm fb}^{-1}$ for ATLAS+CMS. NLC errors are given for a luminosity times efficiency of $L\epsilon = 200\ {\rm fb}^{-1} \times 0.6$ at both $\sqrt{s} = 500\,{\rm GeV}$ and $\sqrt{s}_{Zh_{\rm SM}} \equiv m_Z + m_{h_{\rm SM}} + 20\,{\rm GeV}$. For recoil mass reconstruction we consider tracking/calorimetry cases 1 and 3 (*i.e.* super-JLC [29] and 'standard' NLC [24], respectively); for Higgs peak reconstruction in the $h_{\rm SM} \to b\bar{b}, W^+W^-$ final states, case 5, we assume 'standard' NLC [24] hadronic calorimetry. Beamstrahlung, bremsstrahlung and beam energy smearing effects upon the recoil mass reconstruction are neglected. NLC threshold results are for $L = 50\ {\rm fb}^{-1}$ at $\sqrt{s} = m_Z + m_{h_{\rm SM}} + 0.5\,{\rm GeV}$, *i.e.* just above threshold, and are quoted before including beamstrahlung, bremsstrahlung and beam energy smearing — at the NLC (FMC) these effects increase the error by about 35% (15%). FMC scan errors are for $L = 200\ {\rm fb}^{-1}$ devoted to the scan with beam energy resolution of 0.01%. TeV33 and NLC errors are statistical only. Systematic FMC error is neglected assuming extremely accurate beam energy determination.

Machine/Technique	$\Delta m_{h_{\rm SM}}$ (MeV)			
$\mathbf{m_{h_{SM}}}$**(GeV)**	**80**	m_Z	**100**	**110**
LEP2	250	400	–	–
TeV33	960	?	1500	2000
LHC/$\gamma\gamma$ (stat+syst)	90	90	95	100
NLC/case-3 $\sqrt{s} = 500$	813	674	572	494
NLC/case-1 $\sqrt{s} = 500$	370	264	196	151
NLC/hadronic $\sqrt{s} = 500$	51	?	51	51
NLC/case-3 $\sqrt{s} = \sqrt{s}_{Zh_{\rm SM}}$	27	29	31	34
NLC/case-1 $\sqrt{s} = \sqrt{s}_{Zh_{\rm SM}}$	3.6	3.8	4.1	4.4
NLC/hadronic $\sqrt{s} = \sqrt{s}_{Zh_{\rm SM}}$	15	17	19	22
NLC/threshold	40	70	55	58
FMC/scan	0.025	0.35	0.1	0.08
$\mathbf{m_{h_{SM}}}$**(GeV)**	**120**	**130**	**140**	**150**
TeV33	2700	–	–	–
LHC/$\gamma\gamma$ (stat+syst)	105	110	130	150
LHC/4ℓ (stat+syst)	–	164	111	90
NLC/case-3 $\sqrt{s} = 500$	432	383	343	311
NLC/case-1 $\sqrt{s} = 500$	120	97	80	68
NLC/hadronic $\sqrt{s} = 500$	52	52	53	55
NLC/case-3 $\sqrt{s} = \sqrt{s}_{Zh_{\rm SM}}$	37	40	44	48
NLC/case-1 $\sqrt{s} = \sqrt{s}_{Zh_{\rm SM}}$	4.8	5.2	5.6	6.1
NLC/hadronic $\sqrt{s} = \sqrt{s}_{Zh_{\rm SM}}$	24	27	30	34
NLC/threshold	65	75	85	100
FMC/scan	0.06	0.12	0.20	0.49
$\mathbf{m_{h_{SM}}}$**(GeV)**	**170**	**190**	**200**	**300**
LHC/4ℓ (stat+syst)	274	67	56	90
NLC/case-3 $\sqrt{s} = 500$	261	225	211	153
NLC/case-1 $\sqrt{s} = 500$	50	39	35	20
NLC/hadronic $\sqrt{s} = 500$	58	62	65	113
NLC/case-3 $\sqrt{s} = \sqrt{s}_{Zh_{\rm SM}}$	56	65	70	133
NLC/case-1 $\sqrt{s} = \sqrt{s}_{Zh_{\rm SM}}$	7.1	8.2	8.8	17
NLC/hadronic $\sqrt{s} = \sqrt{s}_{Zh_{\rm SM}}$	41	51	56	140
NLC/threshold	120	150	170	?

Much of the following material is summarized in more detail and with more referencing in [1]. We present here only a very rough summary. We often focus on strategies and results for a relatively light SM-like Higgs boson.

If the $h_{\rm SM}$ is seen in the $\gamma\gamma$ decay mode (as possible at the LHC and at the NLC or FMC with sufficient luminosity in mass regions M1, M2 and M3) or produced at the LHC via gluon fusion (as presumably could be verified for all mass regions) or produced in $\gamma\gamma$ collisions at the NLC, then Yang's theorem implies that it must be a scalar and not a vector, and, of course, it must have a CP$= +$ component (C and P can no longer be regarded as separately conserved once the Higgs is allowed to have fermionic couplings). If the Higgs is observed with substantial rates in production and/or decay channels that require it to have ZZ and/or WW couplings, then it is very likely to have a significant CP-even component given that the ZZ/WW coupling of a purely CP-odd Higgs boson arises only at one-loop. Thus, if there is a Higgs boson with anything like SM-like couplings it will be evident early-on that it has spin-zero and a large CP$= +$ component. Verifying that it is purely CP-even as predicted for the $h_{\rm SM}$ will be much more challenging.

As we have discussed in earlier sections, observation of a Higgs boson in the Zh and/or e^+e^-h mode at LEP2 or the NLC via the missing-mass technique yields a direct determination of the squared coupling $(ZZh)^2$. Other techniques allow determination of $(WWh)^2$. At LEP2 only Zh production is useful; for a SM-like Higgs boson its reach will be confined to $m_{h_{\rm SM}} \lesssim 95\,{\rm GeV}$ and the accuracy of the $(ZZh_{\rm SM})^2$ determination is quite limited ($\sim \pm 26\%$ at $m_{h_{\rm SM}} \sim m_Z$). Errors in the case of $L = 200\ {\rm fb}^{-1}$ at the NLC for a SM-like Higgs boson were quoted in Table X — for $m_{h_{\rm SM}} \lesssim 2m_W$, $(ZZh_{\rm SM})^2$ can be measured to $\pm 3\% - \pm 4\%$ and $(WWh_{\rm SM})^2$ to $\pm 5\% - \pm 8\%$. If the measurement yields the SM value to this accuracy, then the observed Higgs must be essentially purely CP-even unless there are Higgs representations higher than doublets. This follows from the sum rule

$$\sum_i (ZZh_i)^2 = \sum_i (WWh_i)^2 = 1 \qquad (11)$$

(where the $(VVh_i)^2$ – $V = W, Z$ – are defined relative to the SM-values) that holds when all Higgs bosons are in singlet or doublet representations. However, even if a single h appears to saturate the coupling strength sum-rule, the possibility remains that the Higgs sector is exotic and that saturation of the sum rule by a single h is purely accidental. Further, even if the ZZh coupling is not full strength the h could still be purely CP-even. To saturate the sum rule of Eq. (11), one need only have other Higgs bosons with appropriate CP-even components; such Higgs bosons are present in the many attractive models (including the minimal supersymmetric model) that contain additional doublet and/or some number of singlet Higgs representations beyond the single doublet Higgs field of the SM.

When the Zh rate is significant, as particularly true at the NLC, it will be possible to cross check that there is a large CP-even component by examining the angular distribution in

in the Zh (*i.e.* e^+e^-) center of mass. (For summaries, see Refs. [40, 1].) However, the Zh rate is adequate to measure the θ distribution only if the h has significant ZZh coupling, which in most models is only possible if the h has a significant CP-even component (since only the CP-even component has a tree-level ZZh coupling). Further, if the CP-even component dominates the ZZh coupling, it will also dominate the angular distribution which will then not be sensitive to any CP-odd component of the h that might be present. Thus, we arrive at the unfortunate conclusion that whenever the rate is adequate for the angular distribution measurement, the angular distribution will appear to be that for a purely CP-even Higgs, namely $d\sigma/d\cos\theta \propto 8m_Z^2/s + \beta^2 \sin^2\theta$, even if it contains a very substantial CP-odd component. (This insensitivity is numerically explicit in, for example, the results of Ref. [41].) Thus, observation of the above θ distribution only implies that the h has spin-0 and that it is not *primarily* CP-odd.

At machines other than the NLC, measurement of the θ distribution for Zh events will be substantially more difficult. Rates for Zh production will be at most just adequate for detecting the h at LEP2, TeV33 and the LHC. Further, at TeV33 (in the $h \to b\bar{b}$ channel) and at the LHC (in the $h \to \gamma\gamma$ channel) background rates are substantial (generally larger than the signal). Further, Wh production at TeV33 and the LHC cannot be employed because of inability to reconstruct the Wh center of mass (as required to determine θ) in the $W \to \ell\nu$ decay mode.

The $\tau^+\tau^-$ decays of the h provide a more democratic probe of its CP-even vs. CP-odd components [40, 42] than does the θ angular distribution. Further, the τ^+ and τ^- decays are self analyzing. The distribution in the azimuthal angle (ϕ) between certain effective 'spin' directions that can be defined for these decays depends upon the CP mixture for the h eigenstate. However, LEP2 is unlikely to produce the large number of events required for decent statistical precision for this measurement. For $m_h = 90\,\mathrm{GeV}$ and $\sqrt{s} = 192\,\mathrm{GeV}$, $\sigma(Zh) \sim 0.5$ pb, implying some 500 total events for $L = 1000\ \mathrm{pb}^{-1}$. With $BR(h \to \tau^+\tau^-) \sim 0.1$, we are left with only 50 events before taking into account efficiencies and the need for a fully reconstructable Z decay. Expectations at the NLC [40, 42] or FMC [42] are much better. Particularly valuable would be a combination of Zh with $h \to \tau^+\tau^-$ measurements at $\sqrt{s} = 500\,\mathrm{GeV}$ at the NLC and $\mu^+\mu^- \to h \to \tau^+\tau^-$ measurements in the s-channel mode at the FMC. Relatively good verification of the CP-even nature of a light SM-like h is possible. At higher Higgs masses (and higher machine energies) the self-analyzing nature of the $t\bar{t}$ final states of Higgs decay can be exploited in analogous fashion at the two machines.

One should not give up on a direct CP determination at the LHC. There is one technique that shows real promise. The key is the ability to observe the Higgs in the $t\bar{t}h$ production channel with $h \to \gamma\gamma$ or $h \to b\bar{b}$. We saw earlier that separation of the $t\bar{t}h$ from the Wh channel at the LHC can be performed with good efficiency and purity. The procedure for then determining the CP nature of the h was developed in Ref. [43]. The $\gamma\gamma$ decay mode shows the greatest promise because of a much smaller background. It is possible to define certain projection operators are are sensitive to the angular distributions of the t and $\bar{t}$ relative to the h. Assuming $m_h = 100\,\mathrm{GeV}$ and $L = 600\ \mathrm{fb}^{-1}$ for ATLAS+CMS combined, these projection operators distinguish between a SM-like (purely CP-even) Higgs boson and a purely CP-odd Higgs boson at roughly the 6σ to 7σ statistical level. For $m_h = 100\,\mathrm{GeV}$, discrimination between a SM-like Higgs boson and a Higgs which is an equal mixture of CP-even and CP-odd is possible at the 2σ to 3σ level. (These statements assume that the CP-even coupling squared plus CP-odd coupling squared for $t\bar{t}h$ is equal to the SM coupling-squared.) Of course, rates are only adequate for relatively light Higgs bosons. Verification of the efficiencies assumed in this analysis by full simulation will be important. The projection operator technique (but not the statistical significance associated with its application) is independent of the overall event rate.

There is also a possibility that polarized beams at the LHC could be used to look for spin asymmetries in the $gg \to h$ production rate that would be present if the h is a CP-mixed state [44].

Angular distributions in the $t\bar{t}h$ final state in e^+e^- collisions at the NLC or $\mu^+\mu^-$ collisions at the FMC are even more revealing than those in the $t\bar{t}h$ final state at the LHC. The analysis procedures appear in [45, 46] and are summarized in Sec. III.A. By combining Zh measurements with $t\bar{t}h$ measurements verification of the $t\bar{t}$ and ZZ couplings of a SM-like h will be possible at a remarkable level of accuracy [46]. For instance, for $\sqrt{s} = 1\,\mathrm{TeV}$ (we must be substantially above $t\bar{t}h$ threshold), 2 1/2 years of running is expected to yield $L = 500\ \mathrm{fb}^{-1}$ and in the case of $m_{h_{\rm SM}} = 100\,\mathrm{GeV}$ we can achieve a determination of the CP-even $t\bar{t}h_{\rm SM}$ coupling magnitude at the $\sim \pm 3\%$ level, the (CP-even) $ZZh_{\rm SM}$ coupling magnitude at the $\sim \pm 2\%$ level, and a meaningful limitation on the CP-odd $t\bar{t}h_{\rm SM}$ coupling magnitude.

The most elegant determination of the CP nature of Higgs boson is probably that possible in $\gamma\gamma \to h$ production at the $\gamma\gamma$ collider facility of the NLC [47]. Since the CP-even and CP-odd components of a Higgs boson couple with similar strength to $\gamma\gamma$ (via one-loop graphs), there is no masking of the CP-odd component such as occurs using probes involving ZZh or WWh couplings. The precise technique depends upon whether the Higgs is a pure or a mixed CP eigenstate.

- The most direct probe of a CP-mixed state is provided by comparing the Higgs boson production rate in collisions of two back-scattered-laser-beam photons of different helicities [47]. The difference in rates for photons colliding with $++$ vs. $--$ helicities is non-zero only if CP violation is present. A term in the cross section changes sign when both photon helicities are simultaneously flipped. Experimentally, this is achieved by simultaneously flipping the helicities of both of the initiating back-scattered laser beams. One finds that the asymmetry is typically larger than 10% and is observable if the CP-even and CP-odd components of the h are both substantial.

- In the case of a CP-conserving Higgs sector, one must have colliding photons with substantial transverse polarization.

back-scattered laser beams (while maintaining the ability to rotate these polarizations relative to one another) and optimizing the laser beam energy. This optimization has been discussed in Refs. [48, 40]. By computing the difference in rates for parallel vs. perpendicular polarizations divided by the sum, which ratio is $+1$ (-1) for a CP-even (CP-odd) Higgs boson, it is found that $\gamma\gamma$ collisions may well allow direct verification that a SM-like h is CP-even vs. CP-odd.

A $\mu^+\mu^-$ collider might provide an analogous opportunity for directly probing the CP properties of any Higgs boson that can be produced and detected in the s-channel mode [49, 1]. However, it must be possible to transversely polarize the muon beams. Assume that we can have 100% transverse polarization and that the μ^+ transverse polarization is rotated with respect to the μ^- transverse polarization by an angle ϕ. The production cross section for a h with coupling of a mixed CP nature exhibits a substantial asymmetry of the form [49]

$$A_1 \equiv \frac{\sigma(\pi/2) - \sigma(-\pi/2)}{\sigma(\pi/2) + \sigma(-\pi/2)} \,. \tag{12}$$

For a pure CP eigenstate, the asymmetry [1]

$$A_2 \equiv \frac{\sigma(\pi) - \sigma(0)}{\sigma(\pi) + \sigma(0)} \tag{13}$$

is $+1$ or -1 for a CP-even or CP-odd h, respectively. Of course, background processes in the final states where a Higgs boson can be most easily observed (*e.g.* $b\bar{b}$ for the MSSM Higgs bosons) will typically dilute these asymmetries substantially. Whether or not they will prove useful depends even more upon our very uncertain ability to transversely polarize the muon beams while maintaining high luminosity.

III. NON-MINIMAL HIGGS SECTORS

Five new projects were developed and pursued:

A) determining the accuracy with which the $t\bar{t}$ CP-even and CP-odd Yukawa couplings and the ZZ coupling of a general neutral Higgs boson (h) could be measured by using both the $e^+e^- \to t\bar{t}h$ and $e^+e^- \to Zh$ production processes (or the $\mu^+\mu^-$ analogues);

B) determining the extent to which discovery of at least one Higgs boson of the NMSSM is guaranteed at the LHC;

C) detecting $A^0 \to \gamma\gamma$ at the LHC;

D) determining $\tan\beta$ in the MSSM using measurements of $gg \to H^0, A^0$ and $gg \to H^0 b\bar{b}, A^0 b\bar{b}$ production at the LHC;

E) evaluating the prospects for discovering and studying the heavy $H^0, A^0, H^\pm$ in H^0A^0 and H^+H^- pair production at the NLC or FMC and thereby constraining $\tan\beta$ and GUT-scale boundary conditions;

for discovering the H^0, A^0 in s-channel production at the FMC;

G) determining the discovery reach for doubly-charged Higgs bosons in the process $p\overline{p} \to \Delta^{--}\Delta^{++}$ with $\Delta^{--} \to \ell^-\ell^-, \Delta^{++} \to \ell^+\ell^+$ ($\ell = e, \mu, \tau$) at TeV33.

In what follows we motivate the importance of these projects and summarize the results obtained.

A. Determining the $t\bar{t}$ and ZZ couplings of a neutral Higgs boson [46]

It is very possible (some would say probable) that the SM is not correct. In this case, and if there is a weakly-coupled Higgs sector, there will certainly be Higgs bosons that do not have SM-like couplings. In particular, if one neutral Higgs is very SM-like (as for example is very probable in the minimal supersymmetric model), the others must have very small ZZ coupling and can have all manner of $t\bar{t}$ couplings. Thus, it will be crucial to determine if an observed Higgs boson fits into a given model context, such as the two-Higgs-doublet model, and to determine the model parameters and associated couplings for acceptable solutions. By doing this for all the Higgs bosons we would be able to completely fix the Higgs sector model and parameters.

The $t\bar{t}$ and ZZ couplings of a neutral Higgs boson take the form:

$$t\bar{t}h : -\bar{t}(a + ib\gamma_5)t\frac{gm_t}{2m_W} \;, \quad ZZh : c\frac{gm_Z}{cos(\theta_W)}g_{\mu\nu} \;, \tag{14}$$

where g is the usual electroweak coupling constant. For the SM, $a = 1, b = 0, c = 1$. However, these couplings become free parameters in a general Higgs sector model. For example, in the general two-Higgs doublet model, 2HDM, the couplings are

$$a = \frac{R_{2j}}{\sin\beta} \;, \quad b = R_{3j}\cot\beta \;, \quad c = R_{1j}\cos\beta + R_{2j}\sin\beta \;, \tag{15}$$

where $j = 1, 2, 3$ indicates one of the three Higgs mass eigenstates, $\tan\beta$ is the ratio of the vacuum expectation values of the neutral members of the two Higgs doublets (we assume a type-II 2HDM), and R_{ij} is a 3×3 orthogonal matrix which specifies the transformation between the 2HDM Higgs fields and the Higgs boson mass eigenstates. The result is that

$$a = -\frac{s_1c_2}{\sin\beta} \;, \quad b = s_1s_2\cot\beta \;, \quad c = c_1\cos\beta - s_1c_2\sin\beta \;, \tag{16}$$

where $s_i = \sin\alpha_i$ and $c_i = \cos\alpha_i$ and $\alpha_{1,2}$ are free parameters in the range $0 \le \alpha_{1,2} < 2\pi$. The h has CP-violating couplings if either $ab \neq 0$ or $bc \neq 0$.

The optimal technique [45] for extracting the couplings from the $t\bar{t}h$ process is reviewed in [46]. It makes full use of the distribution $d\sigma/d\phi$ of the t, $\bar{t}$ and h in the final state as a function of the final state kinematical variables, ϕ (rather than just the total cross section). One of the t's is required to decay semi-leptonically and the other hadronically in order to reconstruct all

ial (neglecting the 1-loop ZZ coupling to the CP-odd part of the h in comparison to the tree-level ZZ coupling to the CP-even part of h); only the total rate for Zh with $Z \to e^+e^-$ or $\mu^+\mu^-$ (with the Higgs observed as a peak in the recoil mass spectrum) is employed. In order to demonstrate the power of combining the $t\bar{t}h$ and Zh processes, we have considered a NLC or FMC with $\sqrt{s} = 1\,\mathrm{TeV}$ (energy substantially above the $t\bar{t}h$ threshold is needed) and a light Higgs boson with mass $m_h = 100\,\mathrm{GeV}$. We assume integrated luminosity of $L = 500\ \mathrm{fb}^{-1}$ (about 2 1/2 years of running at the presumed design luminosity of $L = 200\ \mathrm{fb}^{-1}$ per year at $\sqrt{s} = 1\,\mathrm{TeV}$). Appropriate efficiency factors (which include relevant branching ratios) are employed. For details see [46]. Our procedure is to input a given 2HDM and determine the accuracy with which the input parameters can be extracted from the data. Our quantitative measure of accuracy is the χ^2 associated with choices for a, b, and c that differ from the values of the input model.[24] The total χ^2 is computed by combining the $t\bar{t}h$ and Zh processes:

$$\chi^2 = \chi^2(t\bar{t}h) + \chi^2(Zh)\,; \tag{17}$$

$\chi^2(t\bar{t}h)$ is computed using the full correlated error matrix.

We discuss one example in detail. We take a 2HDM model with $\tan\beta = 0.5$, $\alpha_1 = \pi/4$ and $\alpha_2 = \pi/2$ as our input model.[25] For the alternative models, we considered $\tan\beta = 0.5$, $\tan\beta = 1.0$ and $\tan\beta = 1.5$, and computed χ^2 as a function of α_1 and α_2 assuming the 2HDM forms of a, b, c as given in Eq. (16).[26] We first note that, in the case of the particular input model specified above, only $\tan\beta = 0.5$ (the input value), and not $\tan\beta = 1$ or 1.5, yields any a, b, c value set (as $\alpha_{1,2}$ are varied) that leads to $\chi^2 \leq 9$. Thus, an approximate determination of $\tan\beta$ would be possible. In Fig. 13, we take $\tan\beta = 0.5$ and plot different χ^2 regions in the (α_1, α_2), (a, b) and (a, c) planes. In each window of the figure, a filled central region, an empty band, and a filled band may all be visible. The central region is the $\chi^2 \leq 1$ region, the empty band is the $1 < \chi^2 \leq 4$ region, and the outer filled band is the $4 < \chi^2 \leq 9$ region. If no filled central region is visible, the central region being empty, then this means that $\chi^2 \leq 1$ was not possible. If only a completely filled region appears, then $\chi^2 \leq 4$ was not possible. From the χ^2 regions of Fig 13 we arrive at the following additional results.

- The $\chi^2 \leq 1$ region for $\tan\beta = 0.5$ corresponds closely to the input values of $\alpha_1 = \pi/4$ and $\alpha_2 = \pi/2$. An alternative region with $\alpha_1 \to \pi - \alpha_1$ develops for $4 < \chi^2 \leq 9$.
- The values of a, b, c are well-determined if we demand $\chi^2 \leq 1$; $\chi^2 \leq 4$ allows only slightly greater flexibility. However, $4 < \chi^2 \leq 9$ allows a a solution with the wrong sign of ac.]

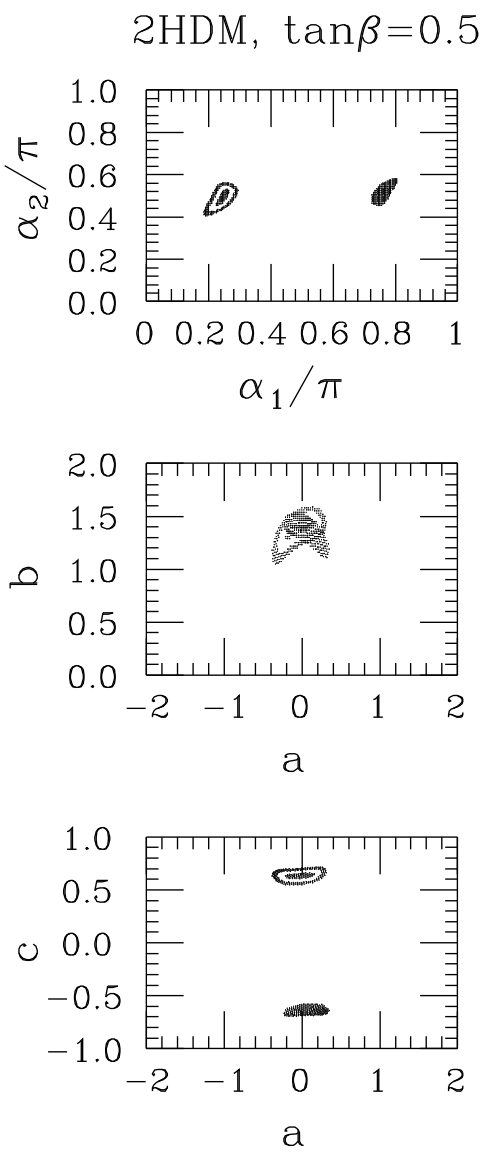

Figure 13: $\chi^2 \leq 1$, $1 < \chi^2 \leq 4$ and $4 < \chi^2 \leq 9$ regions in the $(\alpha_1/\pi, \alpha_2/\pi)$, (a, b) and (a, c) planes, assuming as input a 2HDM model with $\tan\beta = 0.5$, $\alpha_1 = \pi/4$ and $\alpha_2 = \pi/2$.

Of course, if the h being studied is the SM h_{SM} or simply SM-like, the above $t\bar{t}h/Zh$ techniques can be employed to verify the SM a, b, c couplings, see Ref. [46]. Another interesting extreme is a purely CP-odd Higgs boson, a. (For example, the A^0 of the MSSM.) The a might be light enough and $\tan\beta$ small enough that the $t\bar{t}a$ production rate would be large. It was demonstrated in Ref. [45] that the b coupling of a CP-odd a with

[24] Since $d\sigma/d\phi(t\bar{t}h)$ and $\sigma_T(Zh)$ are only sensitive to a^2, c^2, b^2, ac and bc, nothing changes if we simultaneously flip the signs of a, b, c. Thus, there will inevitably be an overall sign ambiguity.

[25] We take $\tan\beta$ to be small so that the $t\bar{t}h$ rate is substantial. If $\tan\beta$ is large, the $t\bar{t}h$ process will have too small an event rate to be terribly useful. If $\tan\beta$ is large enough, the $b\bar{b}h$ final state can be employed in analogous fashion; it would be best to run at smaller $\sqrt{s}$ in such a case.

[26] We considered only $0 \leq \alpha_{1,2} < \pi$ so as to avoid the above-noted overall sign ambiguity.

and significant limits placed on the a, c couplings using $t\bar{t}a$ data alone.[27]

We note that systematic uncertainties in the experimental determination of the overall normalization of the $t\bar{t}h$ and Zh total cross sections could have substantial impact on our ability to determine couplings if the systematic errors are not small compared to the statistical errors. Also, at larger Higgs masses, statistics will deteriorate; higher $L_{\rm total}$ will be required to avoid significant ambiguity in the coupling determinations. However, even when ambiguities emerge, they are usually sufficiently limited that the type of analysis outlined above will make a critical contribution to gaining a clear understanding of the exact nature of all the Higgs bosons. Certainly, the procedures discussed will provide a powerful means for distinguishing between substantially different models.

B. Is discovery of a NMSSM Higgs boson guaranteed with LEP2 plus LHC? [50]

It is well-established [1] that at least one of the Higgs bosons of the MSSM can be discovered either at LEP2 or at the LHC throughout all of the standard $(m_{A^0}, \tan\beta)$ parameter space. Ref. [50] reconsiders this issue in the context of the NMSSM, in which there is greater freedom by virtue of there being three instead of two CP-even Higgs bosons and correspondingly greater freedom in their couplings. It is found that there are regions of parameter space for which none of the NMSSM Higgs bosons can be detected at either LEP2 or the LHC. This result is to be contrasted with the NLC or FMC no-lose theorem [51], according to which at least one of the CP-even Higgs bosons (denoted generically by h) of the NMSSM will be observable in $Z^\star \to Zh$ production.

The detection modes considered for the NMSSM are the same as those employed in establishing the LEP2 plus LHC no-lose theorem for the MSSM: 1) $Z^\star \to Zh$ at LEP2; 2) $Z^\star \to ha$ at LEP2; 3) $gg \to h \to \gamma\gamma$ at LHC; 4) $gg \to h \to ZZ^\star$ or $ZZ \to 4\ell$ at LHC; 5) $t \to H^+ b$ at LHC; 6) $gg \to b\bar{b}h, b\bar{b}a \to b\bar{b}\tau^+\tau^-$ at LHC; 7) $gg \to h, a \to \tau^+\tau^-$ at LHC. Additional Higgs decay modes that could be considered at the LHC include: a) $a \to Zh$; b) $h \to aa$; c) $h_j \to h_i h_i$; d) $a, h \to t\bar{t}$. Because of the more complicated Higgs self interactions, b) and c) cannot be reliably computed in the NMSSM without additional assumptions. The Higgs mass values for which mode a) is kinematically allowed can be quite different than those relevant to the MSSM and thus there are uncertainties in translating ATLAS and CMS results for the MSSM into the present more general context. Finally, mode d) is currently of very uncertain status and might turn out to be either more effective or less effective than current estimates. Thus, to be conservative, any choice of NMSSM parameters for which the modes a)-d) might be relevant is excluded. Even over this restricted region of parameter space, NMSSM parameter choices can be found such that there are no observable Higgs signatures at either LEP2 or

[27] Numerical details for the A^0 of the MSSM would differ slightly due to the fact that the other Higgs bosons would also be light, whereas in Ref. [45] it was assumed that only the a was light.

The free parameters of the model can be chosen to be $\tan\beta$, m_{h_1}, λ, $\alpha_{1,2,3}$, and m_a. Here, m_{h_1} is the mass of the lightest CP-even Higgs mass eigenstate. λ appears in the superpotential in the term $W \ni \lambda \hat{H}_1 \hat{H}_2 \hat{N}$. A crucial ingredient in constraining the model is that $\lambda \lesssim 0.7$ is required if λ is to remain perturbative during evolution from scale m_Z to the Planck scale. This limitation on λ implies a $\tan\beta$-dependent upper limit on m_{h_1} in the range $\lesssim 140\,{\rm GeV}$. The angles $\alpha_{1,2,3}$ are those parameterizing the orthogonal matrix which diagonalizes the CP-even Higgs mass-squared matrix. m_a is the mass of the lighter of the two CP-odd mass eigenstates — the second CP-odd state can be assumed to be very massive for the purposes of establishing the existence of parameter choices for which no Higgs boson can be found. All couplings and cross sections are determined once the above parameters are specified. Details regarding the procedure for scanning the NMSSM parameter space and assessing observability of the various Higgs bosons are given in Ref. [50]. A choice of parameters such that none of the Higgs bosons $h_{1,2,3}$, a or $H^\pm$ are observable at LEP2 or the LHC is declared to be a "point of unobservability" or a "bad point".

The results obtained are the following. If $\tan\beta \lesssim 1.5$ then all parameter points that are included in the search are observable for m_{h_1} values up to the maximum allowed ($m_{h_1}^{\rm max} \sim 137\,{\rm GeV}$ for $\lambda_{\rm max} = 0.7$, after including radiative corrections). For such low $\tan\beta$, the LHC $\gamma\gamma$ and 4ℓ modes allow detection if LEP2 does not. For high $\tan\beta \gtrsim 10$, the parameter regions where points of unobservability are found are also of very limited extent, disappearing as the $b\bar{b}h_{1,2,3}$ and/or $b\bar{b}a$ LHC modes allow detection where LEP2 does not. However, significant portions of searched parameter space contain points of unobservability for moderate $\tan\beta$ values. That such $\tan\beta$ values should be the most 'dangerous' can be anticipated from the MSSM results. It is well-known (see, for example, Ref. [1]) that for stop masses of order 1 TeV and no stop-mixing there is a wedge of MSSM parameter space at moderate $\tan\beta$ and with H^0 and A^0 masses above about 200 GeV for which the only observable MSSM Higgs boson is the light SM-like h^0, and that the h^0 can only be seen in the $\gamma\gamma$ mode(s) at the LHC. (Observation at LEP2 is impossible in this wedge of parameter space since $m_{h^0} + m_Z, m_{h^0} + m_{A^0} > 192\,{\rm GeV}$.) By choosing m_{h_1} and m_a in the NMSSM so that $m_{h_1} + m_Z$ and $m_{h_1} + m_a$ are close to or above the $\sqrt{s}$ of LEP2, then, by analogy, at moderate $\tan\beta$ we would need to rely on the $h_{1,2,3} \to \gamma\gamma$ modes. However, in the NMSSM, parameter choices are possible for which all the $WWh_{1,2,3}$ couplings are reduced relative to SM strength. This reduction will suppress the $\gamma\gamma$ couplings coming from the W-boson loop. All the $h_i \to \gamma\gamma$ widths can be sufficiently smaller than the somewhat enhanced $b\bar{b}$ widths so that the $\gamma\gamma$ branching ratios are *all* no longer of useful size.

To illustrate, we shall discuss results for $\tan\beta = 3$, $\tan\beta = 5$ and $\tan\beta = 10$ (for which $m_{h_1}^{\rm max} \sim 124\,{\rm GeV}$, $118\,{\rm GeV}$ and $114\,{\rm GeV}$, respectively) and $m_{h_1} = 105\,{\rm GeV}$.

- In Fig. 14, we display for $\tan\beta = 5$ both the portions of $(\alpha_1, \alpha_2, \alpha_3)$ parameter space that satisfy our search restrictions, and the regions (termed "regions of unobserv-

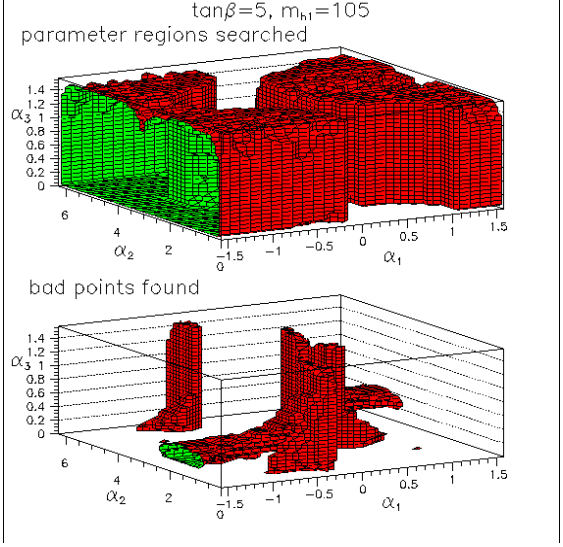

Figure 14: For $\tan\beta = 5$ and $m_{h_1} = 105\,\text{GeV}$, we display in three dimensional $(\alpha_1, \alpha_2, \alpha_3)$ parameter space the parameter regions searched (which lie within the surfaces shown), and the regions therein for which the remaining model parameters can be chosen so that no Higgs boson is observable (interior to the surfaces shown).

ability") within the searched parameter space such that, for *some* choice of the remaining parameters (λ and m_a), no Higgs boson will be detected using any of the techniques discussed earlier.[28] Relatively large regions of unobservability within the searched parameter space are present.

- At $\tan\beta = 3$, a similar picture emerges. The search region that satisfies our criteria is nearly the same; the regions of unobservability lie mostly within those found for $\tan\beta = 5$, and are about 50% smaller.

- For $\tan\beta = 10$, the regions of unobservability comprise only a very small portion of those found for $\tan\beta = 5$. This reduction is due to the increased $b\bar{b}$ couplings of the h_i and a, which imply increased $b\bar{b}h_i, b\bar{b}a$ production cross sections. As these cross sections become large, detection of at least one of the h_i and/or the a in the $b\bar{b}\tau^+\tau^-$ final state becomes increasingly difficult to avoid. For values of $\tan\beta \gtrsim 10$,[29] we find that one or more of the h_i, a should be observable regardless of location in $(\alpha_1, \alpha_2, \alpha_3, \lambda, m_a)$ parameter space (within the somewhat restricted search region that we explore).

It is useful to present details on what goes wrong at a typical point of unobservability. For $\tan\beta = 5$ and $m_{h_1} = 105\,\text{GeV}$, -0.479, $\alpha_2 = 0.911$, $\alpha_3 = 0.165$, and $\lambda = 0.294$ (for which $m_{h_2} = 124\,\text{GeV}$, $m_{h_3} = 206\,\text{GeV}$, and $m_{H^+} = 201\,\text{GeV}$). For this point, the Higgs boson couplings (relative to the SM values) are:

$$\begin{array}{ccc} (VVh_1)^2 = 0.79 & (VVh_2)^2 = 0.21 & (VVh_3)^2 = 0.006 \\ (b\bar{b}h_1)^2 = 5.3 & (b\bar{b}h_2)^2 = 2.5 & (b\bar{b}h_3)^2 = 18 \\ (t\bar{t}h_1)^2 = 0.69 & (t\bar{t}h_2)^2 = 0.29 & (t\bar{t}h_3)^2 = 0.062 \end{array}$$

where $V = W$ or Z. Note that h_3 has very small couplings to VV. The manner in which this point escapes discovery is now apparent. First, the minimum values required for the $(b\bar{b}h_i)^2$ values for h_i observability in the $\tau^+\tau^-$ mode are: 53 ($i = 1$); 32 ($i = 2$); 35 ($i = 3$). The actual values all lie below these required values. Observation of the a at $m_a = 103\,\text{GeV}$ would require $\tan\beta = 8$. Regarding the other discovery modes, h_1 and h_2 are both in the mass range for which the $\gamma\gamma$ mode is potentially viable and the h_3 is potentially detectable in the $ZZ \to 4\ell$ channel. However, the suppressed $t\bar{t}h_{1,2,3}$ couplings imply smallish gg production rates for $h_{1,2,3}$. Relative to a SM Higgs of the same mass we have:

$$\frac{(ggh_i)^2}{(ggh_{\rm SM})^2} = 0.58\ (i=1); \quad 0.43\ (i=2); \quad 0.15\ (i=3)\,. \tag{18}$$

(Note that these strengths are not simply the $(t\bar{t}h_i)^2$ magnitudes; the enhanced b-quark loop contributions interfere with the t-quark loop contributions at amplitude level.) Further, the enhanced Higgs decay rate to $b\bar{b}$ and the reduced W-loop contributions to the $\gamma\gamma$ coupling suppress the $\gamma\gamma$ branching ratios of h_1 and h_2 relative to SM expectations. We find:

$$\frac{BR(h_i \to \gamma\gamma)}{BR(h_{\rm SM} \to \gamma\gamma)} = 0.18\ (i=1)\,; \quad 0.097\ (i=2)\,; \tag{19}$$

i.e. suppression sufficient to make h_1 and h_2 invisible in the $\gamma\gamma$ mode. The suppressed ZZh_3 coupling and the enhanced $h_3 \to b\bar{b}$ decays are sufficient to suppress $BR(h_3 \to ZZ)$ much below SM expectations:

$$\frac{BR(h_3 \to ZZ)}{BR(h_{\rm SM} \to ZZ)} = 0.11\,, \tag{20}$$

i.e. such that the 4ℓ signal has a significance of only 1.5σ, even though a SM Higgs of this mass would yield a $\sim 37\sigma$ signal. In short, there is enough flexibility due to the addition of the singlet Higgs field (which has no couplings to SM fermions and vector bosons!) for *all* the Higgs bosons to escape detection for certain choices of model parameters, provided $\tan\beta$ is moderate in size. Moderate $\tan\beta$ implies that $h \to \gamma\gamma$ decays for light Higgs are suppressed, while at the same time $b\bar{b}h$ production is not adequately enhanced for detection of the $h \to \tau^+\tau^-$ mode.

The regions of NMSSM parameter space where no Higgs boson can be detected will expand if full $L = 600\ \text{fb}^{-1}$ ($L = 1000\ \text{pb}^{-1}$) luminosity is not available at the LHC (LEP2) or efficiencies are smaller than anticipated. Conversely, these "regions of unobservability" could decrease substantially (perhaps

[28] For a given $\alpha_{1,2,3}$ value such that there is a choice of λ and m_a for which no Higgs boson is observable, there are generally other choices of λ and m_a for which at least one Higgs boson *is* observable.

[29] The precise value of the critical lower bound on $\tan\beta$ depends sensitively on m_{h_1}.

calorimeter) in the $\tau\tau$ final state or higher luminosity. Supersymmetric decays of the Higgs bosons are neglected in the above. If these decays are important, the regions of unobservability found without using the SUSY final states will increase in size. However, Higgs masses in the regions of unobservability are typically modest in size ($100 - 200\,\mathrm{GeV}$), and as SUSY mass limits increase with LEP2 running this additional concern will become less relevant. Of course, if SUSY decays are significant, detection of the Higgs bosons in the SUSY modes might be possible, in which case the regions of unobservability might decrease in size. Assessment of this issue is dependent upon a specific model for soft SUSY breaking.

Although it is not possible to establish a no-lose theorem for the NMSSM Higgs bosons by combining data from LEP2 and the LHC (in contrast to the no-lose theorems applicable to the NLC Higgs search with $\sqrt{s} \gtrsim 300\,\mathrm{GeV}$), the regions of complete Higgs boson unobservability appear to constitute a small fraction of the total model parameter space. It would be interesting to see whether or not these regions of unobservability correspond to unnatural choices for the Planck scale supersymmetry-breaking parameters.

C. Detecting $A^0 \to \gamma\gamma$ at the LHC [52]

In this report, a realistic study was performed of observability for the CP-odd Higgs boson (A^0) in the minimal supersymmetric standard model (MSSM) via its photon decay mode ($A^0 \to \gamma\gamma$) with the CMS detector performance. It is demonstrated that it will be possible to discover the CP-odd A^0 and reconstruct its mass (m_{A^0}) with high precision for 170 GeV $< m_{A^0} < 2m_t$ at the LHC if the decays of the A^0 into SUSY particles are forbidden and $\tan\beta$ is close to one. Thus, the $A^0 \to \gamma\gamma$ mode complements the $\mu^+\mu^-$ decay modes ($h^0, H^0, A^0 \to \mu\mu$) that are promising [10, 53] for observing and precisely reconstructing masses for the neutral Higgs bosons at large $\tan\beta$.

The total cross section for the process $pp \to A^0 \to \gamma\gamma + X$ is given by $\sigma(pp \to A^0 + X)BR(A^0 \to \gamma\gamma)$; $\sigma(pp \to A^0 + X)$ is evaluated using the parton distribution functions of CTEQ2L with $\Lambda_4 = 0.190$ GeV and $Q^2 = m^2_{A^0}$.

Gluon fusion ($gg \to A^0$), via the top quark and the bottom quark triangle loop diagrams, is the major source for the CP-odd Higgs pseudoscalar if $\tan\beta$ is less than about 4. At higher $\tan\beta$, $gg \to A^0 b\bar{b}$ dominates since the $(b\bar{b}A^0)^2$ coupling-squared is proportional to $\tan^2\beta$. In the computations, both production mechanisms are included. QCD radiative corrections, which, for example, increase $\sigma(gg \to A^0)$ by about 50% to 80% for $\tan\beta \sim 1$, are not included for either the signal or the backgrounds.

The $b\bar{b}$ mode dominates A^0 decays for $\tan\beta \gtrsim 4$ and $m_{A^0} \leq 2m_t$. For $m_Z + m_{h^0} < m_{A^0} \leq 2m_t$ and $\tan\beta < 4$, $BR(A^0 \to Zh)$ is comparable to $BR(A^0 \to b\bar{b})$. If present, SUSY decay modes would deplete both. In the analysis, parameters were chosen so that $A^0 \to$SUSY decays are kinematically forbidden. Then, for $\tan\beta$ close to 1 and 170 GeV $< m_{A^0} < 2m_t$ $BR(A^0 \to \gamma\gamma) \sim 5 \cdot 10^{-4} - 2 \cdot 10^{-3}$.

Events were simulated at the particle level using PYTHIA 5.7 tribution functions. The PYTHIA/JETSET outputs were processed with the CMSJET program [54], which is designed for fast simulations of "realistic" CMS detector response. Resolution effects were taken into account by using the parameterizations obtained from the detailed GEANT [55] simulations. CMSJET includes also some analysis programs, in particular, a set of jet reconstruction algorithms.

The irreducible backgrounds considered were: (i) $q\bar{q} \to \gamma\gamma$ and (ii) $gg \to \gamma\gamma$ (Box). In addition, reducible backgrounds with at least 1 γ in the final state were included: (i) $q\bar{q} \to g\gamma$, (ii) $qg \to q\gamma$, and (iii) $gg \to g\gamma$ (Box).

The ECAL resolution was assumed to be $\sigma(E)/E = 5\%/\sqrt{E} \oplus 0.5\%$ (CMS high luminosity regime). Each photon was required to have transverse momentum (p_T) larger than 40 GeV and $|\eta| < 2.5$. Both photons were required to be isolated, *i.e.*, (1) no charged particle with $p_T > 2$ GeV in the cone $R = 0.3$; and (2) the total transverse energy $\sum E_T^{cell}$ must be less than 5 GeV in the cone ring $0.1 < R < 0.3$. In this preliminary analysis, no rejection power against π^0's with high p_T was assumed; this means all π^0's surviving the cuts (p_T, isolation, etc.) were considered as γ's.[30] For each m_{A^0} and $\tan\beta$, the mass window around the peak (within the range 2-6 GeV) and the p_T cut (50-100 GeV) were chosen to provide the best value of $S/\sqrt{B}$. For example, the best values of the mass window and p_T cut for $m_{A^0} = 200$ GeV (350 GeV) are 2 GeV (4 GeV) and 60 GeV (100 GeV), respectively.

A typical $M_{\gamma\gamma}$ distribution is shown in Fig. 15. The $L = 100\ \mathrm{fb}^{-1}$ and $300\ \mathrm{fb}^{-1}$ 5σ discovery contours are shown in Fig. 16. Apparently, this channel should provide a good opportunity to observe and precisely reconstruct the CP-odd Higgs boson mass (m_{A^0}) for 170 GeV $< m_{A^0} < 2m_t$ if the $A^0 \to$SUSY decays are forbidden and $\tan\beta$ is close to one. The impact of SUSY decays on this discovery channel might be significant [56] and is under investigation with realistic simulations.

D. Determining $\tan\beta$ in the MSSM from A^0 and H^0 production at the LHC [57]

As noted in a previous subsection (see Ref. [1] for a thorough review), detection of single A^0 and/or H^0 production at the LHC will be possible in several regions of $(m_{A^0}, \tan\beta)$ parameter space. In particular, $gg \to H^0$ and $gg \to A^0$ inclusive production can be isolated in the $H^0, A^0 \to \tau^+\tau^-$ decay mode if $\tan\beta$ is modest in size ($\lesssim 3$) and m_{A^0}, m_{H^0} are below $2m_t$. It is mainly the A^0 which provides a viable signal in this region of parameter space. For masses above $2m_t$, there is also some hope for detection in the $gg \to H^0, A^0 \to t\bar{t}$ decay mode, provided the $t\bar{t}$ background normalization and shape can be determined at about the 5-10% level. Since $m_{A^0} \sim m_{H^0}$ at higher mass, it is the combined $gg \to H^0 + gg \to A^0$ signal that will be observed. At high $\tan\beta$, the H^0 and A^0 have enhanced $b\bar{b}$ coupling resulting in large rates for the $gg \to H^0 b\bar{b}$ and $gg \to A^0 b\bar{b}$ processes; detection of these production modes

[30] This is quite conservative. The background from the π^0 is overestimated, especially in the low mass $M_{\gamma\gamma}$ region.

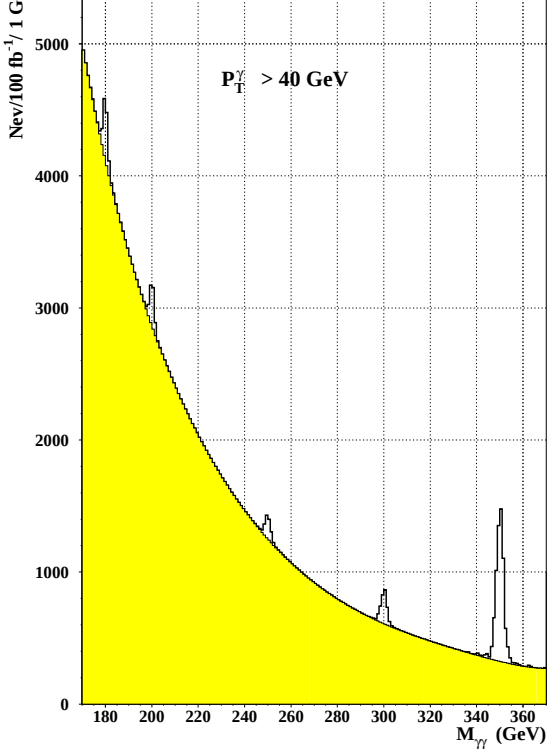

Figure 15: Number of events vs. $M_{\gamma\gamma}$ for the signal and the background at $\sqrt{s} = 14$ TeV with $L = 100$ fb^{-1} and $\tan\beta = 1$. CMS performance is assumed and SUSY parameters are $m_{\tilde{q}} = \mu = 1000$ GeV.

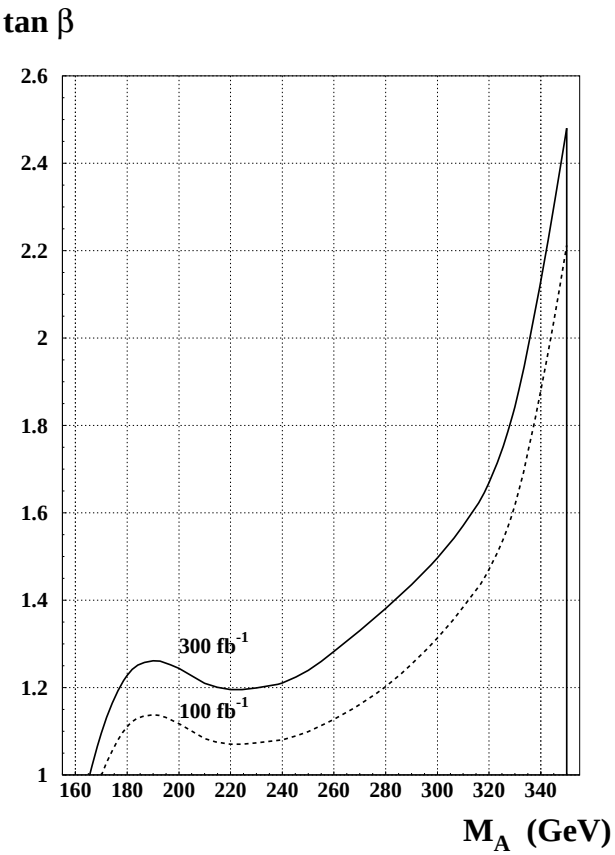

Figure 16: The 5σ $A^0 \to \gamma\gamma$ discovery contours in the $(m_{A^0}, \tan\beta)$ plane at $\sqrt{s} = 14$ TeV with $L = 100$ fb^{-1} and $L = 300$ fb^{-1}. CMS performance is assumed and SUSY parameters are $m_{\tilde{q}} = \mu = 1000$ GeV. The discovery regions lie below the contours shown.

in the $H^0, A^0 \to \tau^+\tau^-$, $\mu^+\mu^-$ and, perhaps, $b\bar{b}$ decay channels will be possible. (At high $\tan\beta$, these are the only important decay modes since they are the only ones associated with enhanced coupling, $\propto \tan\beta$ at the amplitude level.) In the $(m_{A^0}, \tan\beta)$ parameter space, the lowest value of $\tan\beta$ for which $gg \to H^0 b\bar{b}, A^0 b\bar{b} \to \tau^+\tau^- b\bar{b}$ production can be observed ranges from $\tan\beta \gtrsim 3$ at $m_{A^0} \sim 200\,\mathrm{GeV}$ to $\tan\beta \gtrsim 15$ at $m_{A^0} \sim 500\,\mathrm{GeV}$. Still higher $\tan\beta$ values would be required at higher m_{A^0} simply due to the fact that the cross section decreases (at fixed $\tan\beta$) as m_{A^0} increases. A similar range of viability may be possible in the $b\bar{b}b\bar{b}$ final state, if b tagging can be performed at the optimistic end of current efficiency and purity expectations [58]. Higher $\tan\beta$ values are required for viability of the signal in the $\mu^+\mu^- b\bar{b}$ final state (simply because of the much smaller rates deriving from the much smaller $\mu^+\mu^-$ branching ratios for the H^0 and A^0). At high $\tan\beta$, the degeneracy between the A^0 and H^0 is such that their independent signals would not be separable, except, possibly, in the $\mu^+\mu^-$ mode.

The $\tan\beta$ dependence of H^0 and A^0 rates implicit in the above discussion is quantified in Fig. 17, which displays the $gg \to H^0$, $gg \to A^0$, $gg \to b\bar{b}H^0$ and $gg \to b\bar{b}A^0$ cross sections (and separate t and b loop contributions to the first two).[31] At low $\tan\beta$, we see that the $gg \to H^0$ and, especially, $gg \to A^0$ cross sections fall rapidly as the t-loop contribution falls with increasing $\tan\beta$. At high $\tan\beta$, the rapid rise of the $gg \to H^0 b\bar{b}$ and $gg \to A^0 b\bar{b}$ cross sections is apparent.

The strong $\tan\beta$ dependence of the $gg \to H^0, A^0$ and $gg \to b\bar{b}H^0, b\bar{b}A^0$ discovery modes will provide an opportunity for determining the otherwise somewhat elusive $\tan\beta$ parameter. The sensitivity to $\tan\beta$ depends on the accuracy with which these cross sections can be measured and the rate of their variation with $\tan\beta$. The possibility of determining $\tan\beta$ in this manner was noted in Ref. [59] (see remarks above Table 34 of the referenced paper). However, the specific results quoted there disagree with those obtained here, and seem to be in error [60]. In what follows it is demonstrated that a fairly simple global characterization of the $\tan\beta$ errors turns out to be possible.

We start with the signal and background results of Table 34

[31] QCD corrections to these cross sections are not included. They have only been calculated for $gg \to H^0$ and $gg \to A^0$, for which cases they increase the cross section by $\sim 50\% - 100\%$.

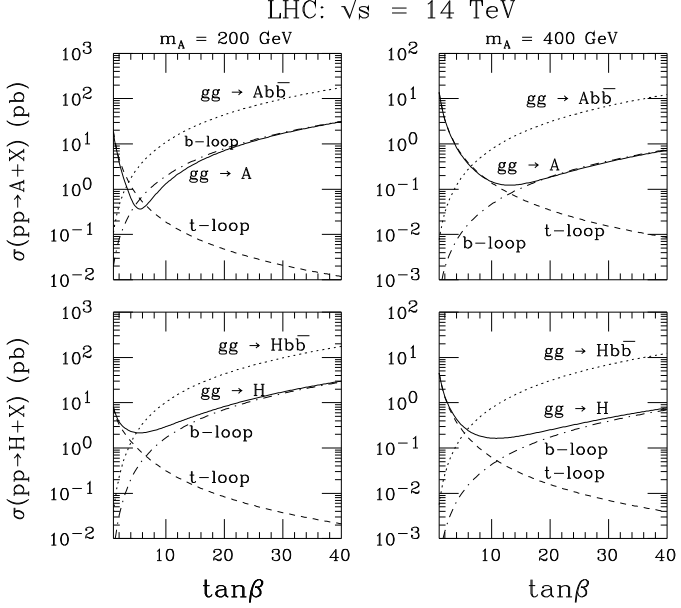

Figure 17: The dependence of $gg \to H^0, A^0$ and $gg \to H^0 b\bar{b}, A^0 b\bar{b}$ cross sections at the LHC on $\tan\beta$ for $m_{A^0} = 200$ and 400 GeV. Also shown are the $gg \to H^0, A^0$ cross sections obtained by retaining only b- or t-loop contributions to the one-loop coupling.

of Ref. [59] for $\tan\beta = 10$ and $A^0 \to \tau^+\tau^-$ only. There S and B are given for $L = 100\ \mathrm{fb}^{-1}$ as a function of m_{A^0}, along with the cross section employed before reduction by the efficiency associated with cuts, particle identification and so forth. By comparing $L\sigma$ (for $L = 100\ \mathrm{fb}^{-1}$) with the tabulated S, we get the signal efficiency, ϵ_S for each m_{A^0}. We then compute an effective statistical significance for the combined H^0 and A^0 signals at $L = 600\ \mathrm{fb}^{-1}$ as follows. First we compute the total H^0 rate S_H

$$S_H = L\epsilon_S[\sigma(gg \to H^0) + \sigma(gg \to H^0 b\bar{b})]BR(H^0 \to \tau^+\tau^-)\,. \tag{21}$$

The analogous equation is used for the total A^0 rate S_A. (The cross section times branching ratio for A^0 is found to be slightly larger, roughly by 10%, than quoted in Table 34 of Ref. [59].) B_H and B_A are computed by scaling up the $L = 100\ \mathrm{fb}^{-1}$ results of Table 34 to $L = 600\ \mathrm{fb}^{-1}$. The net effective $S/\sqrt{B}$ for the combined H^0 and A^0 signals is computed according to the Ref. [59] prescription:

$$\left[\left(\frac{S}{\sqrt{B}}\right)_H^2 + \left(\frac{S}{\sqrt{B}}\right)_A^2 - 2\epsilon_{HA}\left(\frac{S}{\sqrt{B}}\right)_H\left(\frac{S}{\sqrt{B}}\right)_A\right]^{1/2}, \tag{22}$$

where ϵ_{HA} is a function of $r_M \equiv |m_{H^0} - m_{A^0}|/\sigma_M$, with σ_M being the $\tau^+\tau^-$ mass resolution. (At high luminosity we take $\sigma_M = 21\ \mathrm{GeV}$ — see earlier SM LHC discussion for mass region M2.) The value of ϵ_{HA} is: 0 (corresponding to no signal total overlap of the signals) for $r_M < 0.5$. The $\tan\beta$ values required for net $S/\sqrt{B} = 5$, 10, 15 and 20 as a function of m_{A^0} are shown in Fig. 18. For large $\tan\beta$ values, $S/\sqrt{B} > 5$ is always possible. For a limited range of m_{A^0}, $S/\sqrt{B} > 5$ is also possible at low $\tan\beta$.

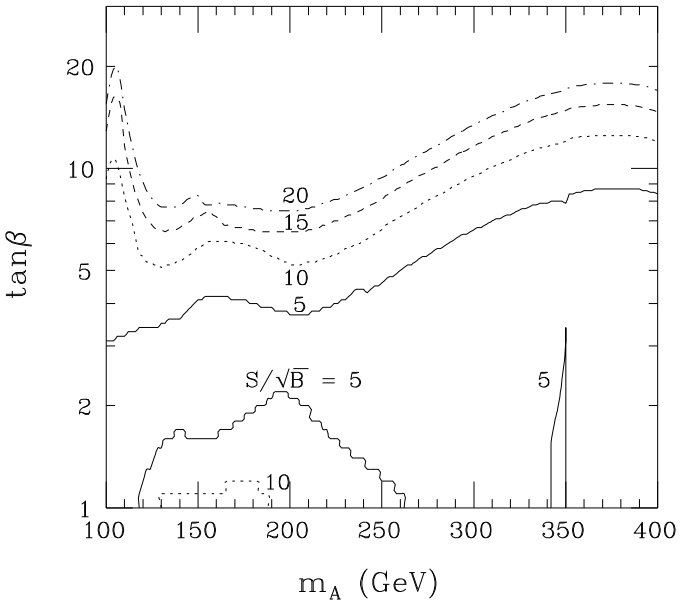

Figure 18: The $\tan\beta$ values required for detection of H^0, A^0 production with $H^0, A^0 \to \tau^+\tau^-$ as a function of m_{A^0} for $S/\sqrt{B} = 5, 10, 15, 20$.

We next compute the error in the cross section determination as

$$\frac{\Delta\sigma}{\sigma} = \left[\frac{S+B}{S^2} + (0.1)^2\right]^{1/2}, \tag{23}$$

where the 0.1 is the presumed systematic uncertainty, assumed independent of parameter choices. We have computed the values of $\Delta\sigma/\sigma$ for the $\tan\beta$ values such that $S/\sqrt{B} = 5, 10, 15, 20$ at $m_{A^0} = 200\,\mathrm{GeV}$ and $400\,\mathrm{GeV}$. For both m_{A^0} values one finds fractional errors of $[\Delta\sigma/\sigma] = 0.22, 0.14, 0.12, 0.11$, respectively. $\Delta\tan\beta$ can be approximately computed as $\Delta\sigma[d\sigma/d\tan\beta]^{-1}$ or with greater precision by searching for those values of $\tan\beta$ such that σ changes by $\Delta\sigma$; the results obtained in these two ways are virtually the same. Dividing the absolute $\Delta\tan\beta$ error by the $\tan\beta$ value required for the given $S/\sqrt{B}$, one discovers that, for $S/\sqrt{B} \geq 10$, the corresponding fractional errors in $\tan\beta$ are roughly independent of m_{A^0}: $\Delta\tan\beta/\tan\beta \sim 0.075, 0.062, 0.056$ for $S/\sqrt{B} = 10, 15, 20$ at both $m_{A^0} = 200$ and $400\,\mathrm{GeV}$. Thus, when a $\geq 10\sigma$ signal can be detected in the $\tau^+\tau^- b\bar{b}$ final state channel a $\leq \pm 8\%$ determination of $\tan\beta$ will be possible, a very useful level of accuracy. At $\tan\beta$ such that $S/\sqrt{B} = 5$, there is more variation. The full results for the high-$\tan\beta$ cases are summarized in Table XIV. At $m_{A^0} = 200\,\mathrm{GeV}$,

$\tan\beta = 3.5$ value at which we summarized results in Table XIV. At $\tan\beta \sim 2$ and $m_{A^0} \sim 200\,\mathrm{GeV}$, the percentage error in the $\tan\beta$ determination is $\sim \pm 30\%$.

Of course, when there are two different $\tan\beta$ values yielding the same signal rate (and also same $S/\sqrt{B}$), as at $m_{A^0} = 200\,\mathrm{GeV}$ above, we would be left with an ambiguity using the totally inclusive procedures considered so far by ATLAS and CMS. This ambiguity can be resolved by b-tagging. For the high-$\tan\beta$ $S/\sqrt{B} = 5, 10, 15, 20$ contours, the signal rate is essentially entirely due to the $gg \to H^0 b\bar{b}, A^0 b\bar{b}$ production mechanisms, while on the low-$\tan\beta$ $S/\sqrt{B} = 5$ and 10 contours, it is the inclusive $gg \to H^0, A^0$ production mechanism that dominates. Tagging or anti-tagging b-quarks in the final state in association with the $\tau^+\tau^-$ from H^0, A^0 decay would definitively separate these mechanisms from one another and avoid any ambiguity as to the correct $\tan\beta$ value.

Table XIV: We tabulate the percentage errors at $m_{A^0} = 200\,\mathrm{GeV}$ and $400\,\mathrm{GeV}$ for the $H^0, A^0 \to \tau^+\tau^-$ signal and the corresponding errors in the determination of $\tan\beta$ for the high-$\tan\beta$ contours such that $S/\sqrt{B} = 5, 10, 15, 20$, assuming $L = 600\ \mathrm{fb}^{-1}$ accumulated at the LHC.

Quantity	Errors			
m_{A^0}	200 GeV		400 GeV	
	$\Delta\sigma/\sigma$	$\Delta\tan\beta/\tan\beta$	$\Delta\sigma/\sigma$	$\Delta\tan\beta/\tan\beta$
$S/\sqrt{B} = 5$	$\pm 20\%$	$\pm 22\%$	$\pm 22\%$	$\pm 12\%$
$S/\sqrt{B} = 10$	$\pm 14\%$	$\pm 7.8\%$	$\pm 14\%$	$\pm 7.4\%$
$S/\sqrt{B} = 15$	$\pm 12\%$	$\pm 6.2\%$	$\pm 12\%$	$\pm 6.2\%$
$S/\sqrt{B} = 20$	$\pm 11\%$	$\pm 5.6\%$	$\pm 11\%$	$\pm 5.7\%$

In the above analysis, we have implicitly assumed that $BR(H^0, A^0 \to \tau^+\tau^-)$ will be either measured or calculable. More generally, conversion of measurements of $\sigma(H^0, A^0)BR(H^0, A^0 \to \tau^+\tau^-)$ to determinations of the cross sections and actual signal rate must include systematic and/or statistical errors due to uncertainty in the $\tau^+\tau^-$ branching ratios. Direct measurement of $BR(H^0, A^0 \to \tau^+\tau^-)$ will require NLC or FMC data. (See next subsection.) If only LHC data is available, then the situation is more complicated, as we now describe.

At high enough $\tan\beta$, the enhancement of the H^0, A^0 couplings to $b\bar{b}$ and $\tau^+\tau^-$ in the MSSM will imply that these are the only modes of importance and that they will be in the ratio[32] $3m_b^2(m_{A^0}) : m_\tau^2$. For such $\tan\beta$ values, systematic uncertainty will be small. However, the $\tan\beta$ values of Fig. 18 required for $S/\sqrt{B} = 5$ and, to a lesser extent $S/\sqrt{B} = 10$, are not always large enough to guarantee that other (*e.g.* SUSY) decays of the H^0, A^0 can be neglected. (See next subsection for some examples.)

Even at high $\tan\beta$ it would be very helpful to directly measure the $BR(\tau^+\tau^-)/BR(b\bar{b})$ ratio(s) as a confirmation of the theoretical prediction. To measure the ratio requires measuring the rates for the $H^0 b\bar{b}, A^0 b\bar{b} \to b\bar{b}b\bar{b}$ final states. This was $S/\sqrt{B}$ values comparable to those in the $b\bar{b}\tau^+\tau^-$ final state are possible if excellent b-tagging efficiency and purity are achieved at high luminosity. Full detector simulation studies by the ATLAS and CMS experimental groups are underway. Accuracy in the measurement of the $H^0 b\bar{b}, A^0 b\bar{b} \to b\bar{b}b\bar{b}$ rates will be limited if S/B is as small as typically associated with $S/\sqrt{B} \sim 5$ signals in the study of Ref. [58]. Precise statements must await the completion of ongoing work.

At lower $\tan\beta$ values, where $gg \to H^0, A^0 \to \tau^+\tau^-$ production mode(s) are dominant, systematic uncertainties associated with imperfect knowledge of the $\tau^+\tau^-$ branching ratios will definitely be a major consideration. At low $\tan\beta$, other decay channels (most notably $H^0 \to h^0 h^0$ and $A^0 \to Zh^0$, not to mention SUSY pair channels if kinematically allowed) are expected to be important in the MSSM, but determining their magnitude will be very difficult without the NLC. Further, isolation of the inclusive $gg \to H^0, A^0 \to b\bar{b}$ production/decay mode is almost certainly impossible.

E. Probing $\tan\beta$ and GUT-scale boundary conditions using H^0A^0 and H^+H^- production at the NLC or FMC [61]

If supersymmetry is discovered, one of our primary goals will be to fully test the model and determine the underlying GUT boundary conditions at the GUT/Planck mass scale. The heavy Higgs bosons of the model are an important component in this program. First, detection of the H^0, A^0 and $H^\pm$ is required in order to verify the Higgs sector content. This may only be possible in the pair production modes H^0A^0 and H^+H^- at a e^+e^- or $\mu^+\mu^-$ collider with $\sqrt{s} \gtrsim 2m_{A^0}$. (Recall that the MSSM Higgs sector structure requires $m_{H^0} \sim m_{A^0} \sim m_{H^\pm}$ at higher masses.) In Ref. [61], the influence of SUSY decays on our ability to detect pair production is assessed and a strategy for using these and other decays to probe the GUT boundary conditions is developed. A related study has recently appeared in Ref. [62].

In Ref. [61], these issues are examined in the context of six not terribly different GUT-scale boundary condition scenarios in which there is universality for the soft-SUSY-breaking parameters $m_{1/2}$, m_0 and A_0 associated with soft gaugino masses, soft scalar masses and soft Yukawa coefficients, respectively [63]. After requiring that the electroweak symmetry breaking generated as a result of parameter evolution yield the correct Z boson mass, the only other parameters required to fully specify a model in this universal-boundary-condition class are $\tan\beta$ and the sign of the μ parameter (appearing in the superpotential $W \ni \mu\hat{H}_1\hat{H}_2$). The six models considered in Ref. [61] are denoted D^-, D^+, NS^-, NS^+, HS^-, HS^+, where the superscript indicates $\mathrm{sign}(\mu)$. Each is specified by a particular choice for $m_0 : m_{1/2} : A_0$, thereby leaving only $m_{1/2}$, in addition to $\tan\beta$, as a free parameter in any given model. Pair production is then considered in the context of each model as a function of location in the kinematically and constraint allowed portion of $(m_{1/2}, \tan\beta)$ parameter space.

Ref. [61] finds that event rates for anticipated machine lu-

[32] $m_b(m_{A^0})$ is the running b-quark mass evaluated at scale $m_{A^0} \sim m_{H^0}$. For m_{A^0} in the $150 - 400\,\mathrm{GeV}$ range, $m_b^2(m_{A^0}) \sim 0.5 m_b^2(pole)$.

detected in final state modes where $H^0, H^0 \to b\bar{b}$ or $t\bar{t}$ and $H^+ \to t\bar{b}, H^- \to b\bar{t}$ even when the branching ratios for SUSY decays are substantial. Further, the mass of the H^0 or A^0 can be determined with substantial accuracy using the fully reconstructable all jet final states associated with these modes. Perhaps of greatest ultimate importance, in much of the kinematically and phenomenologically allowed parameter space Higgs branching ratios for a variety of different decay channels can be measured by "tagging" one member of the Higgs pair in a fully reconstructable all jet decay mode and then searching for different types of final states in the decay of the second (recoiling) Higgs boson.

The power of Higgs pair observations for determining the GUT boundary conditions is most simply illustrated by an example. Let us suppose that the D$^-$ model with $m_{1/2} = 201.7\,\mathrm{GeV}$ and $\tan\beta = 7.5$ is nature's choice. This implies that $m_{A^0} = 349.7\,\mathrm{GeV}$ and $m_{\widetilde{\chi}_1^\pm} = 149.5\,\mathrm{GeV}$. Experimentally, one would measure m_{A^0} as above and $m_{\widetilde{\chi}_1^\pm}$ (the lightest chargino) mass in the usual way and then infer the required parameters for a given model. For the six models the parameters are given in Table XV. Note that if the correct GUT scenario can be ascertained experimentally, then $\tan\beta$ and $m_{1/2}$ will be fixed.

Table XV: We tabulate the values of $m_{1/2}$ (in GeV) and $\tan\beta$ required in each of our six scenarios in order that $m_{A^0} = 349.7\,\mathrm{GeV}$ and $m_{\widetilde{\chi}_1^\pm} = 149.5\,\mathrm{GeV}$. Also given are the corresponding values of m_{H^0}. Masses are in GeV.

	D$^-$	D$^+$	NS$^-$	NS$^+$	HS$^-$	HS$^+$
$m_{1/2}$	201.7	174.4	210.6	168.2	203.9	180.0
$\tan\beta$	7.50	2.94	3.24	2.04	12.06	3.83
m_{H^0}	350.3	355.8	353.9	359.0	350.1	353.2

Determination of the GUT scenario proceeds as follows. Given the parameters required for the observed m_{A^0} and $m_{\widetilde{\chi}_1^\pm}$ for each model, as tabulated in Table XV, the rates for different final states of the recoil (non-tagged) Higgs boson in pair production can be computed. Those for the input D$^-$ model are used to determine the statistical accuracy with which ratios of event numbers in different types of final states can be measured.[33] The ratios predicted in the D$^+$, NS$^-$, NS$^+$, HS$^-$, and HS$^+$models will be different from those predicted for the input D$^-$ model. Thus, the statistical uncertainty predicted for the various ratios in the input D$^-$ model can be used to compute the χ^2 by which the predictions of the other models differ from the central values of the input D$^-$ model. The results for a selection of final state ratios are given in Table XVI. The final states considered are: $b\bar{b}$ and $t\bar{t}$ for the H^0, A^0; h^0h^0 (light Higgs pair, with $h^0 \to b\bar{b}$) for the H^0; h^0W^+ and $\tau^+\nu_\tau$ for the H^+ (or the charge conjugates for the H^-); and SUSY modes (exper-

[33] We focus on ratios in order to be less sensitive to systematic uncertainties in efficiencies *etc.*; however, from Ref. [61] it is clear that absolute rates will also be useful in some instances.

classified according to the number of charged leptons summed over any number of jets (including 0). All branching ratios and reasonable efficiencies are incorporated in the statistical errors employed in constructing this table. The effective luminosity $L_{\rm eff} = 80\ \mathrm{fb}^{-1}$ is equivalent to an overall tagging and reconstruction efficiency for events of $\epsilon = 0.4$ at a total integrated luminosity of $L = 200\ \mathrm{fb}^{-1}$. Results presented are for $\sqrt{s} = 1\,\mathrm{TeV}$.

Table XVI: We tabulate $\Delta\chi_i^2$ (relative to the D$^-$ scenario) for the indicated branching fraction ratios as a function of scenario, assuming the measured m_{A^0} and $m_{\widetilde{\chi}_1^\pm}$ values are $349.7\,\mathrm{GeV}$ and $149.5\,\mathrm{GeV}$, respectively. The SUSY channels have been resolved into final states involving a fixed number of leptons. The error used in calculating each $\Delta\chi_i^2$ is the approximate 1σ error with which the given ratio could be measured for $L_{\rm eff} = 80\ \mathrm{fb}^{-1}$ at $\sqrt{s} = 1\,\mathrm{TeV}$ *assuming that the D$^-$ scenario is the correct one*.

Ratio	D$^+$	NS$^-$	NS$^+$	HS$^-$	HS$^+$
$\langle H^0, A^0\rangle$					
$[0\ell][\geq 0j]/b\bar{b}, t\bar{t}$	12878	1277	25243	0.77	10331
$[1\ell][\geq 0j]/b\bar{b}, t\bar{t}$	13081	2.41	5130	3.6	4783
$[2\ell][\geq 0j]/b\bar{b}, t\bar{t}$	4543	5.12	92395	26.6	116
$h^0h^0/b\bar{b}$	109	1130	1516	10.2	6.2
H^+					
$[0\ell][\geq 0j]/t\bar{b}$	12.2	36.5	43.2	0.04	0.2
$[1\ell][\geq 0j]/t\bar{b}$	1.5	0.3	0.1	5.6	0.06
$h^0W/t\bar{b}$	0.8	0.5	3.6	7.3	0.3
$\tau\nu/t\bar{b}$	43.7	41.5	47.7	13.7	35.5
$\sum_i \Delta\chi_i^2$	30669	2493	124379	68	15272

From Table XVI it is clear that the five alternative models can be discriminated against at a high (often very high) level of confidence. Further subdivision of the SUSY final states into states containing a certain number of jets yields even more discrimination power [61]. Thus, not only will detection of Higgs pair production in e^+e^- or $\mu^+\mu^-$ collisions (at planned luminosities) be possible for most of the kinematically accessible portion of parameter space in a typical GUT model, but also the detailed rates for and ratios of different neutral and charged Higgs decay final states will very strongly constrain the possible GUT-scale boundary condition scenario and choice of parameters, *e.g.* $\tan\beta$ and $m_{1/2}$, therein.

F. Implications of LHC and NLC data for s-channel discovery of the H^0 and A^0 at the FMC

As we have already noted, colliders other than the FMC offer various mechanisms to directly search for the A^0, H^0, but have significant limitations:

- There are regions in $(m_{A^0}, \tan\beta)$ parameter space at moderate $\tan\beta$, $m_{A^0} \gtrsim 200\,\mathrm{GeV}$ in which the H^0, A^0 cannot be detected at the LHC.

but it is limited to $m_{H^0} \sim m_{A^0} \lesssim \sqrt{s}/2$.

- A $\gamma\gamma$ collider could probe heavy Higgs up to masses of $m_{H^0} \sim m_{A^0} \sim 0.8\sqrt{s}$, but this would quite likely require $L > 100\ \mathrm{fb}^{-1}$, especially if the Higgs bosons are at the upper end of the $\gamma\gamma$ collider energy spectrum [34].

In contrast, there is an excellent chance of being able to detect the H^0, A^0 at a $\mu^+\mu^-$ collider provided only that m_{A^0} is smaller than the maximal $\sqrt{s}$ available. This could prove to be very important given that GUT MSSM models usually predict $m_{A^0} \gtrsim 200\,\mathrm{GeV}$.

A detailed study of s-channel production of the H^0, A^0 has been made in Ref. [3], upon which the ensuing discussion is based. The signals become viable when $\tan\beta > 1$ (as favored by GUT models) since the $\mu^+\mu^- H^0$ and $\mu^+\mu^- A^0$ couplings are proportional to $\tan\beta$. In particular, even though $\Gamma^{\rm tot}_{H^0}, \Gamma^{\rm tot}_{A^0}$ are big (see Fig. 1) at high $\tan\beta$, due to large $b\overline{b}$ decay widths, $BR(H^0, A^0 \to \mu^+\mu^-)$ approaches a constant value that is large enough to imply substantial cross sections $\overline{\sigma}_{H^0}, \overline{\sigma}_{A^0}$. (We recall from the earlier SM Higgs FMC discussion that for a general h, $\overline{\sigma}_h \propto BR(h \to \mu^+\mu^-)$ when the Gaussian beam spread $\sigma_{\sqrt{s}}$ is smaller than Γ_h.) The optimal strategy for H^0, A^0 detection and study at the FMC depends upon the circumstances.

First, it could be that the H^0 and/or A^0 will already have been discovered at the LHC. With $L = 300\ \mathrm{fb}^{-1}$ (ATLAS+CMS) of integrated luminosity, this would be the case if $\tan\beta \lesssim 3$ or $\tan\beta$ is above an m_{A^0}-dependent lower bound (*e.g.* $\tan\beta \gtrsim 10$ for $m_{A^0} \sim 400\,\mathrm{GeV}$).[34] Even if the H^0, A^0 have not been detected, strong constraints on m_{A^0} are possible if precision measurements of the properties of the h^0 (such as the $b\overline{b}/WW^\star$ and $c\overline{c}/b\overline{b}$ event rate ratios and the $(\mu^+\mu^- h^0)^2$ coupling-squared) are made via s-channel production at the FMC or in $\sqrt{s} = 500\,\mathrm{GeV}$ running at the NLC, or by combining these two types of data — see earlier discussions associated with the errors tabulated in Tables X, XI and XII. By limiting the $\sqrt{s}$ scan for the H^0 and A^0 in the s-channel to the $m_{A^0} \sim m_{H^0}$ mass region preferred by h^0 measurements, we would greatly reduce the luminosity needed to find the A^0 and H^0 via an s-channel scan as compared to that required if m_{A^0} is not constrained.

With such pre-knowledge of m_{A^0}, it will be possible to detect and perform detailed studies of the H^0, A^0 for essentially all $\tan\beta \geq 1$ provided only that $m_{A^0} \lesssim \sqrt{s}_{\rm max}$.[35] If $\tan\beta \lesssim 3$, then excellent resolution, $R \sim 0.01\%$, will be necessary for detection since the A^0 and H^0 become relatively narrow for low $\tan\beta$ values (see Fig. 1).. For higher $\tan\beta$ values, $R \sim 0.1\%$ is adequate for H^0, A^0 detection, but $R \sim 0.01\%$ would be required in order to separate the rather overlapping H^0 and A^0 peaks (as a function of $\sqrt{s}$) from one another [3].

Even without pre-knowledge of m_{A^0}, there would be an excellent chance for discovery of the A^0, H^0 Higgs bosons in the LHC. This is because non-observation at the LHC implies that $\tan\beta \gtrsim 3$ while it is precisely for $\tan\beta \gtrsim 2.5 - 3$ that detection of the A^0, H^0 is possible [3] in the mass range from 200 to 500 GeV via an s-channel scan in $\mu^+\mu^-$ collisions. (The lower $\tan\beta$ reach given assumes that $L_{\rm total} = 200\ \mathrm{fb}^{-1}$ is devoted to the scan. The detailed strategy outlined in Ref. [3], as to how much luminosity to devote to different $\sqrt{s}$ scan settings in the $200 - 500\,\mathrm{GeV}$ range, must be employed.) That the LHC and the FMC are complementary in this respect is a very crucial point. Together, the LHC and FMC guarantee discovery of the A^0, H^0 after 3 to 4 years of high luminosity operation each, provided $m_{A^0} \lesssim 500\,\mathrm{GeV}$. Once m_{A^0}, m_{H^0} are known, very precise measurements of some of the crucial properties of the H^0, A^0 (including a scan determination of their total widths) become possible [3].

In the event that the NLC has not been constructed, it could be that the first mode of operation of the FMC would be to optimize for and accumulate luminosity at, say, $\sqrt{s} = 500\,\mathrm{GeV}$. In this case, there is still a high probability for detecting the H^0, A^0 if they have not been observed at the LHC. First, if $m_{A^0} \sim m_{H^0} \lesssim \sqrt{s}/2 \sim 250\,\mathrm{GeV}$ then $\mu^+\mu^- \to H^0 A^0$ (and H^+H^-) pair production will be observed. Second, although reduced in magnitude compared to an electron collider, there is a long low-energy bremsstrahlung tail at a muon collider that provides a self-scan over the full range of $\sqrt{s}$ values below the nominal operating energy. Observation of A^0, H^0 s-channel peaks in the $b\overline{b}$ mass ($m_{b\overline{b}}$) distribution created by this bremsstrahlung tail may be possible [3]. The region of the $(m_{A^0}, \tan\beta)$ parameter space plane for which a peak is observable depends strongly on the $m_{b\overline{b}}$ resolution. For excellent $m_{b\overline{b}}$ resolution of order $\pm 5\,\mathrm{GeV}$ and integrated luminosity of $L = 200\ \mathrm{fb}^{-1}$ at $\sqrt{s} = 500\,\mathrm{GeV}$, the A^0, H^0 peak(s) are observable for $\tan\beta \gtrsim 4 - 5$ if $500\,\mathrm{GeV} \geq m_{A^0} \geq 250\,\mathrm{GeV}$.[36]

Finally, if neither the LHC nor a FMC scan of the $\leq 500\,\mathrm{GeV}$ region has discovered the H^0, A^0, but supersymmetric particles and the h^0 have been observed, we would believe that the H^0, A^0 must exist but have $m_{A^0} \sim m_{H^0} \geq 500\,\mathrm{GeV}$. Analyses of the SUSY spectrum in the GUT context and precision h^0 studies might have yielded some prejudice for the probable m_{A^0}, and an extension of the FMC energy up to the appropriate $\sqrt{s} \sim m_{A^0}$ for s-channel discovery of the H^0, A^0 could be considered. However, at this point, even if we have developed a favored range for m_{A^0}, it would probably be most worthwhile to consider a machine with much higher $\sqrt{s}$. A popular reference $\mu^+\mu^-$ collider design is one for $\sqrt{s} = 4\,\mathrm{TeV}$. Ref. [61] shows that such an energy with appropriately matched luminosity would allow discovery of $\mu^+\mu^- \to A^0 H^0$ and H^+H^- pair production, via the $b\overline{b}$ or $t\overline{t}$ decay channels of the H^0, A^0 and $t\overline{b}, \overline{t}b$ decay channels of the H^+, H^-, up to masses very close to $m_{A^0} \sim m_{H^0} \sim m_{H^\pm} \sim 2\,\mathrm{TeV}$, even if SUSY decays of the $H^0, A^0, H^\pm$ are substantial. (This mass range certainly includes that expected in any supersymmetric model that provides a solution to the naturalness and hierarchy problems.) Detailed studies of the $H^0, A^0, H^\pm$ of the type discussed in the previous

[34] For $\tan\beta \lesssim 3$, one makes use of modes such as $H^0 \to h^0 h^0 \to b\overline{b}\gamma\gamma$ and $H^0 \to ZZ^{(*)} \to 4\ell$, when $m_{H^0} \lesssim 2m_t$, or $H^0, A^0 \to t\overline{t}$, when $m_{H^0}, m_{A^0} \gtrsim 2m_t$. At high $\tan\beta$, the enhanced production rates for $b\overline{b}H^0, b\overline{b}A^0$ with $H^0, A^0 \to \tau^+\tau^-$ are employed.

[35] We assume that a final ring optimized for maximal luminosity at $\sqrt{s} \sim m_{A^0}$ would be constructed.

[36] Required $\tan\beta$ values increase dramatically as one moves into the $m_{A^0} \sim m_Z$ zone, but this region is covered by $H^0 A^0$ pair production.

e^+e^- collider with $\sqrt{s} \lesssim 1.5 - 2\,\mathrm{TeV}$ is also probably viable, and could probe $m_{A^0} \sim m_{H^0} \sim m_{H^\pm} \lesssim \sqrt{s}/2$ [61, 62]. In the absence of a strong prejudice based on GUT boundary conditions, only the $2\,\mathrm{TeV}$ option could be presumed (purely on the basis of naturalness) to guarantee $H^0, A^0, H^\pm$ discovery.

G. Searching for a doubly-charged Higgs boson [64]

Doubly-charged Higgs bosons (Δ^{--}, Δ^{++}) appear in many extensions of the Standard Model Higgs sector, such as left-right symmetric models, and can be relatively light, the current bound being $m_{\Delta^{--}} > 45\,\mathrm{GeV}$ from LEP. They have received less attention than neutral and singly-charged Higgs bosons because they can lead to phenomenological difficulties. In particular, $\rho \equiv \frac{m_W^2}{[\cos^2\theta_W m_Z^2]} = 1$ is not natural unless any neutral Higgs boson that is part of the same Higgs multiplet has zero vacuum expectation value.[37] Thus, models with zero vev are favored. In left-right symmetric models, zero vev is natural for the neutral member of the Higgs triplet associated with the left-handed sector; the right-handed sector neutral Higgs must have substantial vev and the associated Δ_R^{--} phenomenology is very different. Of course, representations can be chosen for which there is no neutral member; *e.g.* a $T = 1/2, Y = -3$ representation contains only a Δ^{--} and a Δ^-. Coupling constant unification should also be taken into account. It is amusing to note that coupling constant unification occurs in the non-supersymmetric Standard Model if a single $|Y| = 2$ triplet representation is included in addition to the standard $|Y| = 1$ doublet Higgs representation. On the other hand, in the minimal supersymmetric extension of the SM, inclusion of triplet Higgs field(s) destroys unification. However, this can always be cured by introducing intermediate scale matter so as to maintain unification, as done for example in left-right symmetric models. Thus, potential phenomenological difficulties are not all that difficult to avoid, and we should be on the look-out for signatures of exotic Higgs representations, the clearest signal being the existence of a doubly-charged Higgs boson.

An especially important feature of a Δ^{--} is the fact that for many representation choices $\Delta^{--} \to \ell^-\ell^-$ couplings are allowed. Indeed, in left-right symmetric models the corresponding neutral field couplings give rise to the see-saw mechanism and thereby naturally small neutrino masses. Detection and study of a Δ^{--} provides important opportunities for determining whether such couplings exist and how large they are.

We begin our discussion by considering the phenomenologically natural models in which the vev of any neutral member of the multiplet containing the Δ^{--} is zero. This implies that the $\Delta^{--} \to W^-W^-$ coupling is also zero. If the Δ^{--} also couples to $\ell^-\ell^-$, then the resulting phenomenology is very special and easily identified. There are only two production mechanisms: $\gamma^\star, Z^\star \to \Delta^{--}\Delta^{++}$ and $\ell^-\ell^- \to \Delta^{--}$. For the class of model being considered, it is also very possible bly?) τ. The only competing modes that might be present are $\Delta^{--} \to W^-\Delta^-$ and $\Delta^{--} \to \Delta^-\Delta^-$, where Δ^- is a member of the same SU(2)$_L$ multiplet as the Δ^{--}. Generally, m_{Δ^-} is not very different from $m_{\Delta^{--}}$, and only the $W^-\Delta^-$ mode has a significant likelihood of being two-body allowed; in many models both the $W^-\Delta^-$ and $\Delta^-\Delta^-$ modes can only proceed virtually. Even when the $W^-\Delta^-$ channel is two-body allowed, one finds that $\ell^-\ell^-$ could be the dominant decay channel if the $\Delta^{--} \to \ell^-\ell^-$ coupling is not too much lower than the current bound(s). We note that decay of the Δ^{--} will occur inside the detector even if the $W^-\Delta^-$ decay mode is highly suppressed, so long as the $\Delta^{--} \to \ell^-\ell^-$ coupling is not extremely small (smaller than is preferred, for example, for the Δ_L^{--} of a left-right symmetric model).

The $\ell^-\ell^- \to \Delta^{--}$ ($\ell = e$ or μ) production mechanism was studied in Ref. [65]. It can lead to detectable signals down to remarkably small magnitudes of the $\Delta^{--} \to \ell^-\ell^-$ coupling — far below current limits; for couplings near the current limits very high production rates result, implying the possibility of a Δ^{--} factory. However, for $\ell^-\ell^- \to \Delta^{--}$, one must have $\sqrt{s} \sim m_{\Delta^{--}}$. To avoid wasting time on a scan, it is highly advantageous if $m_{\Delta^{--}}$ is known ahead of time. Thus, prior detection of $\Delta^{--}\Delta^{++}$ pair production would be of great value. Discovery of a Δ^{--} with decays to $\ell^-\ell^-$ would in and of itself provide a compelling motivation for building an $\ell^-\ell^-$ collider designed for use as a Δ^{--} factory.

Pair production of $\Delta^{--}\Delta^{++}$ in e^+e^- or $\mu^+\mu^-$ collisions requires only sufficient $\sqrt{s}$. Although no specific study was performed, it seems very likely that discovery up to $m_{\Delta^{--}} \lesssim \sqrt{s}/2$ would be possible. However, the NLC and FMC are still more than a decade away at best.

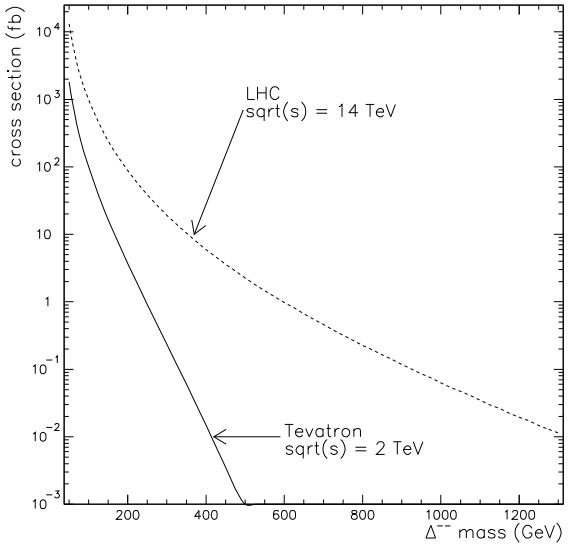

Figure 19: $\Delta^{++}\Delta^{--}$ pair production cross section as a function of Δ^{--} mass for both the Tevatron and the LHC.

[37] Even if the model is constructed so that $\rho = 1$ at tree-level, one loop corrections are infinite unless the vev is zero.

$\Delta^{--} \to \ell^-\ell^-$ and $\Delta^{++} \to \ell^+\ell^+$ is investigated. The $\gamma^\star, Z^\star \to \Delta^{--}\Delta^{++}$ coupling is always present, although slightly model-dependent; for definiteness a $T = 1, T_3 = -1, Y = -2$ Δ^{--} is considered (as found in several popular models). The Tevatron and LHC cross sections for $\Delta^{--}\Delta^{++}$ pair production are plotted as a function of $m_{\Delta^{--}}$ in Fig. 19. Discovery limits for $\Delta^{--}\Delta^{++}$ are obtained assuming that a single $\Delta^{--} \to \ell^-\ell^-$ decay channel is dominant with $\ell = e$, μ or τ. A full Monte Carlo simulation is performed at Tevatron energies. Events are generated in PYTHIA and passed through the Run I CDF detector simulation. For $\ell = e, \mu$ it is found that backgrounds are negligible once a like-sign dilepton pair with high mass is required, and it is purely a matter of having a handful of very clean events. For $\ell = \tau$, the need to identify the τ by its decay to an isolated lepton or hadron leads to a significant background level, implying a smaller discovery reach. Assuming $BR(\Delta^{--} \to \ell^-\ell^-) \sim 1$, it is demonstrated that detection of the Δ^{--} at the Tevatron (operating at $\sqrt{s} = 2\,\mathrm{TeV}$ with $L = 30\ \mathrm{fb}^{-1}$) will be possible for $m_{\Delta^{--}}$ up to $300\,\mathrm{GeV}$ for $\ell = e$ or μ and $180\,\mathrm{GeV}$ for $\ell = \tau$. These results should improve slightly if the greater coverage of the TeV33 detector upgrades is incorporated. The corresponding limits at the LHC are estimated by requiring the same raw number of events before cuts and efficiencies as needed at the Tevatron (~ 10 for $\ell = e, \mu$ and ~ 300 for $\ell = \tau$) yielding $m_{\Delta^{--}}$ discovery up to roughly $925\,\mathrm{GeV}$ (1.1 TeV) for $\ell = e, \mu$ and $475\,\mathrm{GeV}$ ($600\,\mathrm{GeV}$) for $\ell = \tau$, assuming total integrated luminosity of $L = 100\ \mathrm{fb}^{-1}$ ($L = 300\ \mathrm{fb}^{-1}$). For $\ell = e, \mu$, the reach of the LHC detectors will likely be even greater than this, due to the improved lepton acceptance and resolution anticipated over the current generation of hadron collider detectors. For $\ell = \tau$, this simple extrapolation may not account for a different signal-to-background ratio in τ selection at the LHC. A full study is necessary to evaluate this.

Thus, if a Δ^{--} with moderate mass and the assumed properties exists, discovery at TeV33 is not improbable; the LHC allows discovery up to remarkably large masses. Once found, the importance of pursuing $\ell^-\ell^- \to \Delta^{--}$ collisions is easily argued [65]. In particular, it is very likely that the magnitude of the $\Delta^{--} \to \ell^-\ell^-$ coupling can only be determined by doing so. Indeed, observation of $\Delta^{--}\Delta^{++}$ pair production in only a single $\Delta^{--} \to \ell^-\ell^-$ channel provides no information on the $\ell\ell$ coupling magnitude. (Of course, if more than one $\ell\ell$ channel is seen, ratios of the $\ell\ell$ couplings could be obtained.) Only if the $\Delta^{--} \to \Delta^- W^-$ decay channel [for which the partial width can be computed and compared to the $\ell^-\ell^-$ partial width] is also seen, can one get an estimate of the $\ell\ell$ coupling magnitude(s). In contrast, an e^-e^- ($\mu^-\mu^-$) collider would provide a direct measurement of the ee ($\mu\mu$) coupling. This illustrates an important complementarity between the NLC or FMC and hadron colliders. Discovery of a Δ^{--} prior to the construction and operation of the e^+e^-, e^-e^- collider NLC complex or the FMC analogue would be very important in determining the energy range over which good luminosity and good energy resolution for e^-e^- or $\mu^-\mu^-$ collisions should be a priority.

Of course, the possibility that the Δ^{--} is part of a multi-nored. The Δ_R^{--} of the left-right symmetric model must fall into this class. Such a Δ^{--} will have substantial W^-W^- coupling. There has been substantial work on the related phenomenology [66]. An e^-e^- or $\mu^-\mu^-$ collider would be of particular value in exploring such a Δ^{--}. In addition to the possibility of direct s-channel production through the leptonic coupling, the non-zero $W^-W^- \to \Delta^{--}$ coupling will typically yield a substantial cross section for e^-e^- or $\mu^-\mu^- \to \nu\nu\Delta^{--}$ production. Further, if $m_{\Delta^{--}} \gtrsim 2m_W$, then $\Delta^{--} \to W^-W^-$ decays are very likely to be dominant; detection of such a Δ^{--} at a hadron collider might not be straightforward. Thus, it could happen that one would first discover the Δ^{--} in the W^-W^--fusion mode, at which point it would be important to turn to the s-channel production probe of its possible e^-e^- or $\mu^-\mu^-$ couplings by lowering the machine energy.

IV. CONCLUSIONS

There have been two primary focuses in this report.

- We performed a first detailed study of the accuracy with which the branching ratios, couplings, total width and mass of a SM-like Higgs boson can be measured in a model-independent way. A number of new strategies and techniques were developed during the course of these studies. A thorough evaluation of the possibilities and errors at the LHC is still very much in progress. Still, the results obtained to date indicate that many important properties can be measured with substantial accuracy; see Tables II-VIII, Fig. 10, and Table XIII. The simpler and cleaner environment at the NLC or FMC allowed us to perform a reasonably complete study at these machines, with very encouraging results; see Tables IX-XII, Fig. 10, and Table XIII. The errors quoted are those that would materialize after substantial luminosity has been accumulated: $L = 600\ \mathrm{fb}^{-1}$ at ATLAS+CMS at the LHC; $L = 200\ \mathrm{fb}^{-1}$ at the NLC (or FMC) in $\sqrt{s} = 500\,\mathrm{GeV}$ running; and $L = 200\ \mathrm{fb}^{-1}$ in an s-channel scan at the FMC of the SM Higgs resonance peak.

  One significant conclusion is the great desirability of being able to accumulate $L = 200\ \mathrm{fb}^{-1}$ both in $\sqrt{s} = 500\,\mathrm{GeV}$ running and in a FMC s-channel scan if the Higgs mass is below $2m_W$. This could be accomplished if both the NLC and a low-energy FMC were constructed.

- We examined a number of issues and new ideas associated with extensions of the simple one-doublet SM Higgs sector. Of particular interest were supersymmetric extensions of the SM, including the MSSM and NMSSM. Contributions summarized here included:

  1. A demonstration of the substantial accuracy with which the $t\bar{t}h$ and ZZh couplings could be determined for a general h of arbitrary CP nature at a $\sqrt{s} = 1\,\mathrm{TeV}$ NLC.
  2. A demonstration that in the next-to-minimal supersymmetric model (with Higgs sector consisting of

regions of parameter space for which no Higgs boson can be found at the LHC and/or LEP2, implying that in some circumstances Higgs discovery would have to await the NLC or FMC.

3. A demonstration that at low $\tan\beta$, the A^0 of the MSSM could be detected at the LHC in the inclusive $A^0 \to \gamma\gamma$ mode.
4. An assessment of the extent to which the observed rates for $H^0, A^0 \to \tau^+\tau^-$ at the LHC could be used to fix the elusive $\tan\beta$ parameter.
5. A demonstration that $e^+e^- \to H^0A^0, H^+H^-$ pair production at a $\sqrt{s} = 1$ TeV NLC will be observable (even if SUSY decays of the Higgs bosons are substantial) and will provide powerful information for determining the correct boundary conditions at the unification scale.
6. A demonstration that $pp \to \Delta^{--}\Delta^{++}$ (doubly-charged Higgs pair production) will yield an observable signal up to surprisingly substantial Δ^{--} masses at the Tevatron and up to very large masses at the LHC.

Despite the very substantial progress summarized in this report, much work remains to be done, both with respect to fine-tuning procedures for a SM-like Higgs boson and with regard to improving old and finding new techniques for discovering and studying exotic Higgs bosons.

Acknowledgements

This work was supported in part by the U.S. Department of Energy under Grant No. DE-FG03-91ER40674 and by the National Science Foundation under Grant No. PHY94-07194. Further support was provided by the Davis Institute for High Energy Physics. JFG wishes to acknowledge the hospitality of the Institute for Theoretical Physics where a portion of this report was written. We thank R. Settles and P. Janot for their comments and suggestions.

V. REFERENCES

[1] J.F. Gunion, A. Stange, and S. Willenbrock, *Weakly-Coupled Higgs Bosons*, preprint UCD-95-28 (1995), to be published in *Electroweak Physics and Beyond the Standard Model*, World Scientific Publishing Co., eds. T. Barklow, S. Dawson, H. Haber, and J. Siegrist.

[2] *Physics and Technology of the Next Linear Collider: a Report Submitted to Snowmass 1996*, BNL 52-502, FNAL-PUB-96/112, LBNL-PUB-5425, SLAC Report 485, UCRL-ID-124160.

[3] V. Barger, M. Berger, J.F. Gunion and T. Han, UCD-96-6 (January, 1996), to appear in Phys. Rep.

[4] S. Kim, S. Kuhlmann, W.-M. Yao, these proceedings.

[5] W.-M. Yao, these proceedings.

[6] R. Jesik, work in progress.

nion, R. Vega collaboration; C. Kao; and PYTHIA.

[8] The results summarized in this section are based on work by J. Gunion and L. Poggioli.

[9] Atlas Technical Proposal, CERN/LHCC 94-43 (1994).

[10] CMS Technical Proposal, CERN/LHCC 94-38 (1994).

[11] ATLAS study of separating WW fusion at $m_{h_{\rm SM}} \sim 100\,{\rm GeV}$.

[12] ATLAS Internal Note, Phys-No-048.

[13] V. Barger, G. Bhattacharya, T. Han and B. Kniehl, Phys. Rev. **D43**, 779 (1991).

[14] M. Dittmar and H. Dreiner, hep-ph/9608317.

[15] L. Poggioli, preliminary communication regarding a study being performed by the ATLAS collaboration.

[16] Based on work performed by J.F. Gunion.

[17] A. Djouadi, talk presented at the Higgs '96 meeting, Ringberg, Germany, December 1996.

[18] S. Narison, Phys. Lett. **B341**, 73 (1994); for a review, see S. Narison, hep-ph/9510270, presented at the *1995 Europhysics Conference on High Energy Physics*, Brussels, Belgium, July 27-31, 1995.

[19] See the work by P. Burrows *et al.* in the QCD contribution to these proceedings

[20] Work performed by R. Van Kooten and D. Jackson.

[21] P. Janot, The HAZA Monte Carlo Generator, Event Generators for Discovery Physics, CERN Yellow Report, Vol. 3, CERN-96-01.

[22] T. Sjöstrand, Computer Physics Commun. 39 (1986) 347; CERN-TH.7112/93; T. Sjöstrand and M. Bengtsson, Computer Physics Commun. 43 (1987) 367; H. U. Bengtsson and T. Sjöstrand, Computer Physics Commun. 46 (1987) 43.

[23] Chris Damerell, these proceedings.

[24] See p. 25 of Ref. [2].

[25] J.F. Gunion, T. Han and R. Sobey, work in progress.

[26] The strategies and/or estimates outlined were developed by J. Gunion and R. Van Kooten.

[27] Work performed for this workshop by R. Van Kooten.

[28] J.F. Gunion and P. Martin, UCD-96-34, these proceedings; and UCD-96-15 (hep-ph/9607360).

[29] See "JLC-I", KEK-92-16, December 1992.

[30] J. Irwin, private communication.

[31] J.F. Gunion and P. Martin, work performed for this report.

[32] K. Kawagoe, *Proceedings of the 2nd International Workshop on "Physics and Experiments with Linear e^+e^- Colliders"*, eds. F. Harris, S. Olsen, S. Pakvasa and X. Tata, Waikoloa, HI (1993), World Scientific Publishing, p. 660.

[33] Work performed by R. Van Kooten for this workshop.

[34] J.F. Gunion and H.E. Haber, Phys. Rev. **D48**, 5109 (1993).

[35] D. Borden, D. Bauer, and D. Caldwell, Phys. Rev. **D48**, 4018 (1993).

[36] D. Bauer, work performed for this report.

[37] V. Barger, M. Berger, J.F. Gunion and T. Han, work in progress.

[38] P. Janot, private communication.

39 (1996).

[40] M. Kramer, J. Kuhn, M. Stong, and P. Zerwas, Z. Phys. **C64**, 21 (1994).

[41] A. Soni and R.M. Xu, Phys. Rev. **D48**, 5259 (1993).

[42] J.F. Gunion and B. Grzadkowski, Phys. Lett. **B350**, 218 (1995).

[43] J.F. Gunion and X.G. He, Phys. Rev. Lett. **76**, 4468 (1996).

[44] J.F. Gunion, T.C. Yuan and B. Grzadkowski, Phys. Rev. Lett. **71**, 488 (1993).

[45] J. F. Gunion, B. Grzadkowski and X.-G. He, Phys. Rev. Lett. **77**, 5172 (1996).

[46] J.F. Gunion and X.-G. He, these proceedings.

[47] J.F. Gunion and B. Grzadkowski, Phys. Lett. **B294**, 361 (1992).

[48] J.F. Gunion and J. Kelly, Phys. Lett. **B333**, 110 (1994).

[49] D. Atwood and A. Soni, Phys. Rev. **D52**, 6271 (1995).

[50] J.F. Gunion, H.E. Haber, and T. Moroi, these proceedings.

[51] J. Kamoshita, Y. Okada and M. Tanaka, Phys. Lett. **B328**, 67 (1994).

[52] S. Abdullin, C. Kao, and N. Stepanov, CMS TN/96-102, MADPH-96-976.

[53] C. Kao and N. Stepanov, Phys. Rev. D **52**, 5025 (1995).

[54] S. Abdullin, A. Khanov, N. Stepanov, CMS TN/94-180 (1994).

[55] R. Brun *et al.*, GEANT3, CERN DD/EE/84-1 (1986).

[56] H. Baer, M. Bisset, D. Dicus, C. Kao and X. Tata, Phys. Rev. D **47**, 1062 (1993); H. Baer, M. Bisset, C. Kao and X. Tata, Phys. Rev. D **50**, 316 (1994).

[57] Based on work performed by J.F. Gunion, C. Kao and L. Poggioli.

[58] J. Dai, J.F. Gunion and R. Vega, Phys. Rev. Lett. **71**, 2699 (1993); Phys. Lett. **B315**, 355 (1993); Phys. Lett. **B345**, 29 (1995); Phys. Lett. **B371**, 71 (1996); Phys. Lett. **B387**, 801 (1996).

[59] E. Ricther-Was, D. Froidevaux, F. Gianotti, L. Poggioli, D. Cavalli, and S. Resconi, ATLAS Internal Note, PHYS-No-074.

[60] We thank L. Poggioli for checking that the results quoted in Ref. [59] are indeed incorrect.

[61] J.F. Gunion and J. Kelly, these proceedings; detailed results appear in preprint hep/ph-9610495.

[62] J. Feng and T. Moroi, hep/ph-9612333.

[63] See the supersymmetry theory subgroup summary for a definition of these parameters and some discussion of universality.

[64] J.F. Gunion, C. Loomis, and K.T. Pitts, these proceedings.

[65] J.F. Gunion, Int. J. Mod. Phys. **A11**, 1551 (1996).

[66] Phenomenological considerations for Higgs triplet representations, especially in left-right symmetric models, are outlined in J.F. Gunion, J. Grifols, B. Kayser, A. Mendez, and F. Olness, Phys. Rev. **D40**, 1546 (1989); N.G. Deshpande, J.F. Gunion, B. Kayser, and F. Olness, Phys. Rev. **D44**, 837 (1991). Phenomenology for Higgs triplet models, focusing on the $\rho = 1$ model with one $|Y| = 0$ and one $|Y| = 2$ triplet, is considered in: J.F. Gunion, R. Vega, and J. Wudka, Phys. Rev. **D42**, 1673 (1990).